EFFECT OF ENVIRONMENT ON CREEP BEHAVIOR OF AN OXIDE/OXIDE
CFCC WITH ±45° FIBER ORIENTATION

THESIS

Gregory T Siegert, ENS, USN

AFIT/GAE/ENY/06-J15

**DEPARTMENT OF THE AIR FORCE
AIR UNIVERSITY**

AIR FORCE INSTITUTE OF TECHNOLOGY

Wright-Patterson Air Force Base, Ohio

APPROVED FOR PUBLIC RELEASE; DISTRIBUTION UNLIMITED

AFIT/GAE/ENY/06-J15

EFFECT OF ENVIRONMENT ON CREEP BEHAVIOR OF AN OXIDE/OXIDE CFCC WITH ±45° FIBER ORIENTATION

THESIS

Presented to the Faculty

Department of Aeronautics and Astronautics

Graduate School of Engineering and Management

Air Force Institute of Technology

Air University

Air Education and Training Command

in Partial Fulfillment of the Requirements for the

Degree of Master of Science in Aeronautical Engineering

Gregory T Siegert, BS

ENS, USN

June 2006

AFIT/GAE/ENY/06-J15

**EFFECT OF ENVIRONMENT ON CREEP BEHAVIOR OF AN OXIDE/OXIDE
CFCC WITH ±45° FIBER ORIENTATION**

Gregory T Siegert, BS

ENS, USN

Approved:

_____   _____
Dr. Marina Ruggles-Wrenn (Chairman)   Date

_____   _____
Dr. Robert Canfield (Member)   Date

_____   _____
Dr. Som Soni (Member)   Date

AFIT/GAE/ENY/06-J15

Abstract

Aerospace applications require materials capable of maintaining superior mechanical properties while operating at high temperatures and oxidizing environments. Nextel™ 720/A (N720/A), an oxide/oxide ceramic matrix composite (CMC) with a porous alumina matrix was developed specifically to provide improved long-term properties and performance at 1200°C. This research evaluated the creep behavior of N720/A with a ±45° fiber orientation at 1200°C in: laboratory air, steam, and argon environments. Creep-rupture tests at the creep stress levels of: 45, 40, 35, and 15 MPa were conducted in each environment.

The ultimate tensile strength of N720/A with ±45˚ fiber orientation was 55 MPa, the elastic modulus (E) was 45 GPa, and failure strain was 0.265%. The creep-rupture results showed a decrease in creep life with increasing creep stress. The material was found to perform best in air, followed by steam, and then argon. Prior to this effort, N720/A was believed to perform best in non-oxidizing environments such as argon. Tests at stress levels ≤ 35 MPa revealed good creep resistance achieving a run out of 100 h in all test environments at 1200°C. Fracture surface observations with a Scanning Electron Microscope showed a correlation between coordinated fiber bundle failure and increased creep life. A qualitative spectral analysis provided evidence of silicon species migration from the mullite phase of the fiber to the matrix in each environment, but increasingly so in steam and argon.

Acknowledgements

I would like to thank the following people for their assistance during the course of my thesis. First, I would like to thank Dr. Marina Ruggles-Wrenn for her support, guidance and leadership throughout my work. I could not have accomplished it without her. I would like to thank Dr. Seungsu Baek for his help with the microscopy and for helping me to find what I didn't know I was looking for. Also, I would like to thank Dr. Robert Canfield and Dr. Som Soni for their sponsorship of my thesis, and Mr. Barry Page for his constant assistance with all test equipment. Capt John Mehrman, 1st LT John Balconis, and 1st LT Patrick Jackson's assistance on understanding the equipment was invaluable. I am very grateful for all of the help and companionship of ENS Griffin Hetrick who worked with me day in and day out. Most of all I am thankful for my very supportive family and friends who were always there for me.

Gregory T Siegert

Table of Contents

List of Figures

List of Tables

EFFECT OF ENVIRONMENT ON CREEP BEHAVIOR OF AN OXIDE/OXIDE CFCC WITH ±45° FIBER ORIENTATION

I. Introduction

The concept of modifying a material to improve its properties dates back to the pyramids of Egypt. Then, clay bricks were mixed with straw to reinforce them for building purposes. From organic materials to metals to composites, materials have evolved with the needs of man. Every day structures are becoming larger, faster, and stronger. So, materials used in these components have become more advanced. Compared to monolithic materials, composites offer an increase in light weight, high strength, superior toughness, crack tolerance, and non-catastrophic modes of failure. Ceramics matrix composites (CMC) represent one class of today's advanced materials.

Ceramics are lightweight materials that retain high strengths at high temperatures. This is the type of environment where advanced aviation and aerospace components operate. Therefore, ceramic materials are attracting the attention of the aviation community. CMCs offer two significant advantages over conventional nickel-based superalloys to the aerospace engine design community. The major advantages are higher material operating temperatures and a decrease in the cooling air requirements [41:1282]. Many aerospace components must operate at extremely high temperatures. Space reentry vehicles, like the one seen in Figure 1, must withstand temperatures as high as 2000˚C and pressures >200 atm. Due to these high temperatures, advanced reusable space launch vehicles will likely incorporate continuous fiber-reinforced ceramic composites (CFCC)

[30:1]. Aircraft components must operate in many different types of aggressive environments. The thermodynamic stability and oxidation resistance of CMCs have now become recognized as important issues. A new type of ceramic matrix composite was developed where both the matrix and fibers are more resistant to oxidation. This type of material is referred to as an oxide/oxide CMC and is composed of oxide materials. An oxide/oxide CMC is less likely to oxidize and degrade at higher temperatures. This makes oxide/oxide CMCs a good choice for long term operation in oxidizing environments. With the use of ceramics, aerospace components can operate efficiently in extremely harsh environments and reach their full potential [11:9-10].

Figure 1. X-37 Advanced technology demonstrator re-entering the earth's atmosphere [3].

Many different tests have been conducted on CMCs over the years, and they have all reported that oxide/oxide CMCs exhibit excellent tensile and fatigue properties at room and elevated temperature [8:451]. The fiber which possesses the best creep

performance of any commercially available polycrystalline oxide fiber is recognized as

Nextel[TM]720 [30:9]. The superior high-temperature creep-performance of this particular

fiber is the result of a high concentration of mullite. Traditionally, mullite has a better

creep resistance than alumina [39:32]. The objective of this thesis is to assess the creep

rupture behavior of Nextel 720/alumina (N720/A), an oxide/oxide CMC, at 1200° in

several environments. This CMC incorporates the Nextel[TM]720 fiber with an alumina

matrix. The Nextel 720/alumina specimens were tested in air, steam, and argon

environments. Composite specimens had a ±45° fiber orientation. Testing of specimens

with a ±45° fiber orientation permits evaluation of the matrix-dominated response of the

composite.

The next chapter discusses background information of Ceramic Matrix

Composites and their applications. In addition, some comments are given relating to the

creep-rupture behavior of CMCs, as well as factors affecting the creep performance of

these materials. Past work on CMCs is also discussed. Experimental setup used in this

research is discussed in detail. Results are presented and discussed. Finally, conclusions

and recommendations for future work are offered.

II. Background

This chapter introduces ceramic matrix composites (CMCs), including the general material chrematistics and the use of CMCs in advanced applications. The importance of oxide/oxide composites will then be discussed. Next, factors affecting creep performance will be presented. Finally, the effects of environment and past research into this topic will be examined.

2.1 Ceramic Matrix Composites

2.1.1 Structural Applications of Ceramic Matrix Composites

Today, military and commercial aerospace vehicles desire to go higher, farther, and faster. This need has dramatically increased the demand for light weight, high-strength structural materials that can perform in aggressive operating environments at extremely high temperatures. Aircraft such as the F-22 and the Boeing 787 Dreamliner are pushing the technological limits in order to achieve faster cruising speeds, longer operating distances, and improved flight performance. "These goals translate into material requirements involving increased strength-to-weight, stiffness-to-density, and improved damage tolerance - all at significantly higher temperatures" [11:377]. Primary considerations driving the advancement of CMCs are: cost reduction in terms of fabrication and maintenance requirements; weight reduction to decrease specific fuel consumption; higher operating temperatures; and signature reduction. In the past, advanced alloys had been able to meet the aerospace requirements [11:378]. However, in order to meet the challenges of the future, the aerospace industry requires development of

advanced composite materials. "The future is composites," said Boeing's Mike Bair, the head of the 787 Dreamliner program [37]. Ceramic composites can be used in high temperature applications where metallic materials suffer from significant creep and/or oxidation [27:122]. The most advanced fighter aircraft the world has ever seen, the F-22, is made up of approximately 25% composites [2] while the Dreamliner will be made up of 50% composites, with most of it in the fuselage and wing. Composites are also the answer to stronger, lighter, and more efficient aircraft engines [33]. "After waiting three decades for enabling technology to catch up with is design ideas, GE-Aviation is deeply embedding itself in composite materials as a next-generation answer to making engines quieter and cheaper to own and operate" [21:48].

Figure 2. Composite structural parts of F-22 Raptor [36].

Figure 3 Boeing 787 Dreamliner [1].

Ceramic Matrix Composites are not just lighter than most other materials previously used in aviation; they also possess the ability to perform at extremely high temperatures for an extended period of time. "Ceramics are the only class of materials viable at very high temperatures" [11:4]. This is illustrated in Table 1, which compares the service temperatures of several polymers, metals, and ceramics.

Table 1. Service temperature limit of materials [11:4].
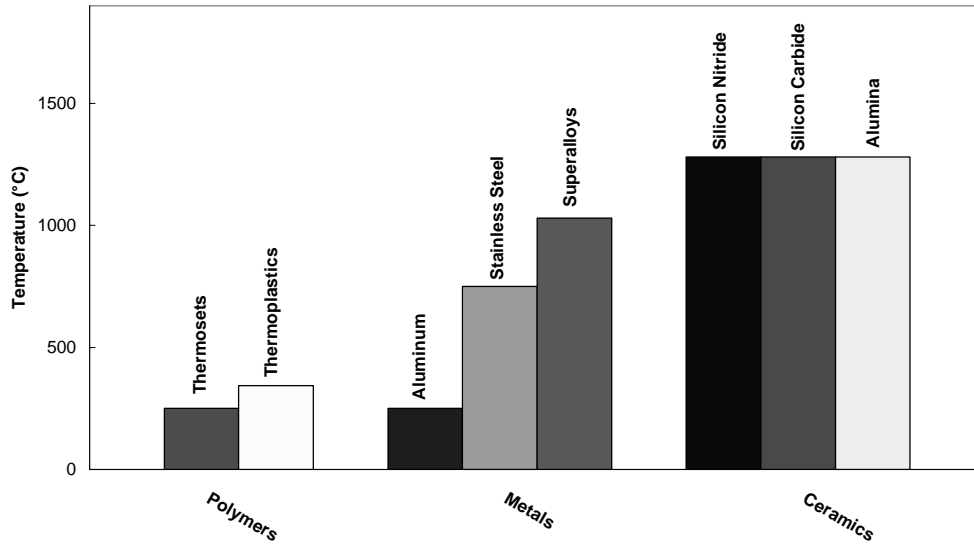
The use of CMCs is not limited to aerospace applications. There are many other areas where CMCs will be of great value, including engine components operating at high temperatures and in corrosive environments, cutting tool inserts, wear resistant parts, nozzles, exhaust ducts, and energy-related applications [6:643, 11:378, 12:951].

2.1.2   Fibers

Fibers used in ceramic matrix composite exhibit high strength and stiffness at high temperatures. The fibers provide the backbone for reinforcing ceramic materials [11:45]. Ceramic fibers can be either continuous or discontinuous fibers based on their size, which can range from smaller multifiber tows (5-15μm diameter) to larger monofilaments (50-100μm). N720/A, classified as a continuous fiber ceramic composite (CFCC), is a ceramic composite reinforced by continuous fibers [20:133]. Discontinuous fibers are very short while continuous fibers are longer and are laid out in bundles. At present both non-oxide and oxide fibers are available. Non-oxide fibers are generally based on silicon carbide (SiC). Oxide fibers are traditionally composed of alumina

(Al$_2$O$_3$) and/or mullite (3Al$_2$O$_3$•2SiO$_2$) [11:12]. The fibers used in Nextel 720/A are

oxide continuous monofilament fibers. In order to achieve high creep resistance,

Nextel™ 720 fibers contain large mullite grains which minimize grain boundary sliding

[17:2333]. The micrograph in Figure 4 shows fiber bundles from a Nextel 720/A

specimen used in this research.

Figure 4. Micrograph of the N720/A specimen subjected to creep at 45 MPa in laboratory air. Fiber bundles and matrix are clearly seen.

2.1.3   Matrix

While the fibers serve as a backbone supporting a composite material, matrix plays an important role as well. The matrix protects the fibers from the surrounding environment allowing the CMC to withstand extremely high temperatures. In the case of the $\pm45°$ fiber orientation studied in this research effort, the matrix provides the load-bearing capability. In designing a CMC, choice of matrix material is as important as the choice of fiber reinforcement. A suitable ceramic matrix material should be able to infiltrate a bundle of fibers, form a mechanical or frictional bond with the reinforcement (fibers), while not reacting chemically with the fiber reinforcement during fabrication or service, and not physically damage the fibers. Furthermore, matrix material must have good creep and fatigue resistance, and be chemically stable [11:40]. A chemically stable matrix is impermeable to moisture and resistant to oxidation. The CMC investigated in this study employs an alumina (Al_2O_3) matrix, which remains stable at temperatures well above 1000°C in oxidizing environments.

Ceramic materials can be divided into two categories: glassy (amorphous) or crystalline. Alumina is a crystalline ceramic. The high strength of the crystalline ceramics is due to the fine grain size and glassy phase present at the grain boundaries [11:41]. The fine alumina particles enhance the packing density, uniformity, and nominal strength of the matrix [19:2077]. Conversely, monolithic alumina is very brittle. Introducing ceramic fiber reinforcement into the ceramic matrix creates a composite designed to exhibit delayed non-brittle failure.

2.1.4   Fabrication of Ceramic Matrix Composites

CMCs are fabricated in a two stage process. During the first phase the reinforcement material, the fibers, are aligned and incorporated into an unconsolidated matrix. Fibers are typically incorporated into the matrix using the slurry infiltration process. This process involves a fiber tow, or bundle, being lead through a tank containing slurry, which is a mixture of the ceramic matrix in a powder form, carrier liquid, and an organic binder. Then the material is wound up onto a drum and dried. Finally, the "tape" which results from this process is cut into sections, stacked into the proper fiber orientation and consolidated [11:151].

There are a multiple techniques for consolidating the ceramic matrix, but hot pressing is the most commonly used. Hot processing produces composites with superior quality provided the thermal mismatch between the constituents of the composite is low. Another process, which produces composites, is cold pressing followed by sintering. The sintering process causes the matrix to shrink and the shrinkage cracks form in the matrix [11:127-128].

Finally, when pairing together a matrix material with a fiber, one must consider their thermal and chemical compatibility. If the materials do not match thermally (i.e. possess significantly different coefficients of linear thermal expansion), the high processing temperatures and the low ductility of the ceramic can lead to matrix cracking during the cooling process [14:607]. The matrix micro-cracks form during the cooling down period in the manufacturing process due to the stresses caused by the difference in thermal expansion between the matrix and fibers [5:572]. This can be seen in Figure 5 and Figure 6. If the materials are chemically compatible, there will be no degradation of

the fiber matrix interface at the elevated temperatures encountered during processing and heat treatment. Conversely, fiber and/or matrix degradation can be caused by a chemical reaction between these materials [24:10].
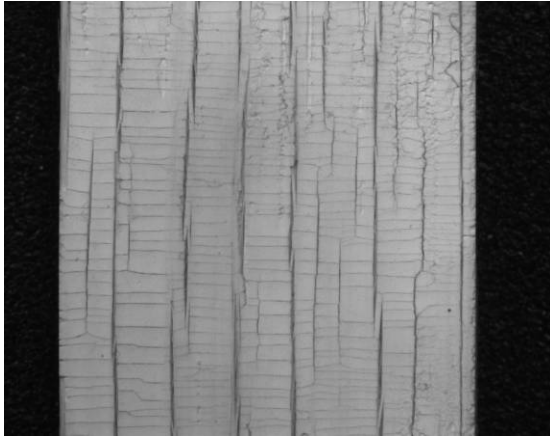
Figure 5. As-processed surface micro-cracking [24:28].
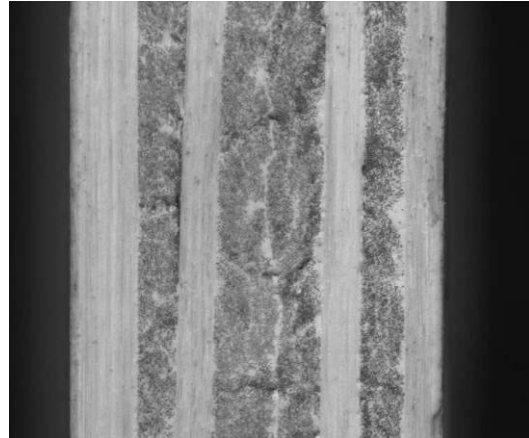
Figure 6. As-processed interlaminar micro-cracking [24:28].

2.2   Oxide/Oxide Composites

A CMC, which is composed of an oxide ceramic matrix and reinforced by oxide fibers, is designated as an oxide/oxide composite. N720/A is an oxide/oxide composite because it is composed of an alumina (Al_2O_3) matrix and alumina-mullite ($3Al_2O_3 \bullet 2SiO_2$) fibers. Oxide/oxide composites are designed to resist oxidation at high temperatures, and thus improve composite properties and performance [8:451]. Oxide/oxide composites have been designed in an attempt to prevent high temperature oxidation damage both in the fibers and the entire composite [10:139]. Oxide/oxide composites developed for aerospace applications are intended for use in turbine engines, combustors, exhaust washed structures, exhaust nozzle flaps, and blade outer air seals [8:617, 26:211].

A composite is considered a non-oxide when none of its phases are oxidized or it possesses a combination of oxidized and non-oxidized phases. When a non-oxide CMC is exposed to an environment such as water vapor or oxygen over a period of time and cracking occurs within the matrix, the oxidants can permeate through the matrix and cause degradation of the fibers. Such oxidation induced degradation results in a shorter life at elevated temperatures by reducing the strength of the composite. One way to prevent this type of oxidation in non-oxide CMCs is to limit the operating temperature below that of the matrix cracking stress level [19:2077].

2.3   Creep-Rupture Behavior

Before Ceramic Matrix Composites can be incorporated into a structural application, the operating conditions must be determined. Because oxide/oxide CMCs exhibit excellent fatigue resistance, but poor creep performance, thorough understanding of the CMCs creep-rupture behavior is critical to evaluating the stability of the composite for a particular application. Furthermore, based on the creep performance of the CMC over a range of temperatures, temperature limitations on the use of this material in operational service can be established.
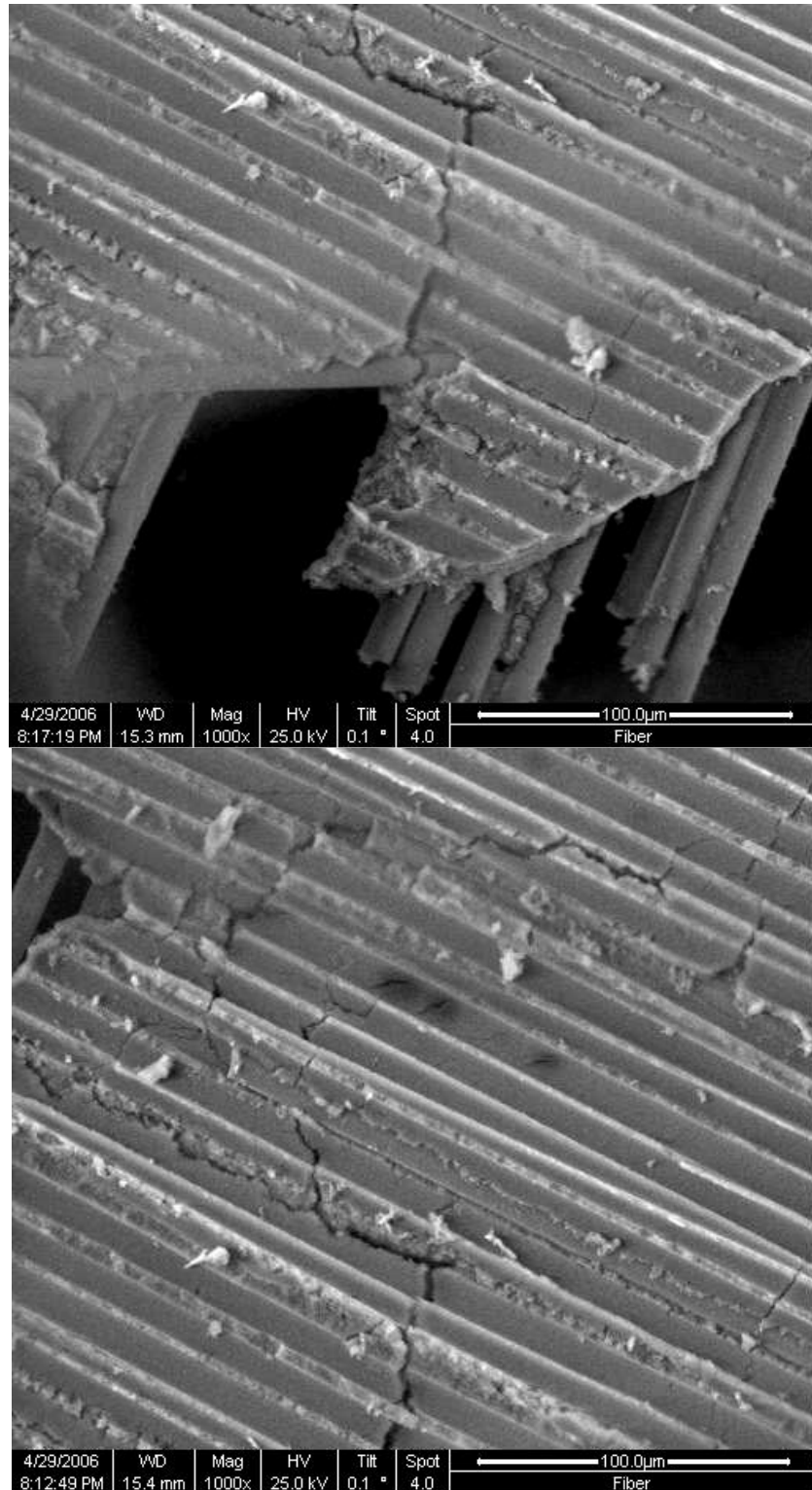
Figure 7. Micrograph of the N720/A specimen subjected to creep at 40 MPa in the 100% argon environment. Crack propagation from a fiber through the matrix is shown.

There are a variety of variables that can affect a material's creep-rupture life. Some of these factors include: applied stress, grain size, porosity, and impurities. All of which occur during processing. However, the primary factor affecting creep-rupture behavior of a traditional non-oxide CMC is the matrix. During a creep test, cracks form within the matrix and expand. These expanding cracks allow oxygen ingress into the composite which causes the matrix and exposed fiber to deteriorate due to oxidation [18]. An image of N720/A with crack propagation due to a creep test in 100% argon can be seen in Figure 7. In a composite with $\pm 45°$ fiber orientation, the ability of the matrix to withstand high creep strengths becomes even more important. Creep-rupture behavior of the CMC can be the limiting factor of its operational life. However, Nextel^{TM}720 is a fiber specifically designed to be creep resistant due to its high mullite concentration [23].

2.4   Previous Efforts

This section of the chapter will discuss previous research involving Ceramic Matrix Composites and particularly Nextel 720/Alumina CMC. There has been little work performed on oxide/oxide CMCs and no previous reported work regarding creep of an oxide/oxide CMC in an argon environment.

Harlan [13] studied the creep-rupture behavior of N720/A with a 0/90° fiber orientation in air and in steam environments. Harlan reported that the CMC exhibited relatively good creep resistance at 1200°C in air. Harlan also studied the creep-rupture behavior of the CMC at 1330°C. He found that there was a substantial decrease in creep life for a given creep stress. Harlan also observed that the presence of steam significantly

reduced the creep life at both test temperatures. The primary damage mechanisms seemed to be fiber fracture and fiber pullout [13:69-71]. Ruggles-Wrenn expanded on Harlan's work and showed that the creep curves produced from those test exhibited very short primary creep. The creep rapidly transitioned to secondary creep which remained linear until failure. Also, the creep strain accumulated in creep tests exceeded the failure strain obtained during tension tests [30:19-20].

Mehrman [22] investigated the response of the N720/A composite with the 0/90˚ fiber orientation in creep-fatigue interaction experiments. Mehrman showed that in air, prior fatigue improved the creep life of the CMC. Furthermore, Mehrman's results revealed that time the CMC spent at maximum stress governed damage accumulation and time to failure. Merman also showed that performance of the CMC in the steam environment was significantly worse than that in the laboratory air. Steam attacked the fibers causing a decrease in the time to failure. Qualitative EDS analysis showed evidence of water vapor attacking the silicon in the mullite phase of the fiber and causing migration of silicon species from fiber to matrix. The depletion of the mullite phase of the fiber led to reduced creep resistance of N720/A in a steam environment [22:83-84].

It is extremely rare that a material will only be subjected to on-axis loads in a real world application. Therefore the off-axis behavior of a material must also be studied. However, little has been reported on the response of oxide/oxide CMCs to off-axis loading conditions. Testing on N720/AS with the ±45˚ fiber orientation produced much lower ultimate tensile strength (UTS) compared to the UTS obtained for the 0/90° fiber orientation (Figure 8). Previous work also shows that the CMC with the ±45˚ fiber orientation produced dissimilar stress/strain curve when compared to that obtained for the

0/90° fiber orientation [8:457]. Figure 9 shows that regardless of fiber orientation, high

creep rates generally correspond to a short creep life. However, Zawada et al [8:457]

reported that the ±45° cross-ply exhibited higher secondary creep rates and shorter creep

life compared to those obtained for the 0/90° cross-ply.
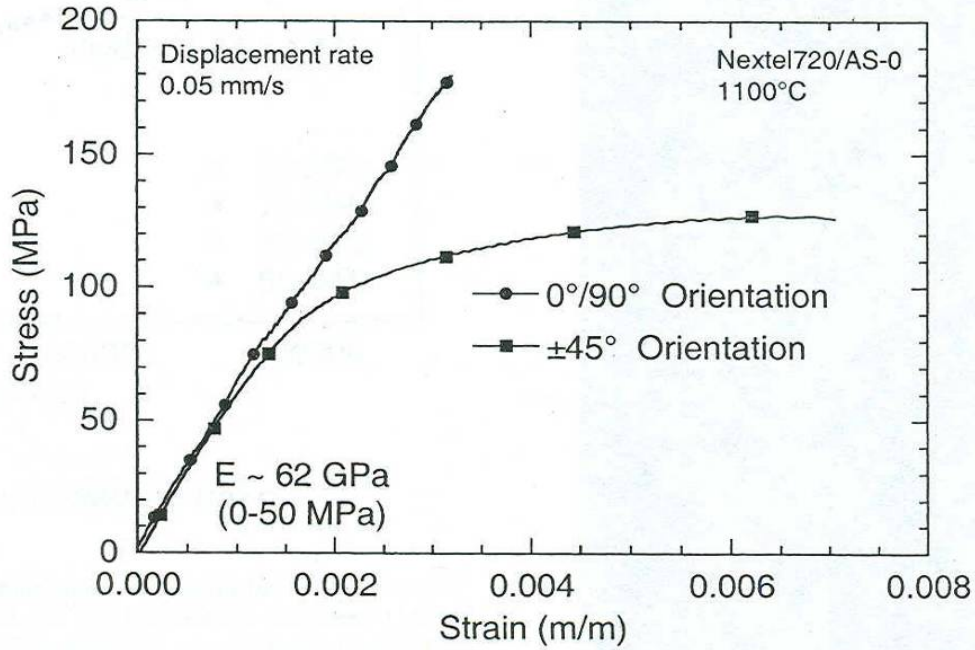
Figure 8. Stress vs. strain of N720/AS in 0/90˙ and ±45˙ orientation at 1100°C. N720/AS with the ±45˙ fiber orientation produced much lower ultimate tensile strength (UTS) compared to the UTS obtained for the 0/90° fiber orientation. [8:457].
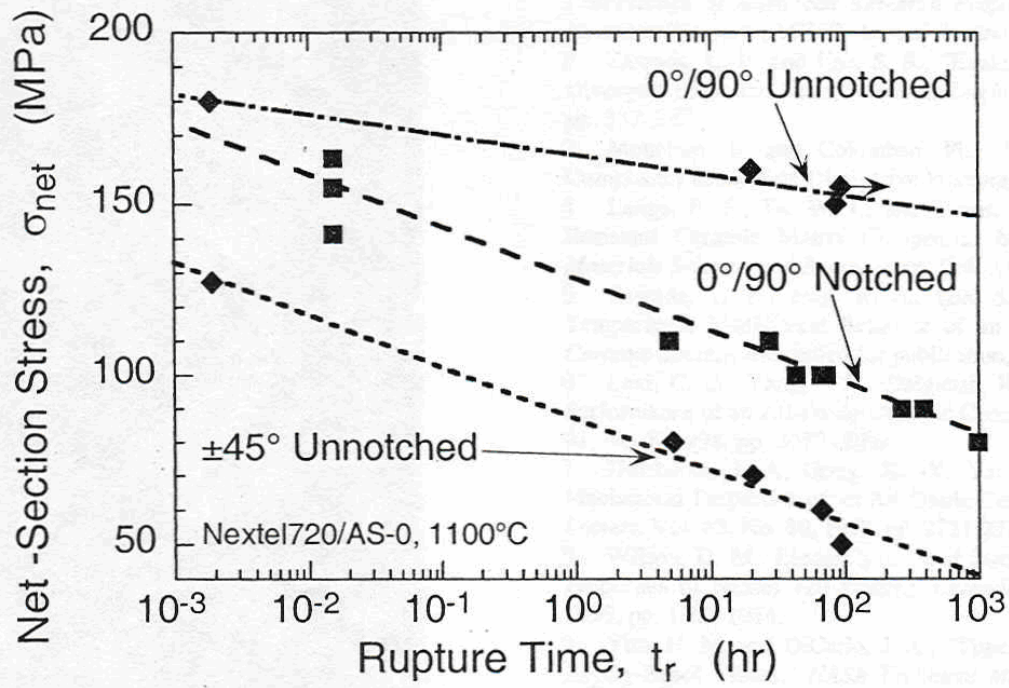
Figure 9. Creep rupture behavior of N720/AS in 0/90˚ and ±45˚ orientation at 1100°C. Shows that high creep rates generally correspond to a short creep life [8:457].

III. Material and Test Specimen

This chapter describes the material investigated, Nextel™ 720/A, and the test specimen geometry.

3.1 Material Description

The material studied in this thesis was the oxide/oxide ceramic matrix composite consisting of Nextel™ 720 (N720) fibers in a porous alumina matrix. N720/A was developed to operate at high temperatures and to retain a high strength while exhibiting improved creep performance. The N720 fibers were produced by the Minnesota Mining and Manufacturing Company or 3M™. The microstructure of the N720 fibers consisted primarily of small, long grains of α-Al_2O_3. Typically the grain sizes were smaller then 0.1 μm; however, there were some grain sizes as large as 0.5 μm from crystals of mullite and α-Al_2O_3. The N720 fibers are produced by using the sol-gel process, however the process details are proprietary to 3M™. The sol-gel process consisted of the following steps. First sol was formed, and then concentrated to form a viscous gel. Next, the precursor fiber was spun, and finally sintered to obtain the oxide fiber [11:70]. The mechanical properties of N720 fiber compared to those of other oxide fibers are presented in Table 2.

Table 2. Mechanical properties of N720 and other oxide fibers [23:41].

Property	Nextel™ 720	Nextel™ 610	Nextel™ 650
Composition (wt%)	$85Al_2O_3$ $15SiO_2$	$>99Al_2O_3$	$89Al_2O_3$ $10ZrO_2$ $1Y_2O_3$
Crystal Phases	$\alpha\text{-}Al_2O_3$ + mullite	$\alpha\text{-}Al_2O_3$	$\alpha\text{-}Al_2O_3$ + cubic ZrO_2
Filament Diameter (μm)	10-12	10-12	10-12
Tensile Strength (Gpa)	2.1	3.3	2.5
Modulus (GPa)	260	373	358
Density (g/cc)	3.4	3.9	4.1
Thermal Expansion (ppm/°C)	6.0	7.9	8.0

The N720/A CMC was manufactured by Composite Optics Inc. (COI) in the form of 12" X 12" panels. The composite panel was fabricated by the slurry infiltration process of the woven N720 fiber into an alumina based matrix [28]. The matrix was reinforced by 12 0/90° woven layers. The fiber orientation changed to ± 45° only when the specimens were cut from the panel using a high powered water jet. The properties of the panel from which the specimens were cut can be seen in Table 3. Also, an example of COI Ceramic's fabrication process can be seen in Figure 10.

Table 3. Physical properties of N720/A laminate panel [9].

Laminate Identification Number	Fired Laminate Thickness (mm)	Fabric Composition (% Volume)	Matrix Composition (% Volume)	Porosity (%)	Density (g/cm³)
4569-4	0.1055	46.8	30	23.2	2.79
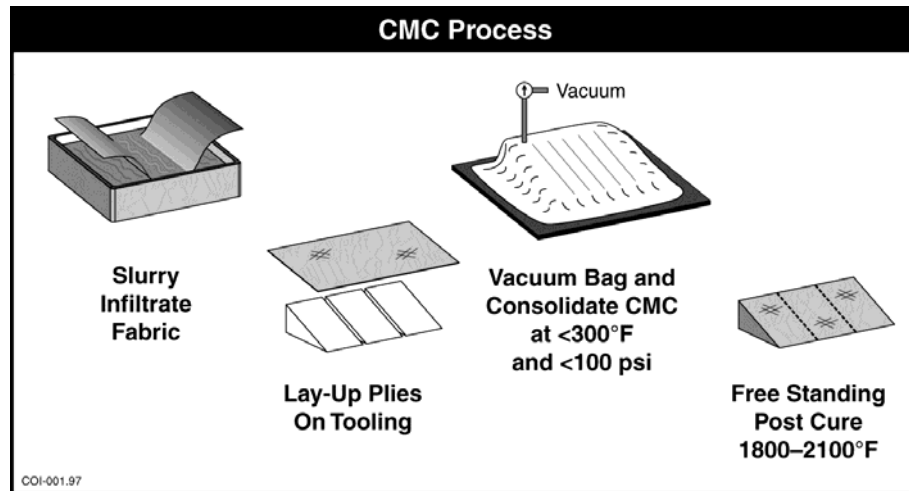
Figure 10. Fabrication process for N720/A CMC [9].

Figure 11 (a) and (b) show as-received N720/A material. Figure 11 (a) shows the $\pm 45°$ fiber orientation. Figure 11 (b) shows the side view of the specimen, where the plies are clearly visible.
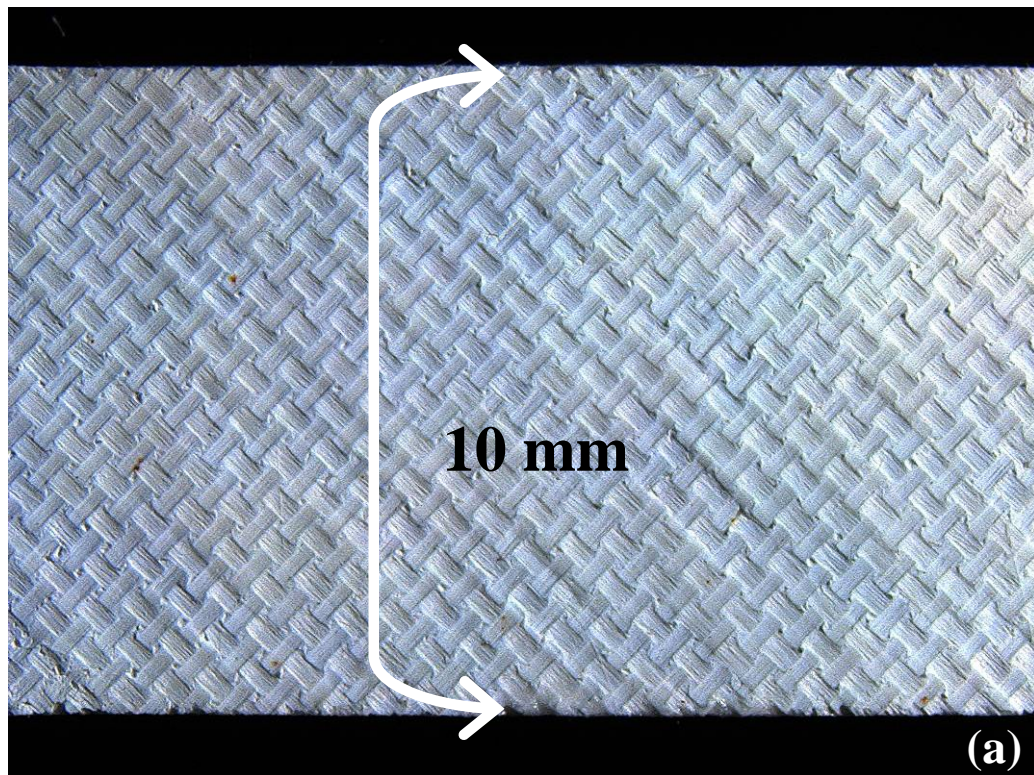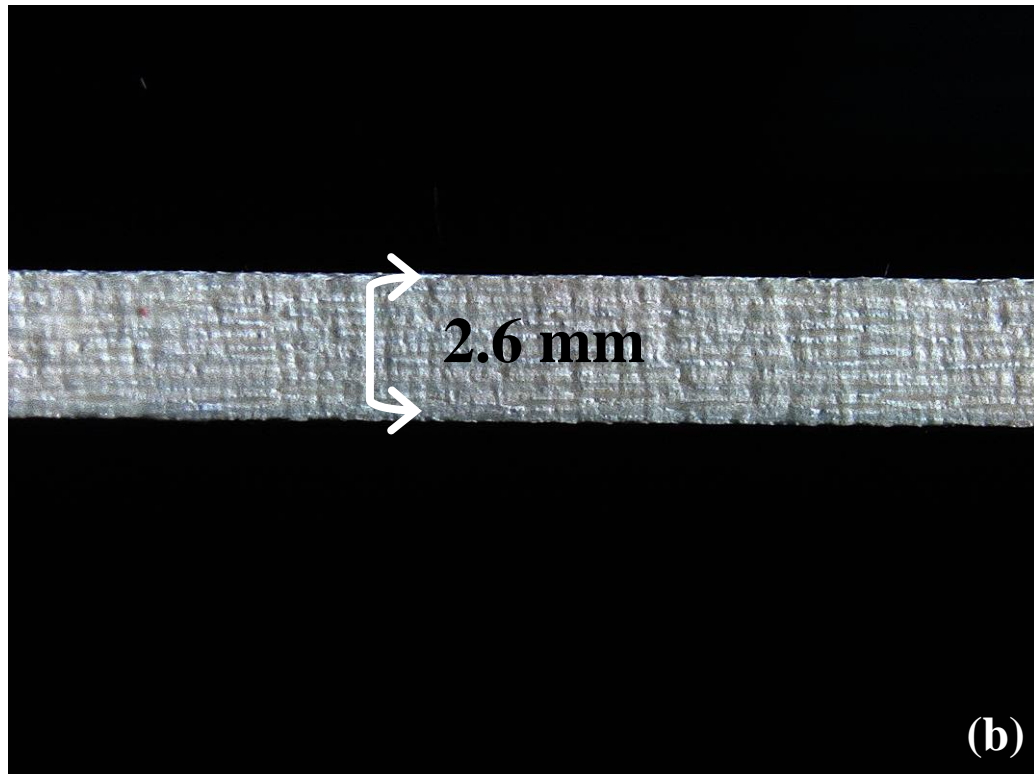
Figure 11. As-received N720/A material showing (a) ± 45˙ fiber orientation and (b) plies.

3.2 Specimen Geometry

Test Specimens were cut from a single composite panel using an abrasive water-jet machine by Kerf Waterjet. A dog-bone specimen design was used to insure that failure would occur within the gage section of the specimen. The total length of the specimens was 152 mm (6 in.), and the width of the gripping section was 16 mm. The reduced width of the gage section was 10 mm. The nominal specimen thickness was 2.62 mm. A specimen drawing is shown below in Figure 12, and an actual specimen used in testing is shown in Figure 13.
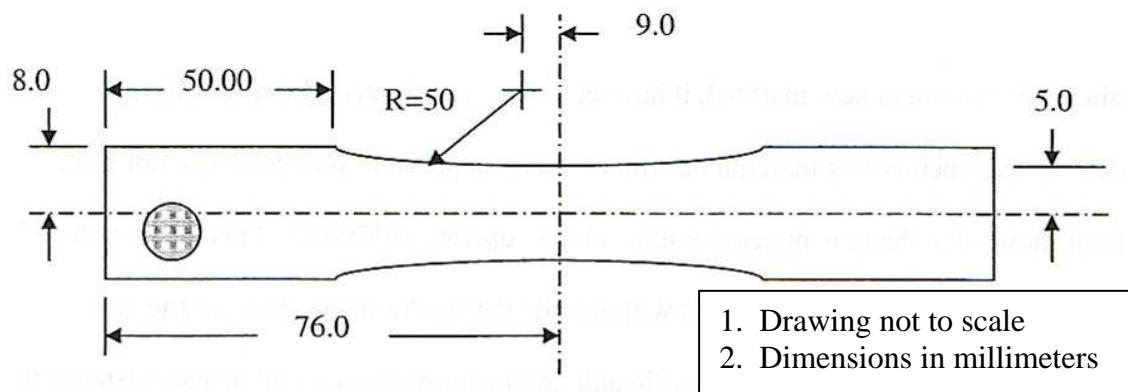
Figure 12. Dog-bone specimen used for testing [13:28].
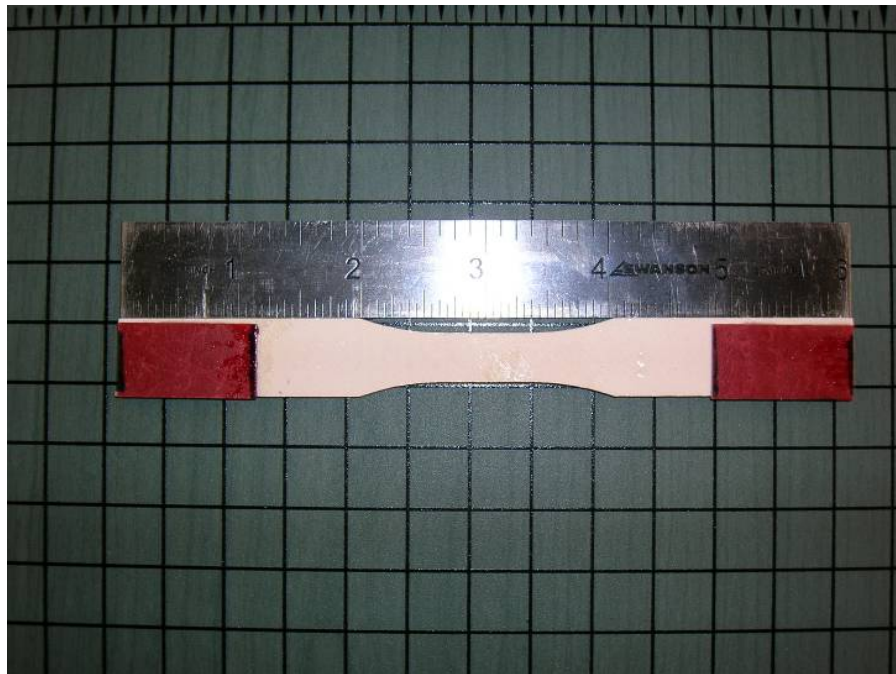
Figure 13. Dog-bone specimen used for testing.

IV. Experimental Setup and Testing Program

The following chapter describes the test setup and support equipment used in this research effort. Test procedures are presented as well.

4. 1   Mechanical Testing

The equipment used for testing included: the mechanical test apparatus, environmental control equipment, and the microstructure characterization equipment.

4.1.1   Mechanical Test Apparatus

The mechanical test equipment included the main servo hydraulic testing machines, the chilled water system, the extensometer, and the computer software. Three different Material Test System (MTS) Corporation servo-hydraulic machines were used during testing. Each one used the axial 810 Material Testing system and was set up for a specific environment. All initial tensile tests and creep rupture tests in the air environment were conducted using a 13kN (3 kip) capacity machine. All creep rupture tests conducted in the 100% steam environment were performed using a testing machine with a 25kN (5.5 kip) capacity. Finally, a 100kN (22 kip) capacity machine was used for all tests in a 100% Argon environment. A picture of the 22 kip test machine is shown in Figure 14. Each MTS machine used is similar to the 22 kip model shown. The applied load during each test was measured by a MTS Force Transducer (model 661.19E-04). The transducer was located just above the top wedge grip.
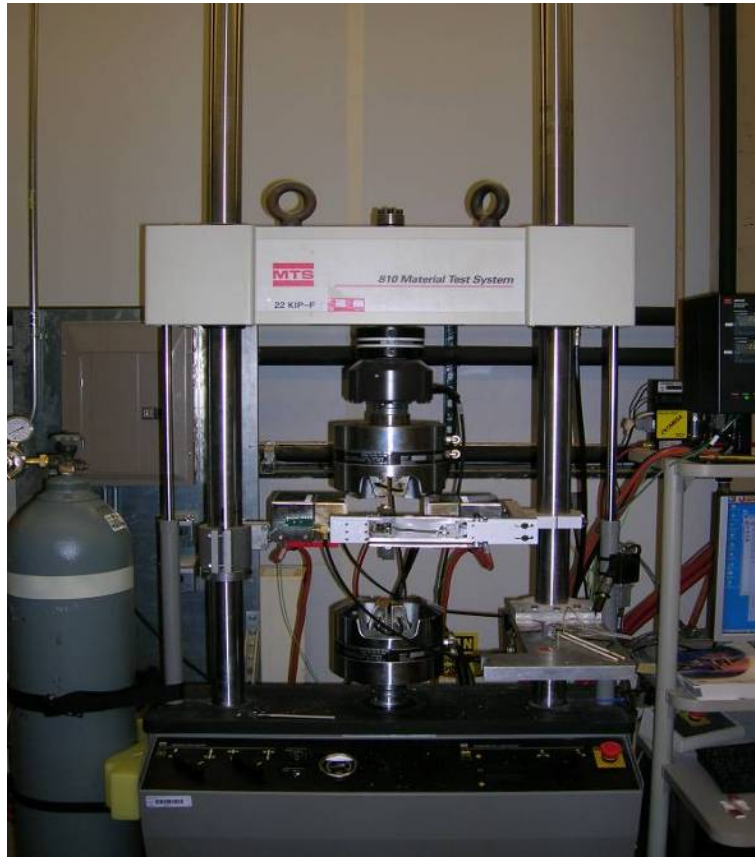
Figure 14. MTS 22 kip.

Each machine was equipped with a MTS 647 water-cooled Hydraulic Wedge

Grip System. Grips utilized interchangeable wedges with flat griping surfaces. In order to

prevent the slippage of a specimen, each wedge was coated with a layer of surf alloy. The

grips contained an inlet and outlet which allowed cooling water from the chiller to pass

through. The grip pressure was controlled by an MTS 685 Hydraulic Grip Controller. The

controller could apply pressure ranging from 0-20 MPa. The grip pressure was carefully

determined by the size of the grips and the maximum load required for each test.

Choosing the correct grip pressure was important in order to insure the specimen was not

crushed when gripped. The grip pressure used on the 3 kip and 5 kip machines was 8

MPa, while the grip pressure applied on the 22 kip machine was only 2.5 MPa. The values of grip pressure were different because the 22 kip machine employed much larger grips. The grip alignment on each machine was preformed prior to testing, and a visual inspection was carried out before each test.

Figure 15. Hydraulic pump and chiller system.

The chiller for cooling the grips was the NESLAB model HX-75 chilled water system. This machine chilled the water in order to provide a safe operating temperature for the grips while the specimen operated in a 1200°C atmosphere. Using a water pressure regulator, the system chilled the distilled water to 10°C and re-circulated it through the wedge grips using 6.35 mm (1/4 in) diameter plastic tubing.

The computer software system used to gather all data and control both the servo hydraulic machine and the temperature controller was the MTS Test Star™ II. It employed the fully automated Multi Purpose Testware (MPT) software to program each specific test and then acquire data during the test. Most often the data acquired during each test was the following: time, furnace temperature (both left and right), temperature command, displacement, force, force command, and strain. All of this data was then formatted into Microsoft excel where it could be further analyzed.
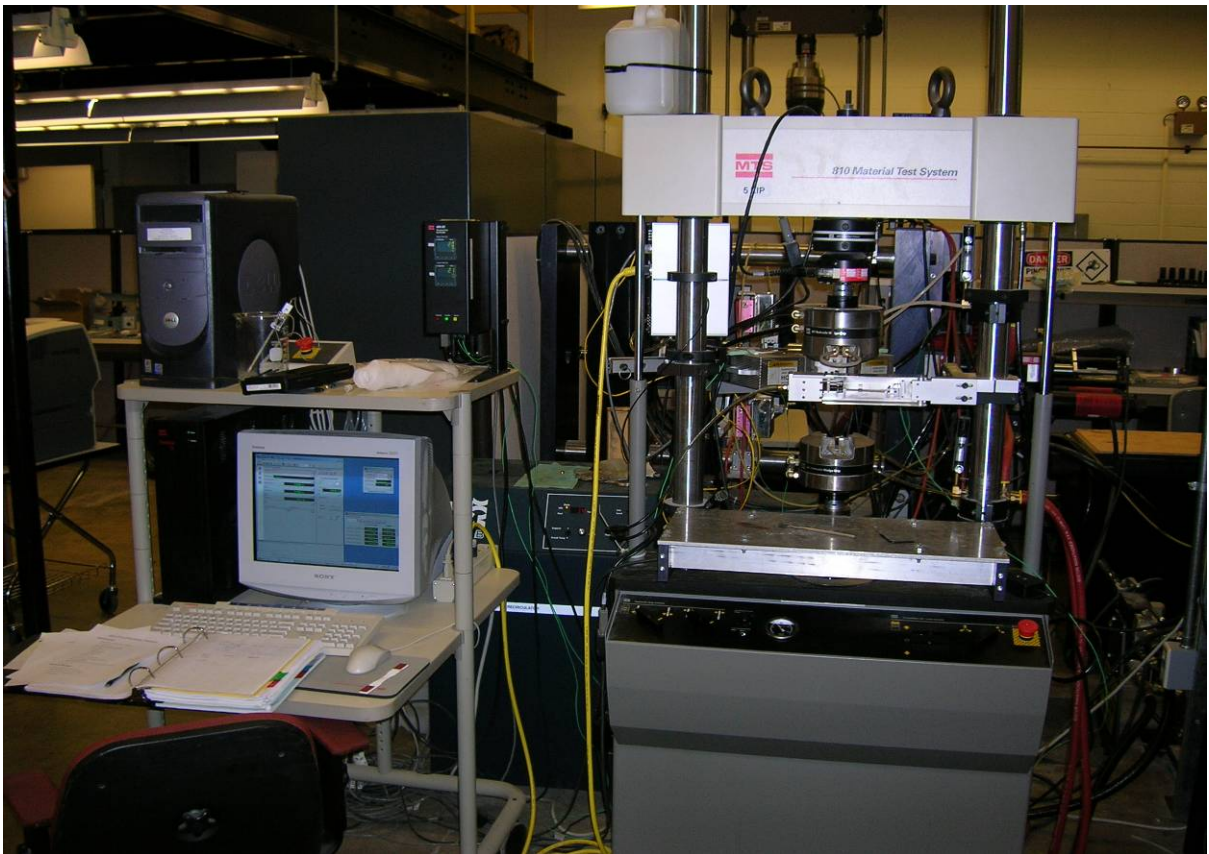
Figure 16. MTS Test Star™ II.

Figure 17. Extensometer on a fractured specimen.

The strain from each experiment was measured using a highly sensitive MTS high temperature uniaxial extensometer model number 632.53E-14. The extensometer included two 3.5 mm diameter alumina rods with a 12.77 mm gage length. The rods implemented a cone shaped tip for mounting onto flat specimens and maintained a contact force with the use of a spring. The extensometer was able to measure strains between ± 20% at temperatures up to 1200˚C. A heat shield and air cooling system were mounted around the extensometer in order to protect it and the delicate electronics from the extreme temperatures. Prior to testing, the extensometer was calibrated using a MTS

calibrator model 650.03. Properly mounting the extensometer on the specimens was the most difficult task when preparing a test.
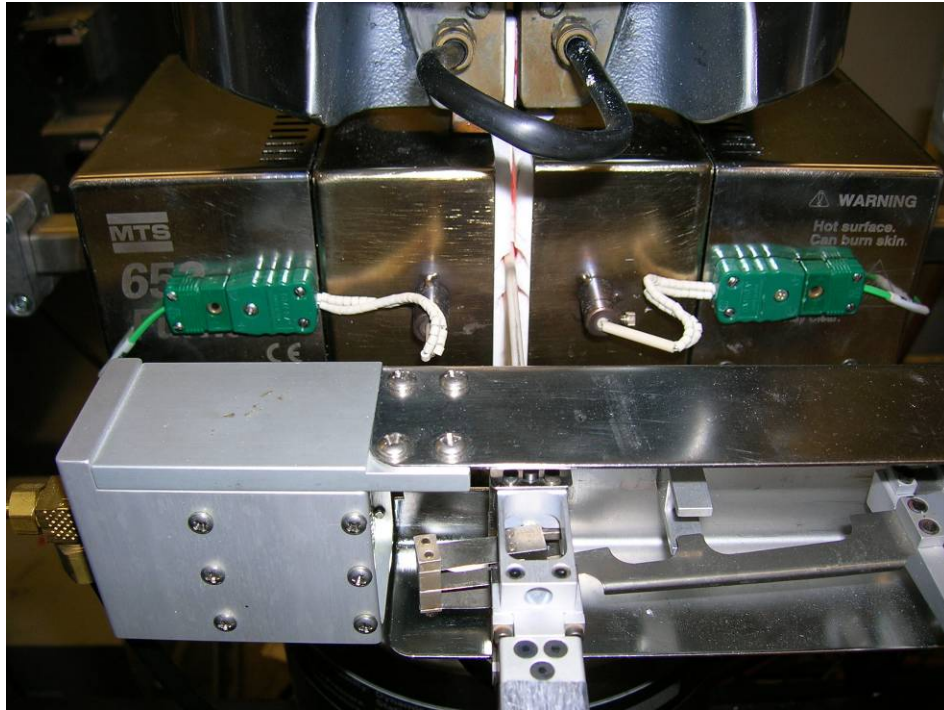
Figure 18. Extensometer platform.

4.1.2 Environmental Equipment

The environmental equipment consisted of a furnace, external temperature controller, steam generator, and an argon environment system.

The furnace systems used to achieve the high temperature of 1200°C were the Amteco Hot Rail Furnace System and the MTS 653 High Temperature Furnace. The 3 kip machine utilized a single zone MTS 653 High Temperature Furnace, the 5 kip machine used a two-zone Amteco Hot Rail Furnace System, and the 22 kip machine used a two-zone MTS 653 High Temperature Furnace. Each furnace was made up of two identical halves which slid on a rail to completely enclose the gauge area of the specimen. The extreme heat was created by silicon carbide heating elements placed within the

furnace chamber. The inner furnace chambers were made up of removable fibrous

alumina inserts. These could be cut and shaped to allow room for only the specimen,

susceptor, and extensometer rods. By enclosing the chamber as tightly as possible,

minimal heat loss was achieved during testing. The furnaces were controlled by a MTS

409 Temperature Controller unit. This system can be seen below. Two S-type

thermocouples, mounted on each furnace, penetrated into the heating chamber and then

provided temperature feedback to the controller system. The MTS 409 Temperature

Controller then provide the adequate power output to each unit until the temperature

sensed by the thermocouples within the chamber matched the programmed control

temperature.
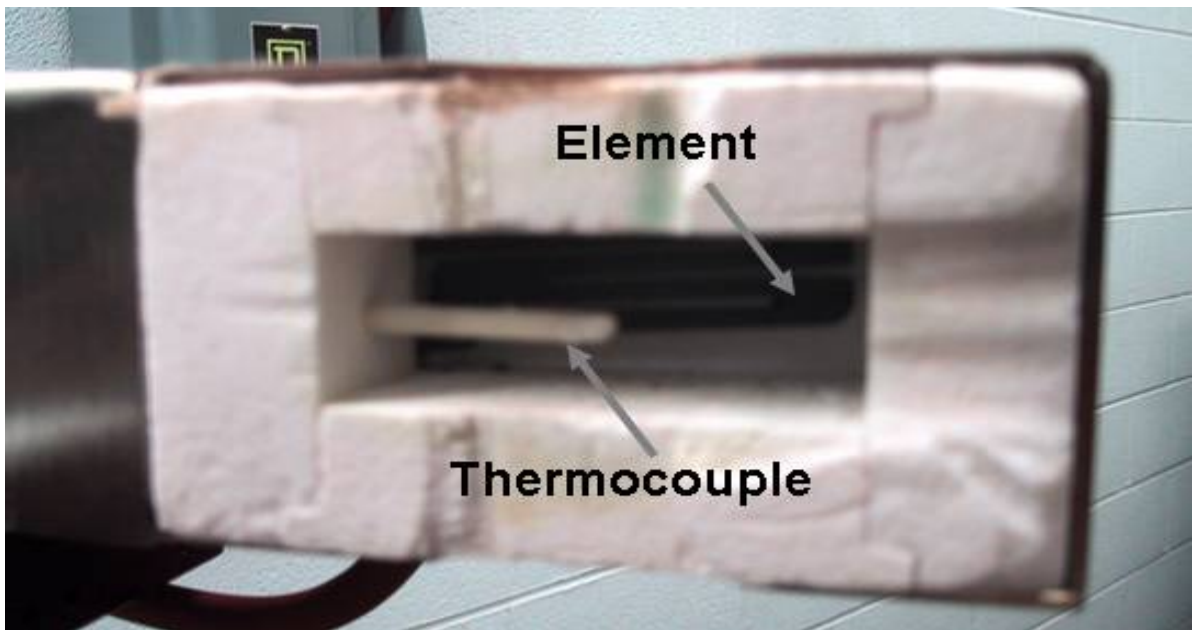
Figure 19. Interior view of oven half [15].
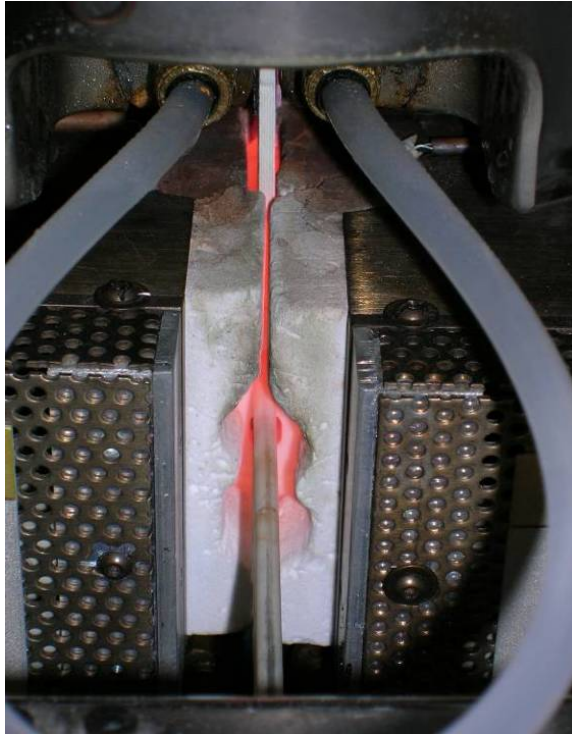
Figure 20. Closed view of furnace chamber.

Figure 21. Temperature controller.

Tests in both the steam and argon environments employed an alumina susceptor, which was assembled around the mounted specimen prior to testing. This can be seen in Figure 22.
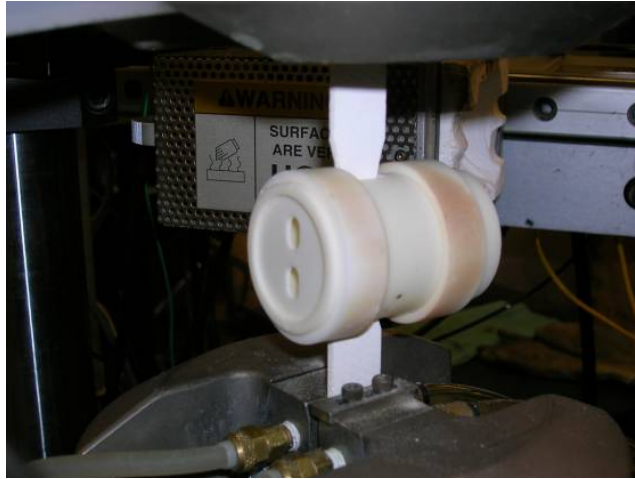
Figure 22. Alumina susceptor assembled around the test specimen.

The 100% steam environment was created using an AMTECO HRFS-STMGEN Steam Generation System. The steam was introduced into the alumina susceptor through a ceramic feeding tube attached to the Steam Generation System at a slight positive pressure expelling dry air from the susceptor and creating a 100% steam environment around the gage section of the test specimen. The pump flow rate for the steam generator was 30.31 mL/h.

Testing in argon environment was accomplished in a similar fashion. An Omega Mass Flow Controller was used to pump high purity argon into a susceptor enclosing a test specimen and creating a 100% argon environment within the susceptor. The measured pump flow rate for testing in the argon environment was 40.8 mL/min. The Omega Mass Flow Controller is shown in Figure 23.

Figure 23. Omega mass flow controller.

4.1.3   Imaging Devices

Specimen microstructure was analyzed using both optical microscope and a Scanning Electron Microscope (SEM). The optical microscope was a Zeiss Stemi SV II equipped with a Zeiss AxioCam HRc digital camera and the Axiovision version 4.4 software. Optical micrographs could be taken at different levels of magnification up to 100x. The optical microscope is shown in Figure 24.
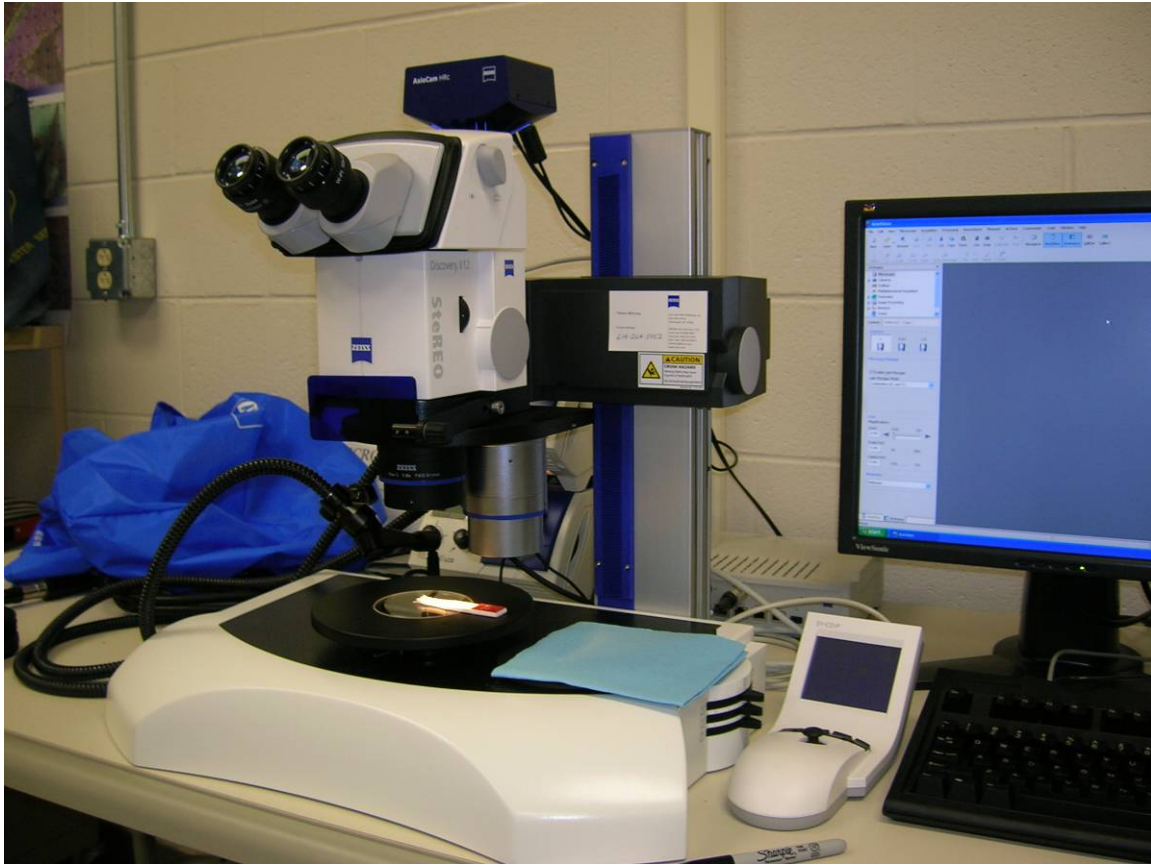
Figure 24. Zeiss Stemi SV II optical microscope.

A scanning electron microscope (SEM) was used to produce high resolution

images at magnifications up to 20,000x. The SEM is different from the optical

microscope in that it does not use reflected light to characterize the image. Instead, the

SEM works by emitting a steady beam of electrons and then, using special detectors,

captures the backscatter electrons emitted back from the specimen [4]. This collection of

backscatter electrons then produces an image. The SEM used was a FEI FP 2011/11

Quanta 200 HV Scanning Electron Microscope. It is shown in Figure 25. Most ceramic

materials are not good conductors and can build up a charge of electrons which would

distort the SEM image. Therefore the SEM specimens were mounted with carbon paint,

which grounded the specimen. Every specimen was viewed using the environmental

scanning electron microscopy (ESEM) mode. In the ESEM mode water vapor is present

within the vacuum chamber enabling the non-conductive samples to become conductive.

For observations at higher magnification, samples were coated with carbon paint using

the SPI Module Carbon Coater. In addition, the SEM included an EDAX Genesis 4000

Energy Dispersive X-Ray Spectroscopy (EDS) system. This system permitted a detailed

examination of fractured surfaces in order to determine what elements were present.

Figure 25. FEI FP 2011/11 Quanta 200 HV scanning electron microscope.

4.2 Test Procedure

The test setup and procedures for both monotonic tension test and creep tests are

described below. Also described are the operations required prior to testing and the

calibration methods employed to ensure accurate data is acquired. Before each test the

servo hydraulic machine was warmed up by cycling in displacement control for

approximately half an hour. For mounting, the specimen was gripped in the upper wedges first under displacement control. Then a level was placed on the specimen to ensure it was vertical. Finally, control was switched from displacement to force, and command was zeroed to ensure zero load on the specimen. Then the bottom of the specimen was gripped.

4.2.1 Specimen and Equipment Preparation

After machining, specimens were cleaned. First, five specimens at a time were placed in an ultrasonic bath for twenty minutes. Then, the specimens were soaked in 200 proof Ethel Alcohol for another twenty minutes. Finally, the specimens were placed in an oven and dried at 250˚C for one hour.

Fiberglass/epoxy tabs were bonded to the gripping portions of each specimen in order to prevent any damage from the high pressure applied by the grips. The cut tabs were bonded to the specimen using M-Bond 200 adhesive. A specimen with tabs is shown in Figure 26.
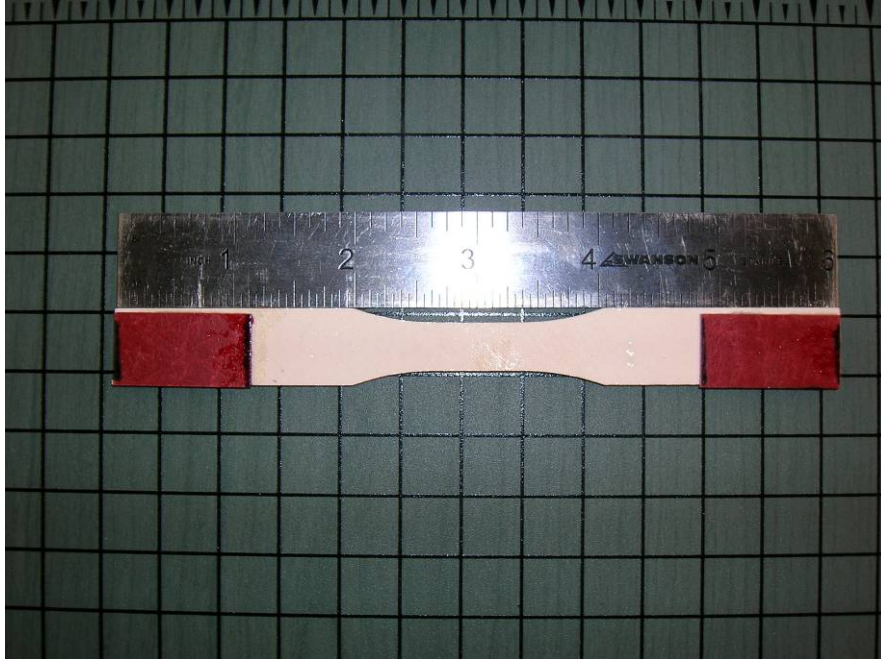
Figure 26. Specimen with tabs.

Prior to testing, each MTS machine was tuned for the ± 45˚ Nextel™ 720/A specimens using a standard procedure. The proportional, integral, differential, and forward gains obtained for the aforementioned specimen are presented in Table 3.

Table 3. Tuning parameters for testing in load control.

		Machine		
		3 kip	**5 kip**	**22 kip**
Gains	**P:**	4.3	6	2.2
	I:	3.5	3	0.1
	D:	0	0	0
	F:	0	0	0

To obtain the temperature controller setting that would yield a 1200˚C temperature on the test specimen, two thermocouples were bonded to the specimen, one on each side, using Zircar alumina cement. Figure 27 shows a test specimen instrumented with thermocouples, which was used for temperature calibration.
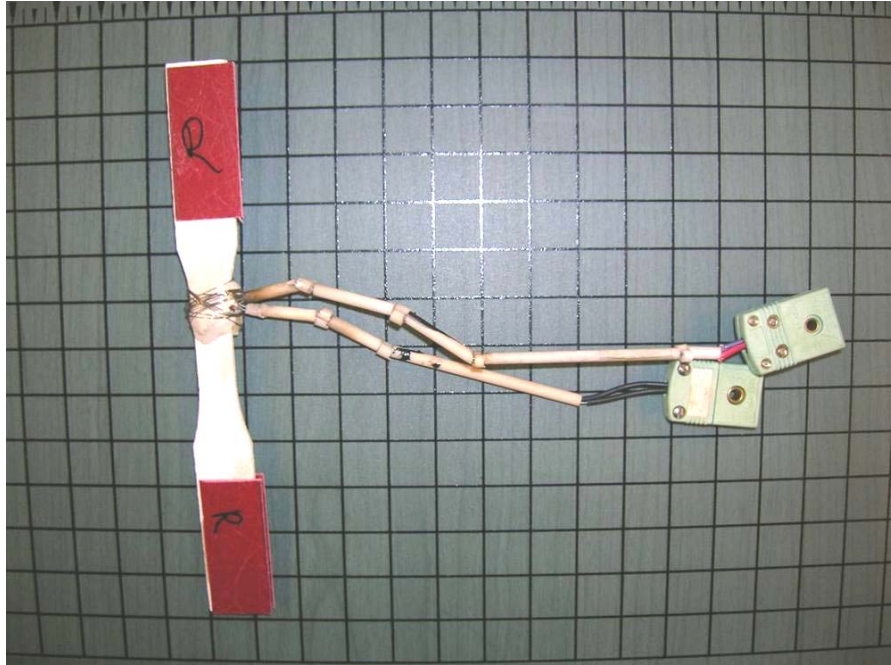
Figure 27. Temperature calibration specimen.

The temperature calibration specimen was mounted in the grips and placed under zero load, the two thermocouples were connected to an Omega Engineering, Inc. OMNI-CAL-8A-110 portable temperature sensor for read-out. For calibration in steam (argon) environment, the susceptor was placed around the gauge section of the calibration specimen and filled with steam (argon). Then the furnace temperature was raised at a rate of 1°C per second until the specimen temperature reached 1200°C. The furnace controller settings that produced a specimen temperature of 1200°C were recorded and used in subsequent tests. The temperature controller settings obtained for each furnace are given in Table 4 for testing in air, steam, and argon environments.

Table 4. Temperature calibration set points.

	Machine		
	3 kip	5 kip	22 kip
Environment	air	steam	argon
Test Temperature	1200	1200	1200
Left Oven Set Point	1220	1095	1315
Right Oven Set Point	NA	1105	1305

37

4.2.2 Monotonic Tension Tests

Monotonic tension tests to failure were carried out to determine the ultimate tensile strength (UTS), modulus of elasticity (E), and coefficient of thermal expansion (α) of an as-processed specimen. Tensile test were preformed in displacement control with a constant tensile displacement of 0.05 mm/s at 1200˚C in laboratory air. In all tests, the specimen was heated to 1200˚C at a rate of 1˚C/s and then allowed to dwell at 1200˚C for at least 15 min. During tension tests time, furnace temperature, force, displacement, displacement command, and strain were recorded. An example of a monotonic tensile test procedure is shown in Figure 28.
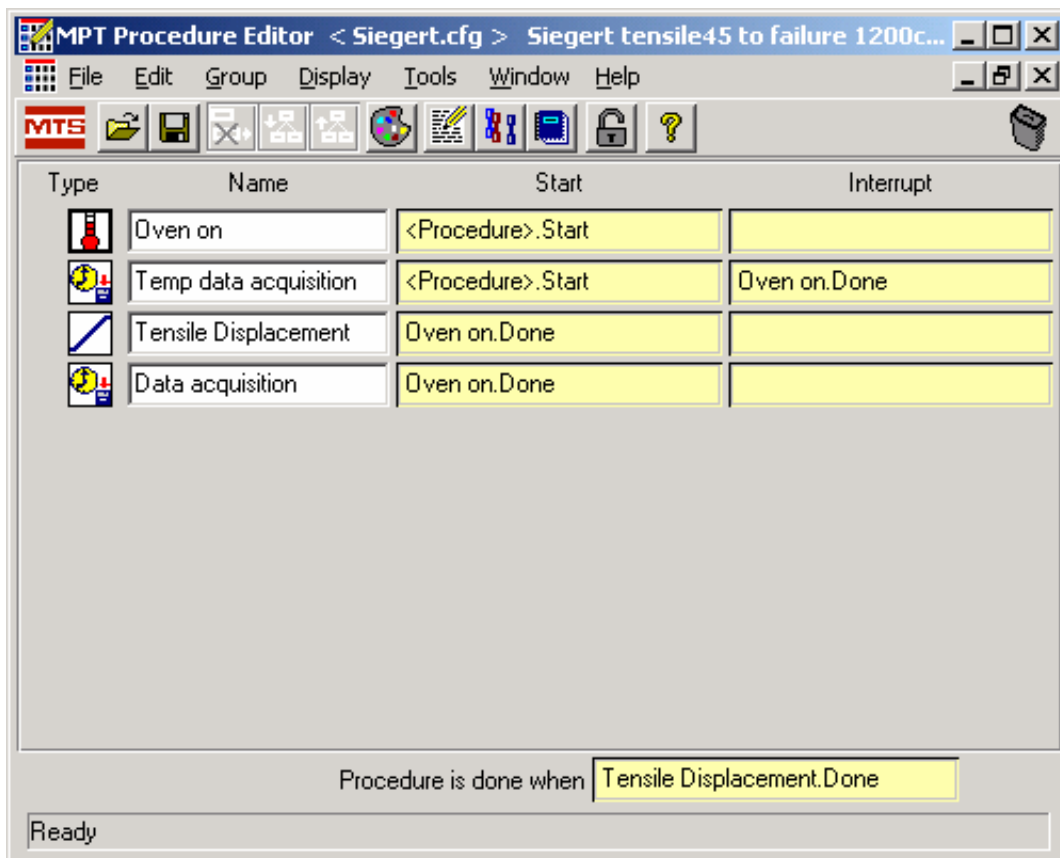
Figure 28. Monotonic tension test procedure.

4.2.3   Creep-Rupture Tests

All creep-rupture tests were conducted in load control at 1200°C. Creep stress levels were 45, 40, 35, and 15 MPa. All specimens were loaded to the desired creep stress at a stress rate of 15 MPa/s. The data acquired during a creep test included time, furnace temperature, displacement, force, force command, and strain. During load ramp up, data points were recorded every 0.5s. Once the creep stress was reached, data was collected every second for the first hour, then once every ten seconds for the next ten hours and finally once every thirty seconds for the remainder or the tests. This data was used to analyze the stress-strain behavior during ramp-up to the creep stress level and the evolution of strain with time during the creep period [7]. Under load, creep proceeds in three regimes: primary, secondary, and tertiary creep. During the primary creep regime, the strain rate decreases over time. During the secondary creep regime, the specimen deformation keeps proceeding at a steady strain rate. For specimens tested at 35 MPa and below, secondary creep was the dominant deformation mode. The last stage of deformation is tertiary creep. Here strain rates increase very rapidly until the test specimen ruptures. Tertiary creep was found in specimens tested at 45 MPa regardless of environment. The modulus of elasticity was obtained from the stress-strain curve produced during the initial loading to the creep stress. Data collected during the creep period were used to determine the creep rates, accumulated creep strain, and the time to rupture [29]. All tests were continued to failure or until run-out. The run-out condition was defined as survival of 100 h at creep stress, which represents a typical amount of time an aerospace component would be expected to survive under sustained load at 1200°C. A typical procedure for a creep-rupture test can be seen in Figure 29.
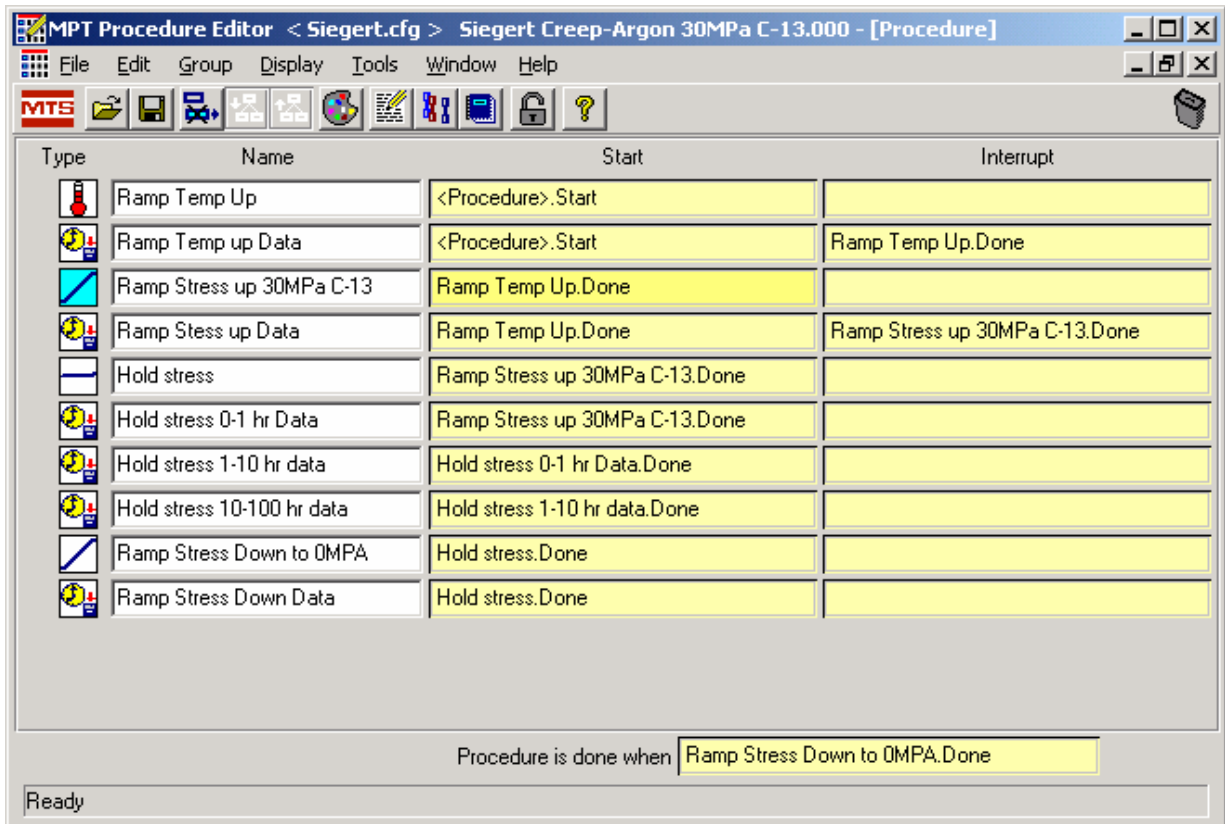
Figure 29. Creep-rupture test procedure.

V.   Results and Discussion

This chapter presents the detailed findings of this research. It will begin with

Table 5 summarizing the tests conducted in this investigation. Then the results of the

tensile and creep tests will be reported. Next, an analysis of the optical micrographs is

discussed. Following, results of the SEM observations will be presented. Finally, a deeper

look into the microstructure will be taken using the EDS. Results obtained in tests

conducted in the air environment are discussed first, followed by test results obtained in

steam and argon environments. All tests were conducted using specimens from a single

panel, number 4569-4. All test specimens had a ±45° fiber orientation. Table 5 shows that

there were a large number of tests conducted, but only a few tests conducted per

condition. The focus of this research was to identify the major trends from mechanical

tests which would require further investigation.

Table 5. Summary of tests conducted at 1200°C.

Specimen #	Test	Environment	σ_{max} (MPa)	Time to Failure (h)	ε_{max} (%)
T-1	Tensile	Air	54.9	0.0009	0.27
C-1	Creep	Air	45	0.033	1.48
C-2	Creep	Air	15	100	3.38
C-3	Creep	Air	35	100	13.30
C-4	Creep	Air	40	23.716	12.07
C-8	Creep	Steam	45	0.016	0.71
C-9	Creep	Steam	15	100	4.80
C-10	Creep	Steam	35	100	16.52
C-11	Creep	Steam	40	0.733	5.07

C-12	Creep	Argon	45	0.006	4.07
C-13	Creep	Argon	30	50	4.46
C-14	Creep	Argon	40	0.009	2.59
C-15	Creep	Argon	15	100	5.67
C-16	Creep	Argon	35	100	20.90
C-17	Creep	Argon	45	0.006	0.72
C-18	Creep	Argon	40	0.018	3.78
Load (MPa)	**% of UTS**				
45	82				
40	73				
35	64				
30	55				
15	27				

5.1 Monotonic Tension

Two tensile tests to failure were performed to determine the ultimate tensile strength (UTS) and the modulus of elasticity (E) of the N720/A specimens with a ±45° fiber orientation at 1200 and 1100°C. Each test was preformed in displacement control at the rate of 0.05 mm/s. At 1200°C, the UTS was 54.9 MPa, and E was 46 GPa. The second tensile test, conducted at 1100˚C, produced the UTS of 52.45 MPa and modulus, E, of 44 GPa. Based on the UTS of ~55 MPa at 1200°C, the information gathered from these two tests led to determining the creep stress levels of 45, 40, 35, and 15 MPa, selected for investigation.

Thermal strain values were recorded during the temperature ramp-up for each test. Then, the thermal strain values were used to calculate the coefficient of thermal expansion (CTE), α, calculated using the following equation: $\varepsilon_{th} = \alpha * \Delta T$ where

ε is the thermal strain and ΔT is the change in temperature. The CTE was determined to be 6×10^{-4} (1/°C). The coefficients of thermal expansion, as seen in Figure 30, were consistent throughout testing.
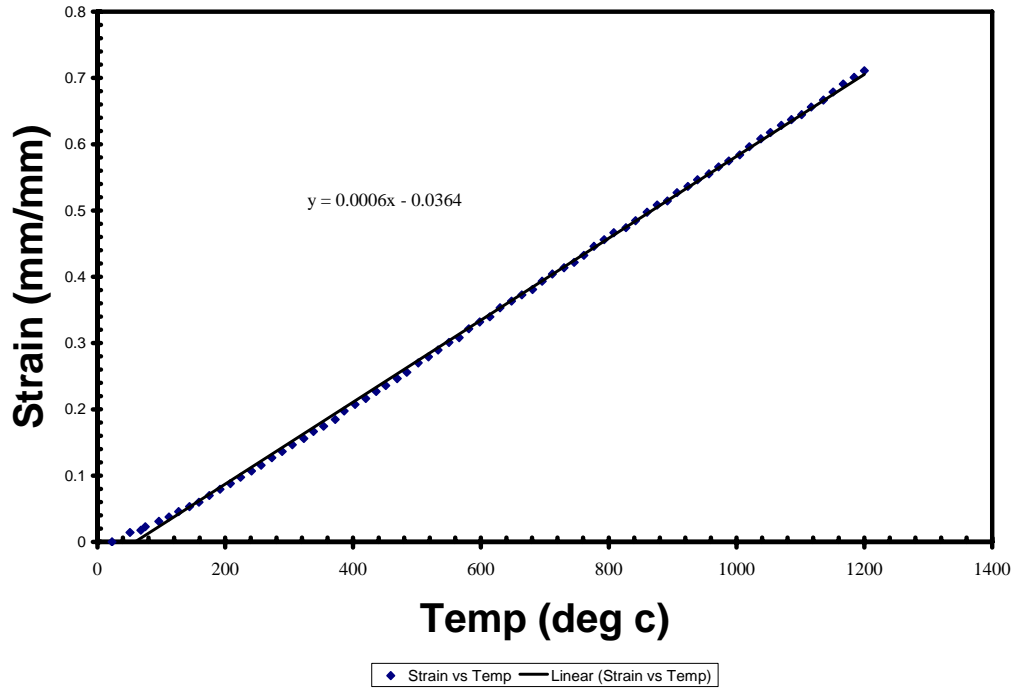
**Figure 30. T-1 strain vs. temperature for the N720/A composite with ±45°
fiber orientation.**

A tensile stress-strain curve obtained at 1200°C is shown in Figure 31, where the stress-strain curve for N720/A with 0/90° fiber orientation from Harlan [13] is also shown. The stress-strain curve for the 0/90° fiber orientation is nearly linear. However, the stress-strain curve for the ±45° cross-ply exhibits a short linear region and then departs from linearity. The tensile curve for the ±45° cross-ply is a shear stress-strain curve of the 0/90° cross-ply. Note that the stress-strain curves for both 0/90° and ±45° fiber orientations are qualitatively similar to the corresponding stress-strain curves reported by Zawada [8] for the N720/AS CMC (see Figure 32).
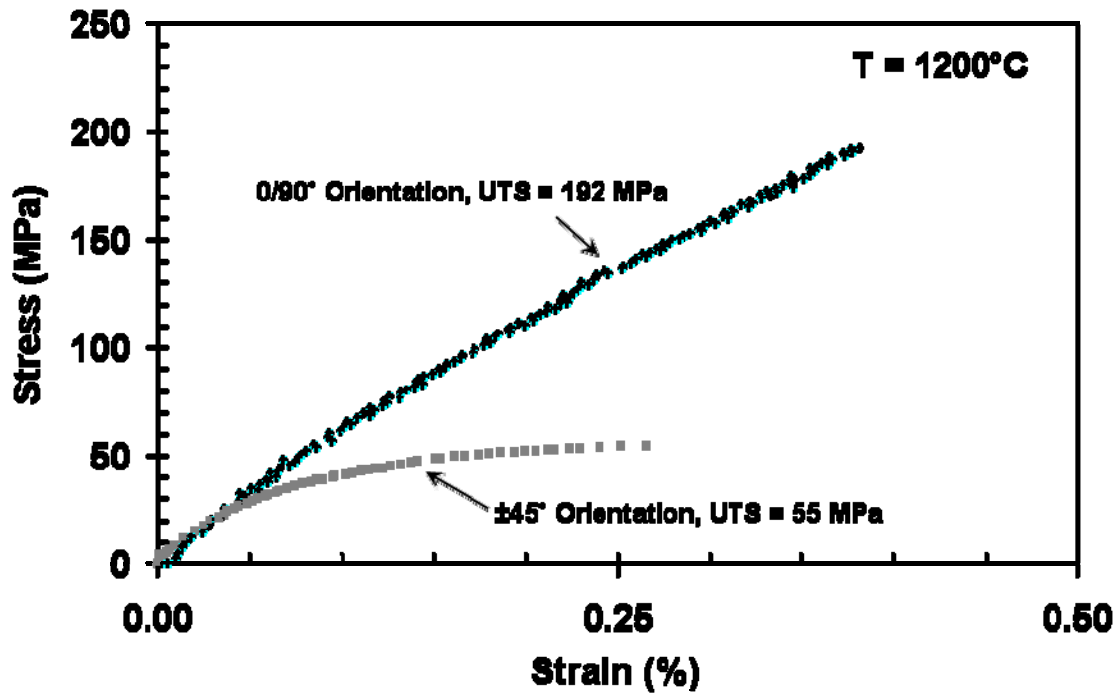
Figure 31. N720/A stress-strain curves for N720/A ceramic composite at 1200˚C
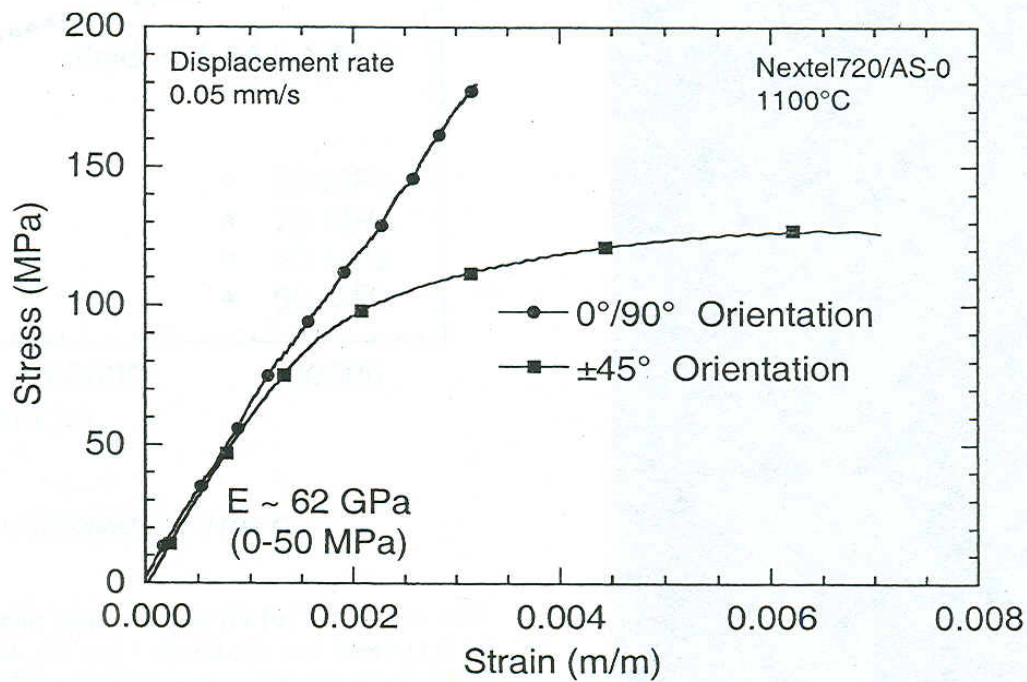
Figure 32. Tensile stress-strain curves for N720/AS at 1200˚C [8].

5.2   Creep-Rupture Test

Creep tests were conducted at the following stress levels: 45, 40, 35, and 15 MPa. Creep tests were conducted at 1200°C in laboratory air, 100% steam, and 100% argon environments. The modulus of elasticity, E, was calculated to ensure each specimen exhibited the same retained strength. The average E from all tests was ~46 GPa. The average E for each load and environment can be seen in Table 6.

Table 6. Average modulus of elasticity of N720/A at 1200°C.

	Load (MPa)				Environment		
	45	**40**	**35**	**15**	**Air**	**Steam**	**Argon**
Average E (GPa)	45.05	45.43	45.6	46.57	46.48	43.65	46.41

The results of creep tests conducted at 1200°C in laboratory air are summarized in Table 7.

Table 7. Creep-rupture results in air at 1200˙C.

Specimen #	Creep Stress (MPa)	Time to Failure (h)	Accumulated Creep Strain (%)
C-1	45	0.033	0.65
C-2	15	100	3.38
C-3	35	100	13.30
C-4	40	23.716	11.08

The table above shows that time to failure for a creep stress of 15 MPa, the lowest stress, was much longer than that for the creep stress of 45 MPa, the largest stress. The 15 and 35 MPa creep tests achieved run-out and were subsequently subjected to a tensile test to failure in order to determine the retained strength and stiffness. Note that the 40 MPa creep test failed after 24 h, while the time to rupture in the 45 MPa test was only 0.03 h. The largest amount of creep strain (13.3%) was accumulated in the 35 MPa test. The tests

results were checked for any extensometer slippage and none was found. Creep curves

obtained vs. time in seconds at 1200°C in air are shown in Figure 33. In all the tests in

Figure 33, primary creep is seen and then rapidly transitions into secondary creep. In the

case of the 45 MPa test, secondary creep rapidly transitions into tertiary creep, for the

creep strain levels ≤ 40 MPa, secondary creep persists until failure or to run-out. Results

in Table 7 indicate that in air the creep run-out stress is between 35 and 40 MPa.
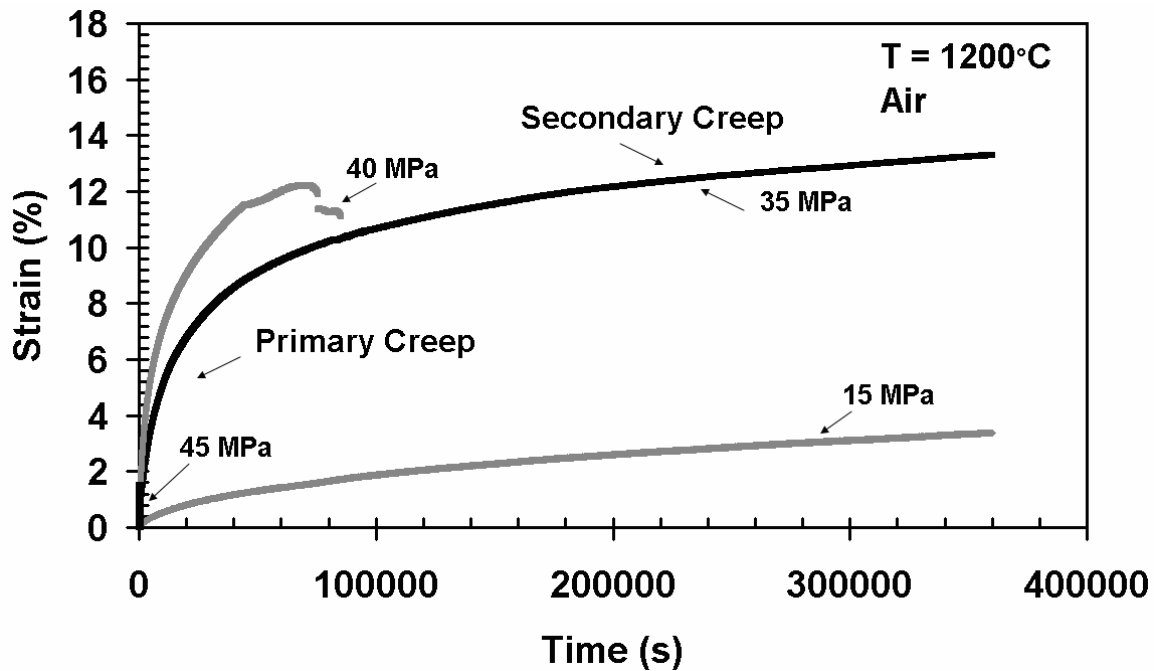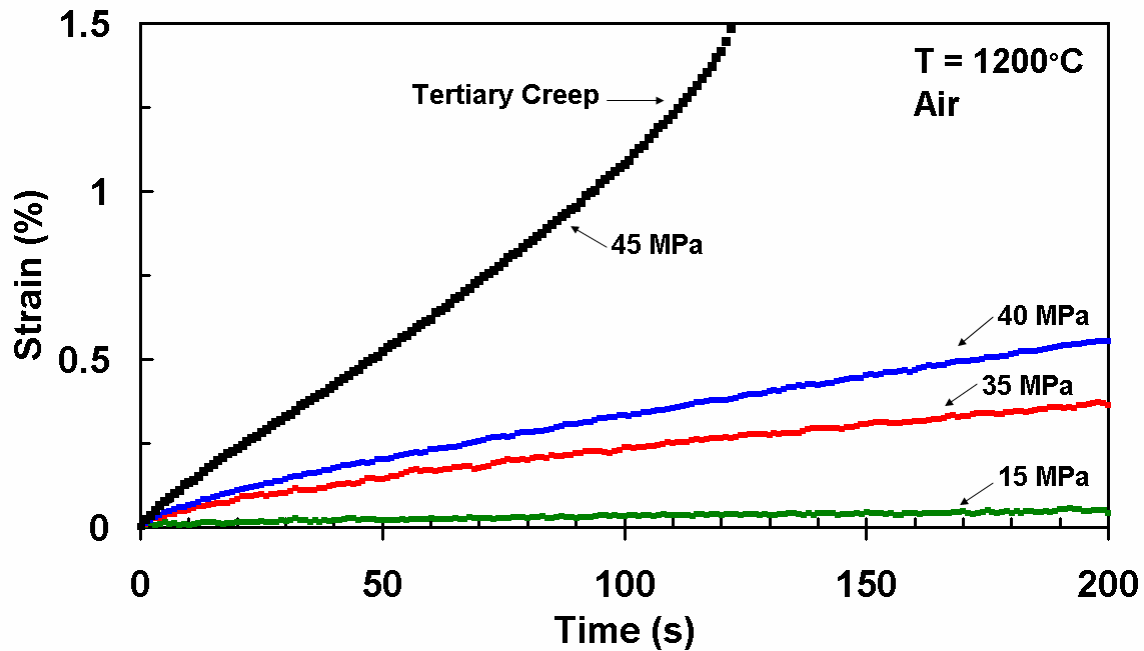
Figure 33. Creep-strain vs. time in air at 1200˚C.

Results of the creep-rupture tests conducted at 1200°C in 100% steam are summarized in Table 8.

Table 8. Creep-rupture results in 100% steam at 1200˚C.

Specimen #	Creep Stress (MPa)	Time to Failure (h)	Accumulated Creep Strain (%)
C-8	45	0.016	0.65
C-9	15	100	4.80
C-10	35	100	16.52
C-11	40	0.733	5.05

The creep curves obtained at 1200°C in steam are presented in Figure 34.
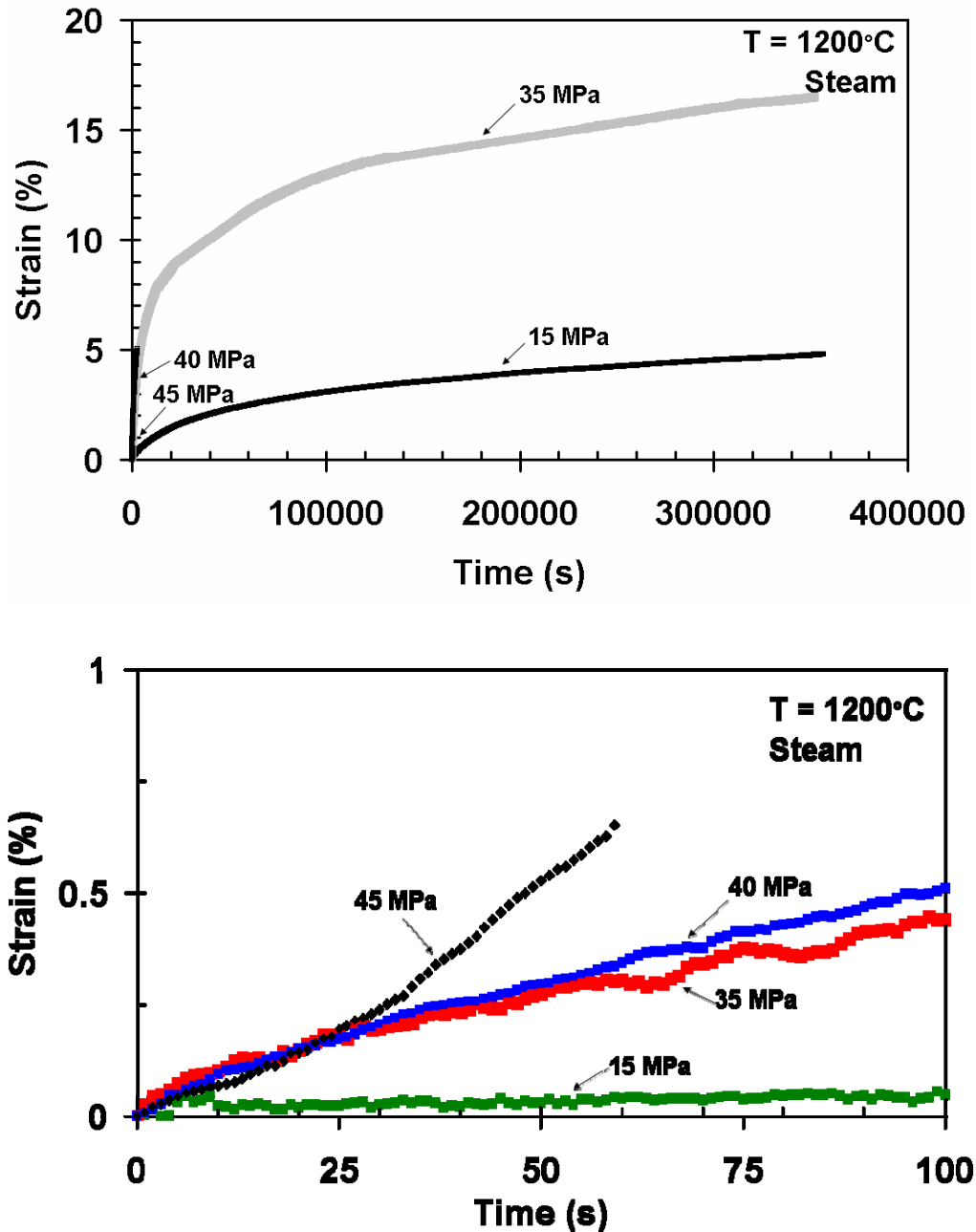
Figure 34. Creep-strain vs. time in 100% steam at 1200˚C.

It is seen that the creep curves produced in steam (Figure 34) are qualitatively similar to those obtained in air. All creep curves exhibit short primary creep and secondary creep that are continuous to failure or run-out. As in the air environment, the 45 MPa creep test in steam represents an exception. At 45 MPa, both primary and

secondary creep regimes are short and tertiary creep develops early. However, it should be noted that while rupture times obtained at 15, 35, and 45 MPa were similar for both environments. At 40 MPa, creep accelerated and the creep life in steam was significantly shorter than that in air.

Harlan reported that for the 0/90˚ fiber orientation, the presence of steam severely decreased creep life [13:52]. In the case of the ±45˚ fiber orientation, the presence of steam did not affect creep performance at stress levels below 40 MPa. The creep run-out stress remains the same in both air and steam environments.

Prior to this research effort, no tests on N720/A in a 100% argon environment have been reported. The creep stress levels of 45, 40, 35, 30, and 15 MPa were used in tests conducted in argon. The tests at 45 and 40 MPa were repeated in order to confirm results. The 30 MPa test was interrupted after 50 h due to a malfunction of the testing machine. The results of the tests conducted in a 100% argon environment are summarized in Table 9. The creep curves obtained in argon are presented in Figure 35.

Table 9. Creep-rupture results of 100% argon at 1200˚C.

Specimen #	Creep Stress (MPa)	Time to Failure (h)	Accumulated Creep Strain (%)
C-12	45	0.006	3.72
C-13	30	NA	4.46
C-14	40	0.009	2.36
C-15	15	100	5.67
C-16	35	100	20.9
C-17	45	0.003	0.72
C-18	40	0.000	3.58
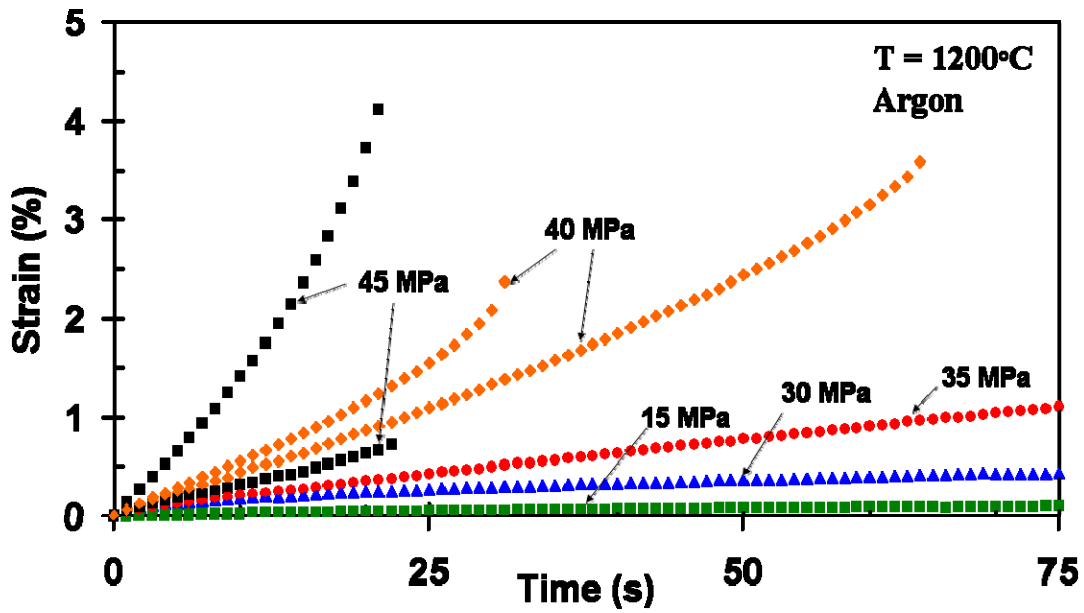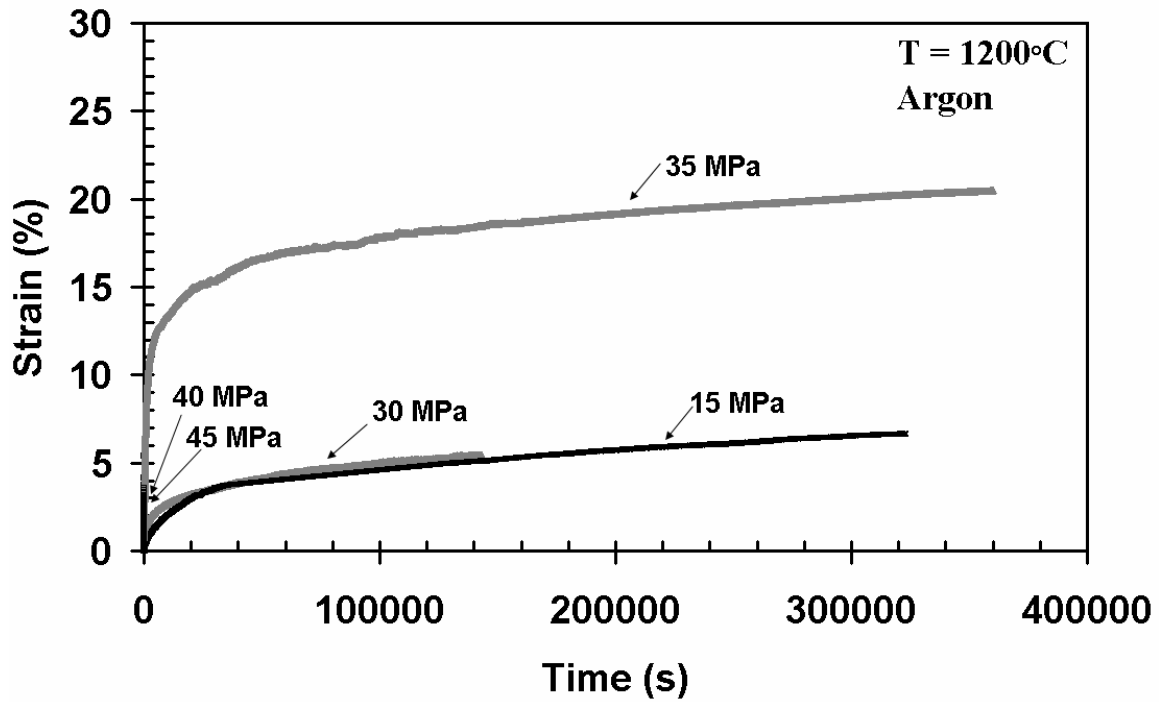
Figure 35. Creep-strain vs. time in 100% argon at 1200˚C.

The results obtained in the tests in 100% argon were not as expected. The

N720/A is an oxide/oxide CMC designed to maintain its strength properties when

exposed to high temperatures and an oxidizing environment. The presence of an

oxidizing environment, such as air or steam, generally decreases the performance and strength of any CMC, including oxide/oxide CMCs [34:141]. Therefore, it was not surprising when some degradation in performance was observed in tests conducted in a steam environment. When the N720/A specimens are exposed to 100% argon environment, no further oxidation can occur because there is no oxygen present. Furthermore, because argon is an inert gas, the chemical balance within the material should be maintained and no chemical reactions should occur. This type of environment would allow the specimen to maintain its properties and possibly extend its creep life. Specimens tested at stress levels ≤ 35 MPa achieved a run-out of 100 h at 1200°C. However, creep strains accumulated in argon were higher than those accumulated in air and steam environments at the same stress level. At the higher stress levels of 40 and 45 MPa, the specimens failed within a minute of creep. In all four tests conducted at 40 and 45 MPa, early onset of tertiary creep was observed, leading to an early failure. Conversely, at lower creep stress levels, both primary and secondary creep regions are present, but no tertiary creep was observed. This is consistent with the results obtained in air and steam.

Because the results achieved in the 100% argon environment were somewhat surprising, every aspect of the test procedure was checked for accuracy. Also, tests at 40 and 45 MPa were repeated for confirmation. Furthermore, COI, the manufacture of the CMC, was contacted for further information [9]. This was done in order to gain insight into possible reasons why N720/A did not perform better in a 100% argon environment where no oxidation was occurring. Researchers at COI were also surprised with the results and could not offer any additional information.

Retained strength and modulus of the specimens that reached run-out in creep tests are summarized in Table 10. Each specimen retained over 89% of its tensile strength (55 MPa), with most retaining over 100% of their tensile strength. The modulus retention was also over 100% with the only loss of 1.5%. Prior creep had minimal effect on the failure strain [31]. The air and steam environments produced similar results while specimens tested in argon achieved lower strains at failure. Strength retention is related to the accumulated creep stress. The tests at 35 MPa in steam and argon achieved the highest creep strain of 16.52 and 20.9% respectively. These specimens were also the only ones not to achieve 100% strength retention. Table 10 shows that prior creep had no qualitative effect on tensile stress-strain behavior.

Table 10. Retained properties of N720/A specimens subjected to prior creep at 1200°C.

Specimen #	Environment	Creep Stress (MPa)	Retained Strength (MPa)	Strength Retention (%)	Retained Modulus (GPa)	Modulus Retention (%)	Strain at Failure (%)
C-2	Air	15	61.07	111.04	53	113.81	0.161
C-3	Air	35	61	110.91	45	98.68	0.161
C-9	Steam	15	67	121.82	45	103.49	0.147
C-10	Steam	35	53.4	97.09	52	114.04	0.160
C-15	Argon	15	73.04	132.80	47.6	102.21	0.100
C-16	Argon	35	49.39	89.80	47.7	104.61	0.024

The objective of this research effort was to evaluate the creep behavior of the N720/A composite with a ±45° fiber orientation in air, steam, and argon environments, and to assess the effect of environment on creep response. Results revealed that in all test environments creep life decreased with increasing creep stress. Figure 36 shows applied stress as a function of rupture time. It is seen that for stress levels ≤ 35 MPa, run-out was

achieved in all test environments. However, at creep stress levels above 35 MPa, specimens tested in air exhibited the longest creep lives followed by those tested in steam. Specimens tested in argon at creep stress levels above 35 MPa exhibited the shortest creep lives. Steady-state (minimum) creep strain rate was reached in all tests. Creep rates were determined by evaluating the strain just before failure. A trend line was drawn along the data points collected prior to failure, and the slope of that trend line indicated the specimens creep rate at failure. The creep rates are plotted vs. creep stress in Figure 37. Once again results revealed that while similar creep strain rates were obtained in all test environments at creep stress levels ≤ 35 MPa, at creep stress levels above 35 MPa the highest creep rates were produced in argon. At 40 MPa the creep strain rate in steam was at least one order of magnitude higher then that in air, while the creep strain rate produced in argon was nearly three orders of magnitude higher than that in air. At 45 MPa similar creep rates were produced in air and in steam, and higher creep rates were observed in argon. However, the difference in creep rates produced in different test environments at 45 MPa was not as dramatic as that noted at 40 MPa. This discrepancy is likely due to data scatter or strength variation between individual specimens.
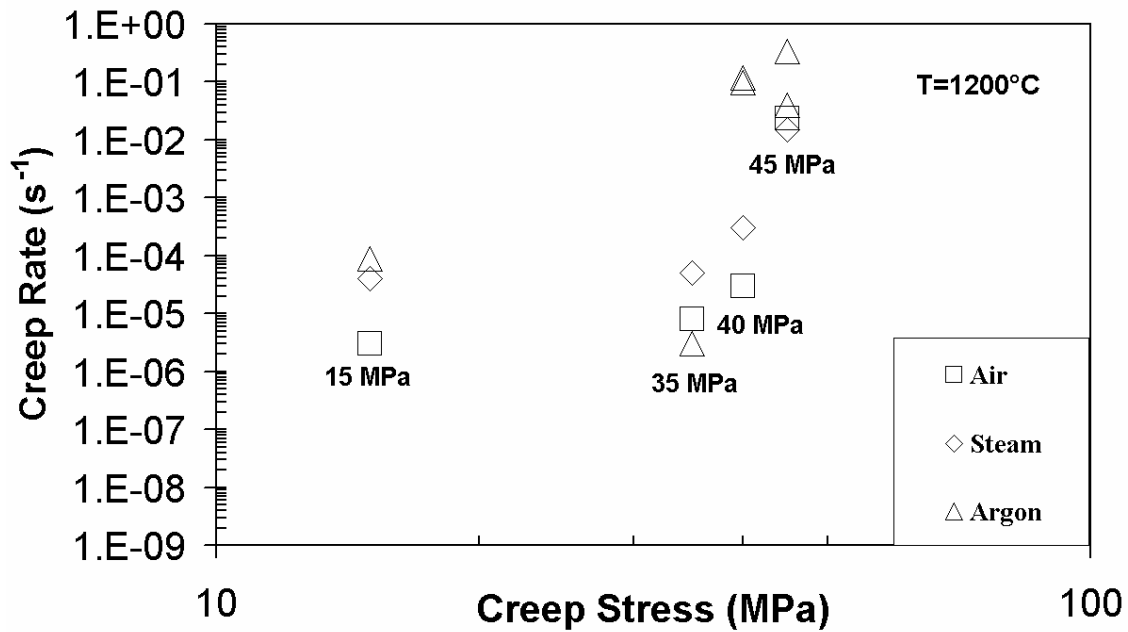
Figure 36. Creep stress vs. time to failure at 1200°C in air, steam, and argon environments.
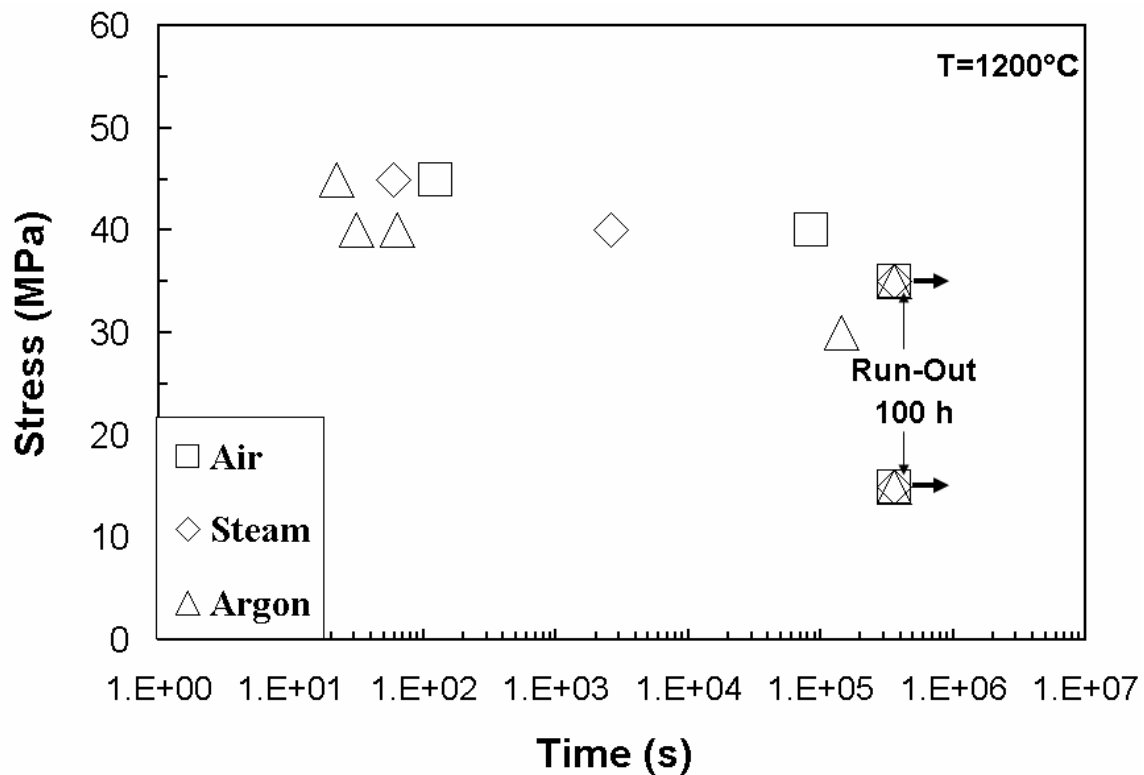
Figure 37. Creep strain rate vs. creep stress at 1200°C in air, steam, and argon environments.

A detailed comparison of creep curves produced at a given stress level in air, steam, and argon is presented in Figure 38 through Figure 41. Results in Figure 38 and Figure 39 show that at applied stresses of 15 and 35 MPa, the largest creep strains are accumulated in argon, followed by those accumulated in steam. The lowest creep strains are produced in air. Significantly different creep strains are accumulated in the primary creep regime. During secondary creep, tests in all environments produced similar rates of creep strain accumulation and similar creep strain.
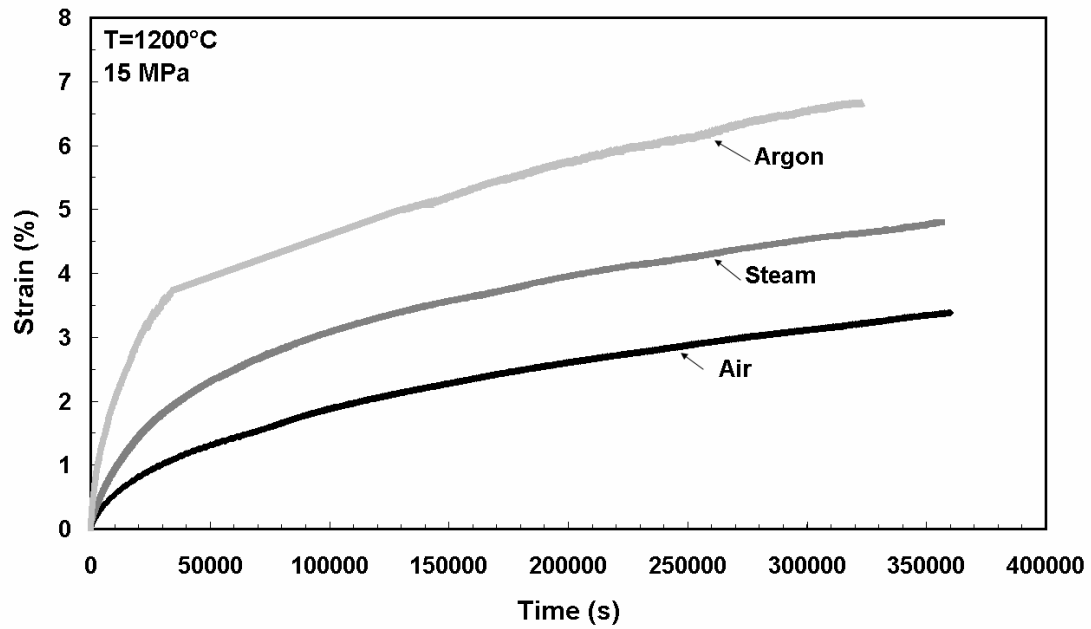
Figure 38. Creep strain vs. time obtained for creep stress of 15 MPa in air, steam, and argon environments at 1200°C.
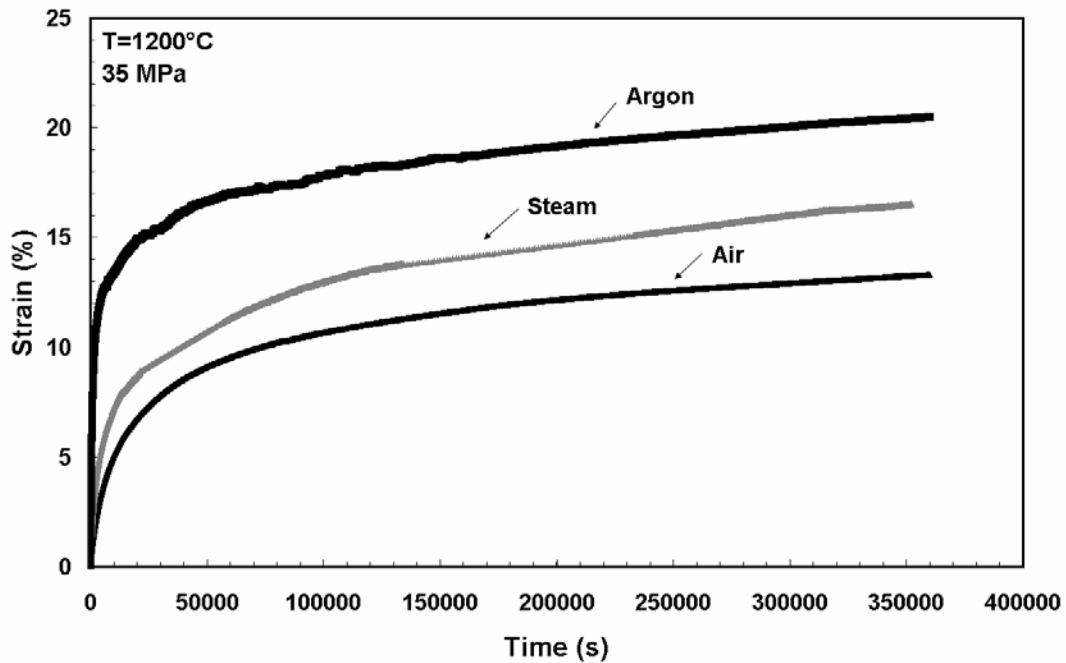
Figure 39. Creep strain vs. time obtained for creep stress of 35 MPa in air, steam, and argon environments at 1200°C.
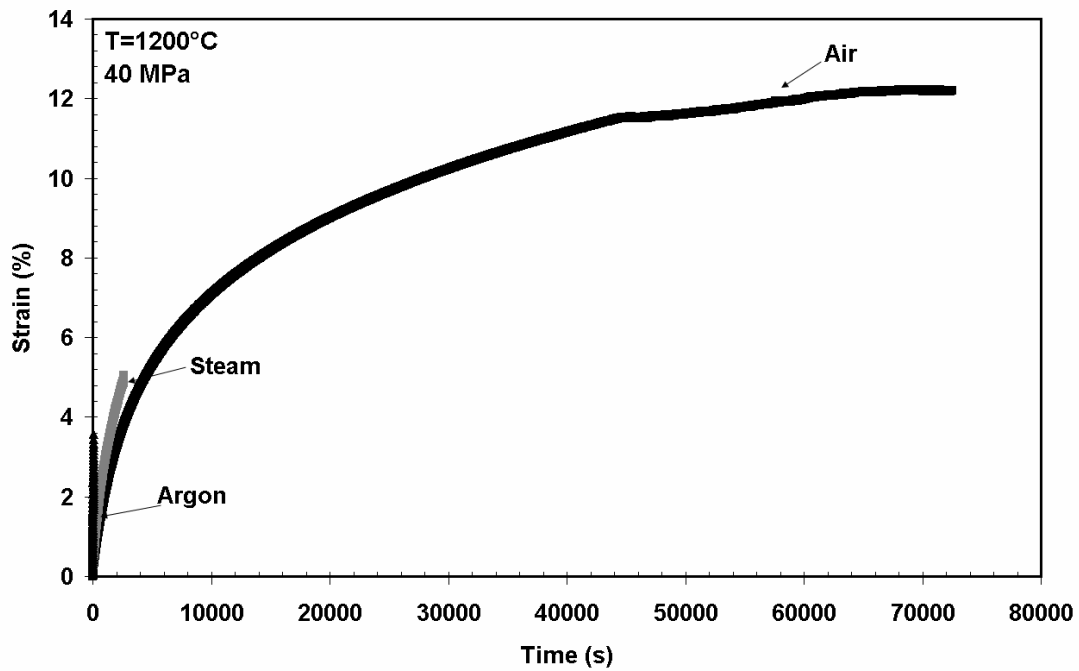
Figure 40. Creep strain vs. time obtained for creep stress of 40 MPa in air, steam, and argon environments at 1200°C.
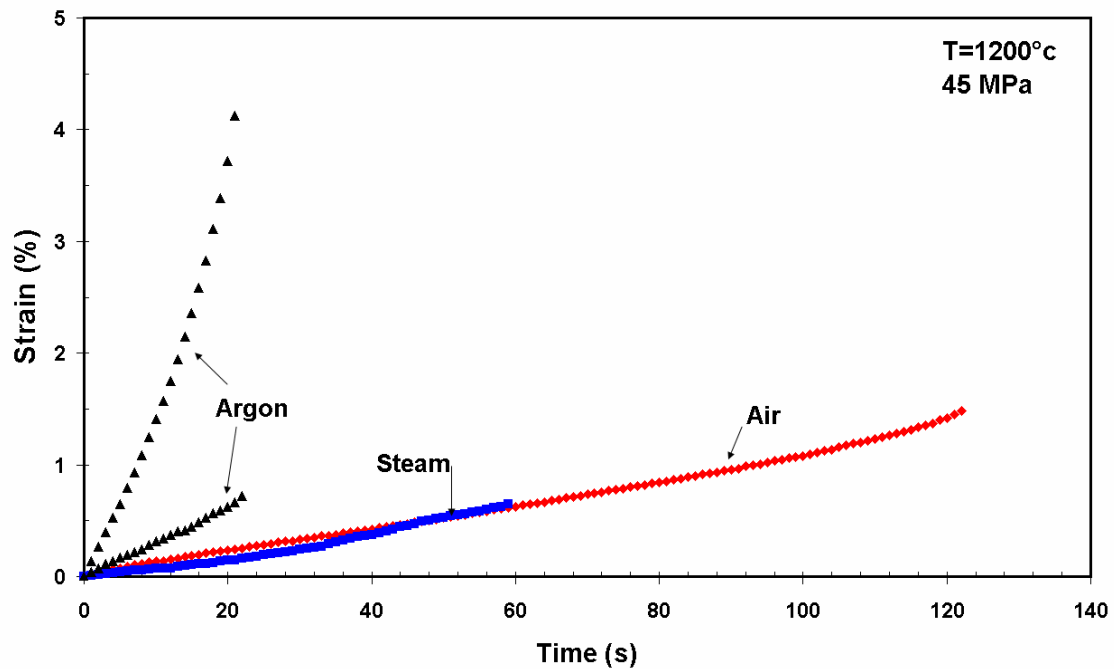
Figure 41. Creep strain vs. time obtained for creep stress of 45 MPa in air, steam, and argon environments at 1200°C.

57

Results in Figure 38 and Figure 39 once again demonstrate that specimens tested at creep stress levels ≤ 35 MPa exhibit primary and secondary creep, but no tertiary creep regimes. The tests conducted at higher stress levels of 40 and 45 MPa also display the same trend. At each stress level, the largest creep strains are accumulated in argon. At 40 MPa, creep curves produced in air and in steam are dominated by secondary creep. Conversely, the 40 MPa creep curves produce in argon exhibit an early transition to tertiary creep which results in rapid accumulation of large creep strain. The same observation can be made regarding the 45 MPa tests. In argon, tests at 40 and 45 MPa were repeated in order to confirm results.

In an earlier investigation, Harlan [13] evaluated the creep performance of N720/A with a 0/90° fiber orientation in air and in steam. In the case of the 0/90° fiber orientation, the composite exhibits a typical fiber-dominated behavior with fibers carrying most of the load. Therefore, composites with 0/90° fiber orientation exhibit much higher tensile strengths than the ±45° cross-ply. The UTS for the 0/90° specimens was 192 MPa and the UTS for the ±45° specimens was 55 MPa. In the case of the ±45° fiber orientation, composite behavior is matrix dominated, with only a small fraction of the load being carried by fibers. With weaker matrix carrying most of the load, ±45 cross-ply exhibits a lower tensile strength than its 0/90° counterpart. However in real-world applications, the N720/A composite would not be loaded strictly along the fiber direction. Therefore it is important to assess the effects of fiber orientation on mechanical performance of the CMC. Creep lives produced by the N720/A composite with 0/90° and

±45° fiber orientation are compared in Figure 42, where applied stress is plotted vs.

rupture time obtained in air and in steam environments at 1200°C.
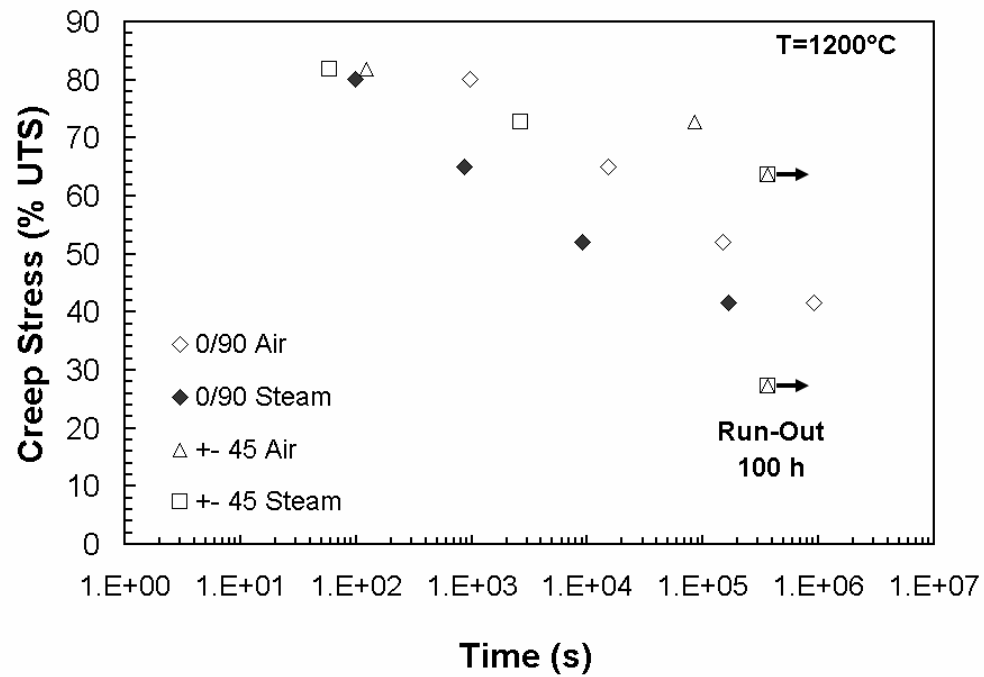
Figure 42. Creep-stress vs. time to failure for N720/A with 0/90° and ±45° fiber orientations at 1200°C in air and in steam environments.
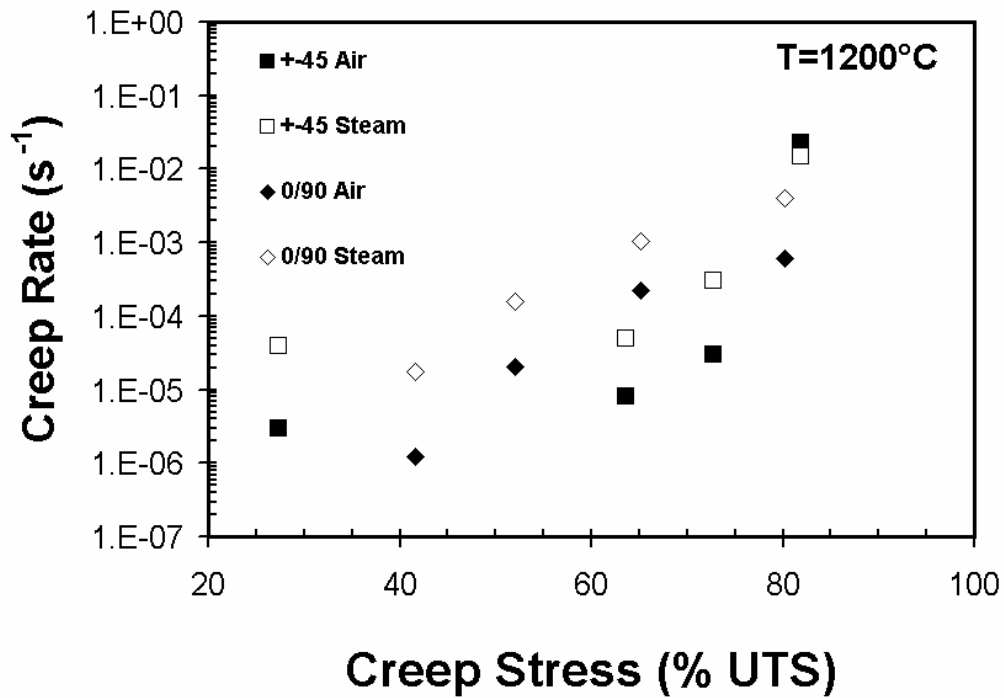
Figure 43. Creep rate vs. creep-stress for N720/A with 0/90° and ±45° fiber orientations at 1200°C in air and in steam environments.

Figure 42 shows that N720/A with 0/90° fiber orientation can operate at larger creep-stresses. In fact, the UTS of the 0/90° cross-ply is approximately 3.5 times that of the ±45° cross-ply. Furthermore, Figure 42 reveals that N720/A with 0/90° fiber orientation is more vulnerable to environmental degradation when operating in a steam environment than the ±45 cross-ply. Figure 43 shows the creep strain rates versus the creep stress for both fiber orientations. It is seen that the creep rate increases with increasing stress regardless of fiber orientation. Furthermore, results in Figure 43 reveal that the presence of steam accelerates creep of the 0/90° cross-ply at all stress levels investigated. As expected, the ±45° cross-ply exhibits higher overall creep rates than the 0/90° cross-ply.

5.3 Composite Microstructure

In this section, the results of the microstructural analysis of N720/A specimens will be presented. An optical microscope, scanning electron microscope (SEM), and an energy dispersive x-ray spectroscopy (EDS) were used to analyze the specimens following the creep-rupture tests.

The fracture surfaces of all specimens were observed with an optical microscope. For each specimen multiple pictures were taken including a picture of the complete fracture surface, and multiple close-up views of the damage zone. Both face and side views of each specimen were examined, as seen in Figure 44. For each specimen, the gauge width was 10 mm and the gauge thickness was 2.6 mm. Figure 45 through Figure 48 show the fracture surfaces within the 10 mm gauge width. Each specimen fractured within the gauge section, and every fracture surface shown is no wider then 10 mm.
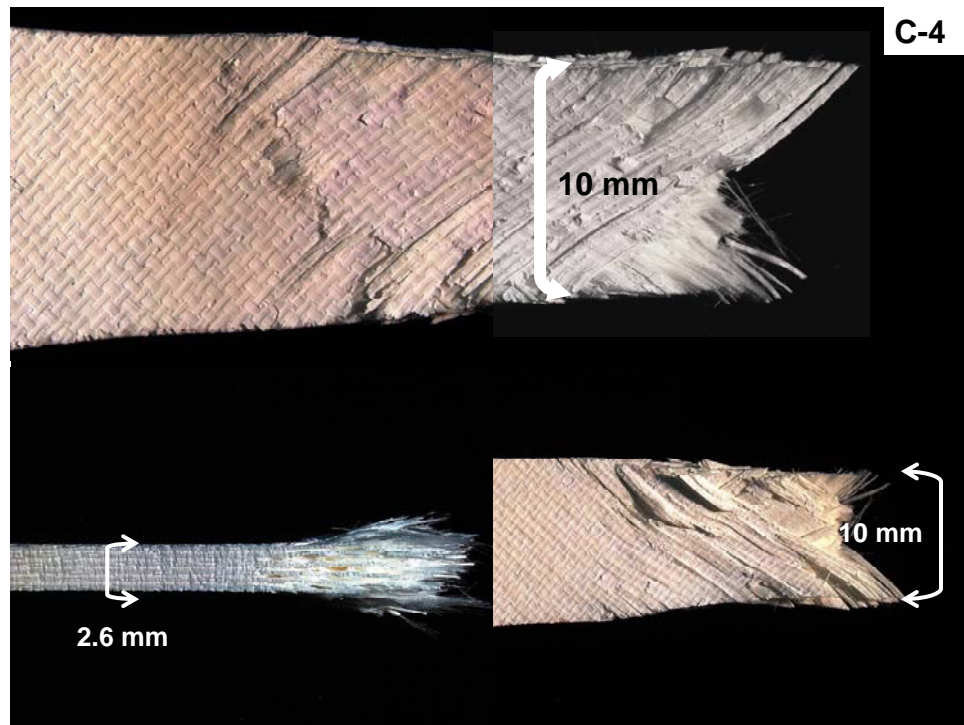
Figure 44. Fracture surfaces of N720/A specimen subjected to 40 MPa creep test at 1200°C in laboratory air.

The optical micrographs show that most of the fractures presented a V shape, caused by pullout of the ±45° fibers. Regardless of the test environment, specimen fracture retained the V shape. Fracture surfaces reveal evidence of individual fiber pullout as well as coordinated fracture of fiber bundles. Furthermore, there was no discernable increase in the amount of fiber pullout or the size of the damage zone with increasing creep stress. Specimens tested at 35 MPa in steam and in argon represent an exception. Both of these specimens achieved a run-out and were subjected to tension test to failure in order to measure retained strength and stiffness. These specimens produced flat fracture surfaces as opposed to the V shaped ones. Also, there was a noticeable increase in the damage zone found in specimens tested in argon compared to those tested in air and steam. This was especially obvious at higher loads. The figures below show the fracture surfaces produced in all creep tests. Each fracture surface is no wider then 10mm. In Figure 45 to Figure 48, the stress decreases from left to right and from top to bottom. Thus, the top left photo shows specimens tested at 45 MPa, the top right at 40 MPa, the bottom left at 35 MPa, and the bottom right at 15 MPa. Specimen information is summarized in Table 11.

Table 11. Specimen data of optical pictures.

Specimen #	Creep Stress (MPa)	Time to Failure (h)	Accumulated Creep Strain (%)
C-1	45	0.033	0.65
C-2	15	100	3.38
C-3	35	100	13.30
C-4	40	23.716	11.08
C-8	45	0.016	0.65
C-9	15	100	4.80
C-10	35	100	16.52
C-11	40	0.733	5.05

C-12	45	0.006	3.72
C-14	40	0.009	2.36
C-15	15	100	5.67
C-16	35	100	20.9
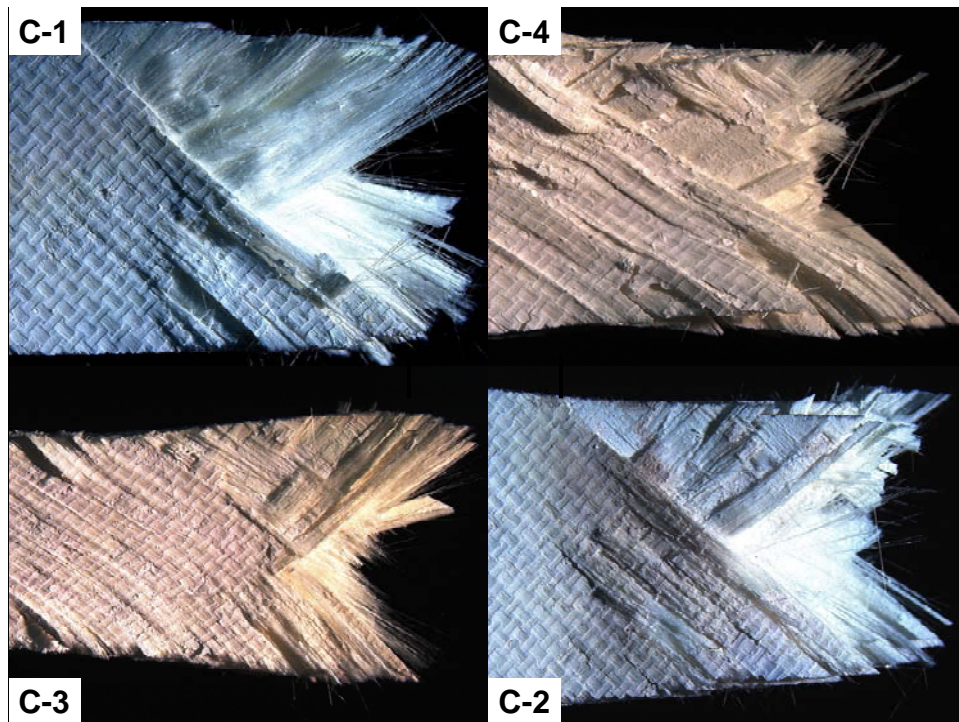
Figure 45. Fracture surfaces of N720/A specimens tested in creep at 1200°C in laboratory air.
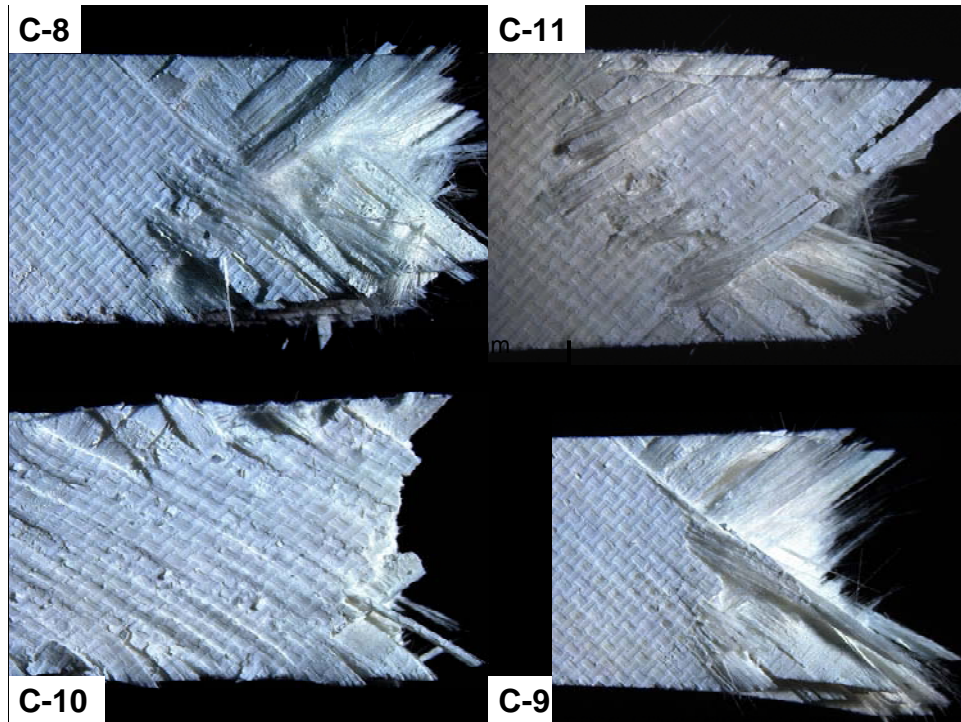
Figure 46. Fractures surfaces of N720/A specimens tested in creep at 1200°C in 100% steam environment.
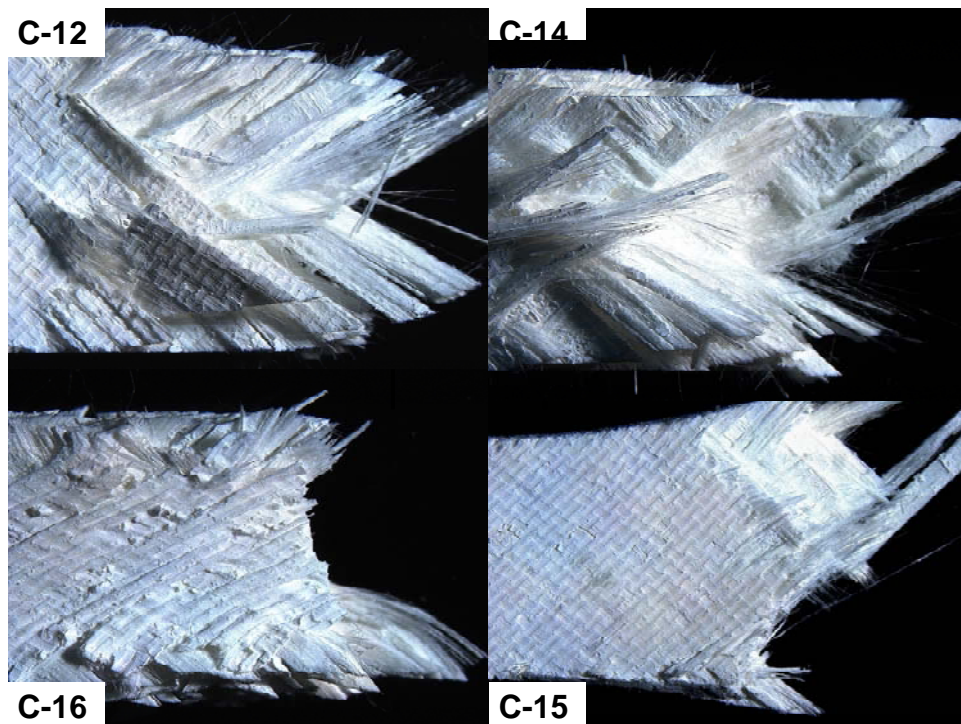
Figure 47. Fracture surfaces of N720/A specimens tested in creep at 1200°C in 100% argon environment.

Figure 48 shows fracture surfaces obtained in 45 MPa creep tests conducted in each environment. The top left figure shows an untested specimen, top right a specimen in air, bottom left a specimen tested in steam, and bottom right a specimen tested in argon.
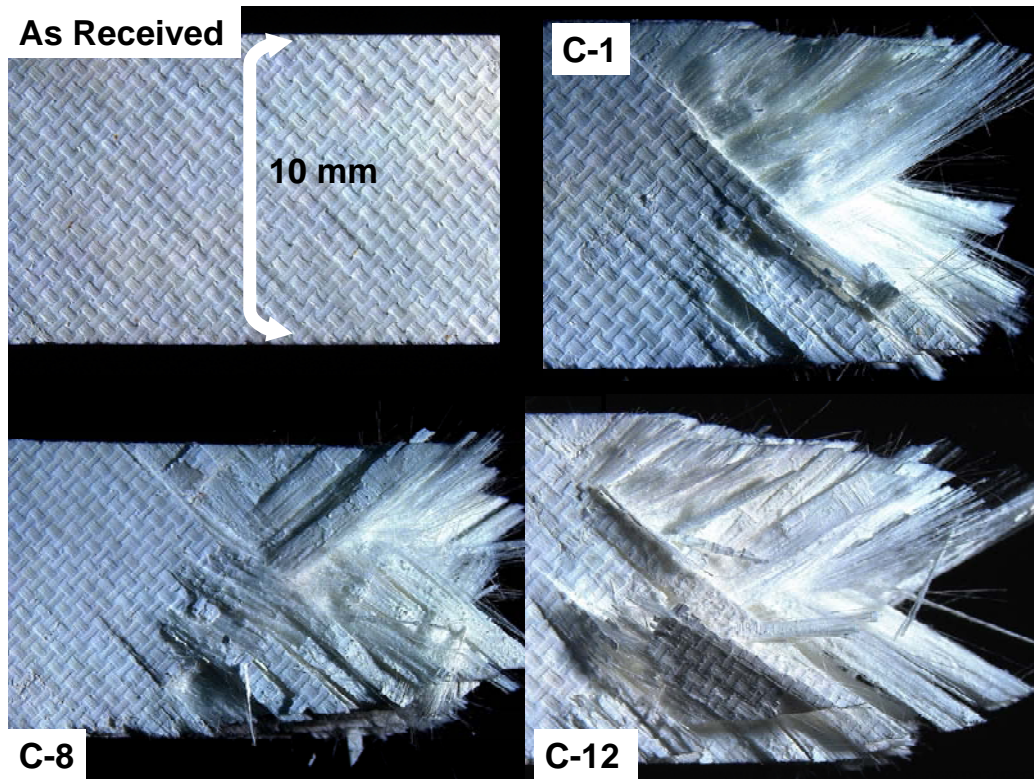
Figure 48. Fracture surfaces of N720/A specimens subjected to 45 MPa in air, steam, and argon.

The fracture surfaces produced by the 0/90° specimens are very different from those produced by the ±45° specimens. Fracture surfaces of specimens with the 0/90° fiber orientation are flatter and do not exhibit a V pattern. The damage zone is also smaller. Examples of fracture surfaces of 0/90° fiber orientation specimens tested in creep at 1200°C from reference [13] are shown in Figure 49.
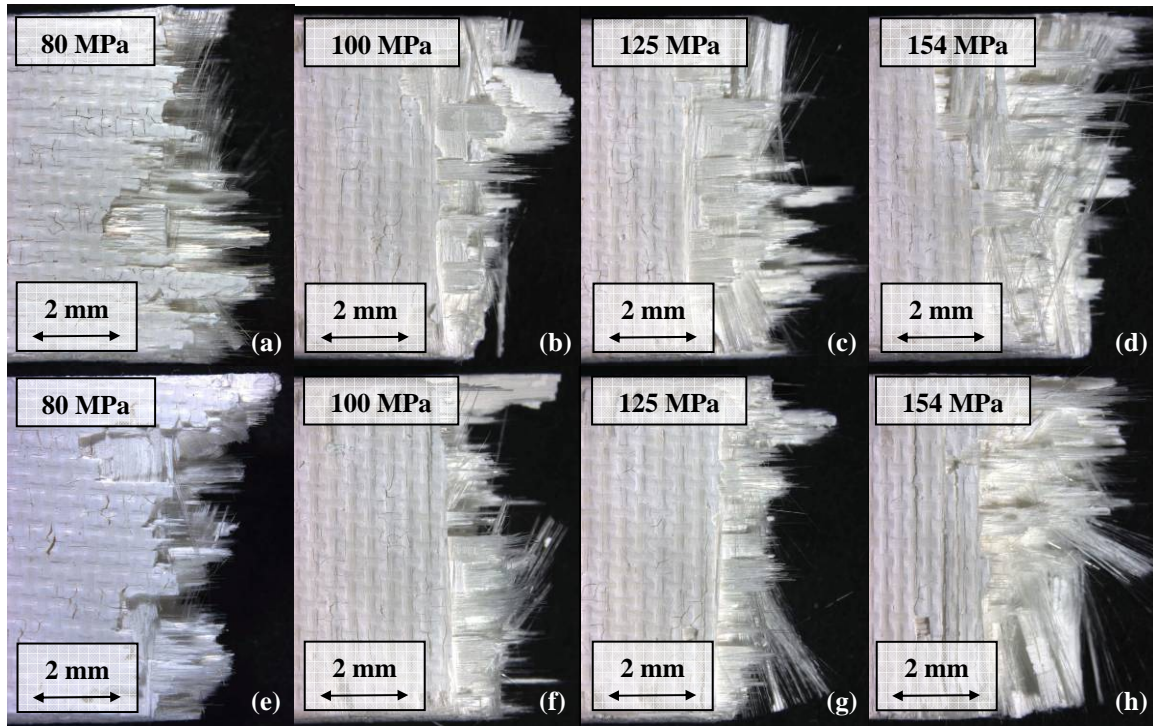
Figure 49. Fractured N720/A [0/90] creep specimens tested in air (a, b, c, d) and steam (e, f, g, h) at 1200°C [13:61].

The use of optical microscopy provides an overall picture of the specimen's fracture. However, an SEM is needed for an in-depth investigation of microstructural damage and failure mechanisms. This section will show the results of the SEM characterization. First, an overall examination of the fibers and matrix will be presented. Then the typical damage characteristics observed throughout the specimens will be shown. Next, the microstructural analyses of specimens tested under different loading conditions and different environments will be compared. Finally, microstructure of the 0/90° and ±45° specimens will be compared. Figure 50 shows a typical fracture surface obtained in creep tests.
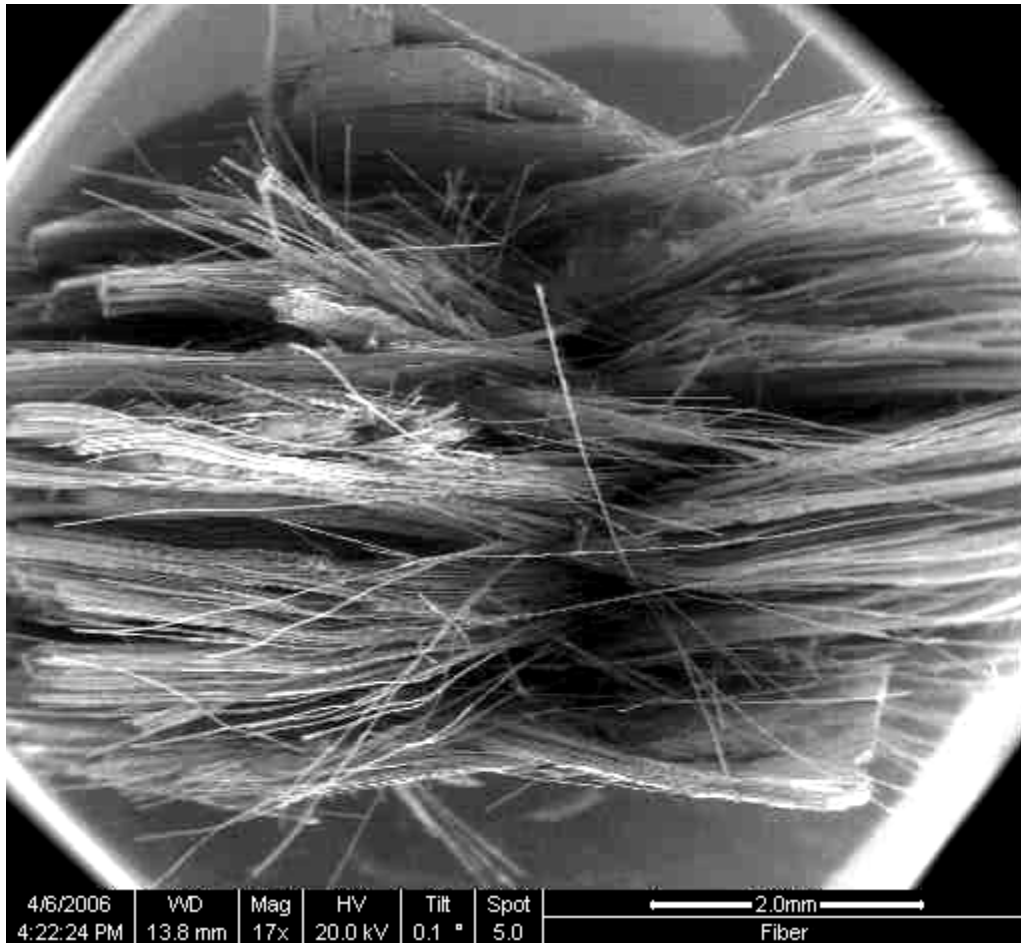
Figure 50. SEM micrograph of C-1, 45 MPa in laboratory air.

As stated earlier, the N720/A composite consist of N720 fibers in a porous alumina matrix. Figure 51 shows an individual fiber while Figure 52 shows the matrix of a fractured specimen. Pieces of matrix that remain bonded to the fiber are seen in Figure 51. This was common for most fibers, especially those pulled out away from the bundles. As the creep stress increased, the amount of individual fiber pullout decreased, but the pulled out filaments had larger amounts of matrix still attached to them. The grains of the porous matrix, which can be seen in Figure 52, are loosely packed and easily distinguishable.
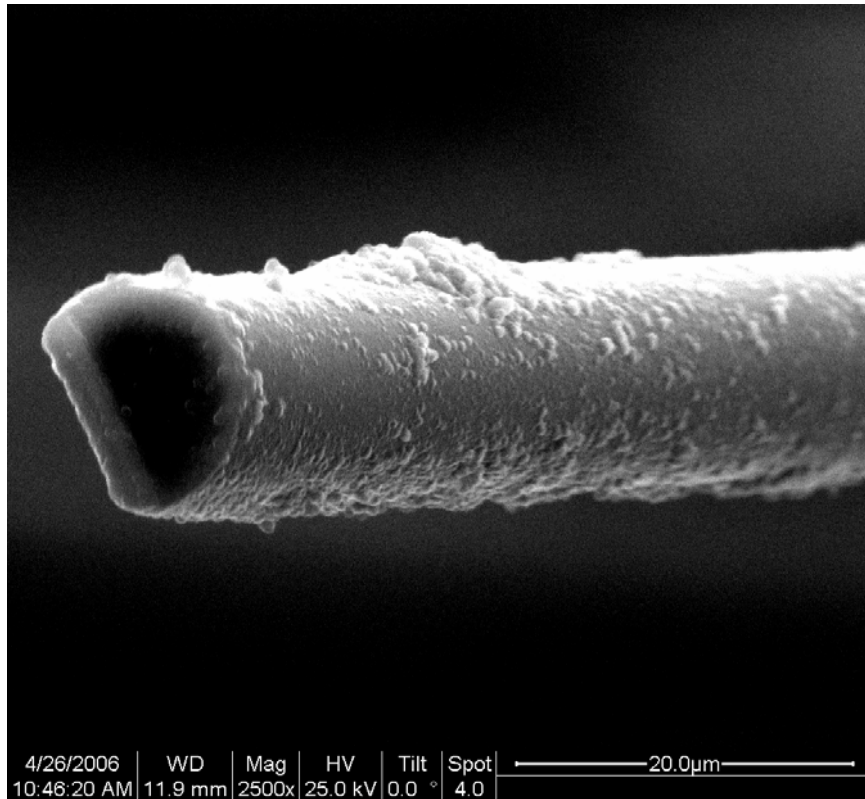
Figure 51. SEM micrograph of N720 fiber.
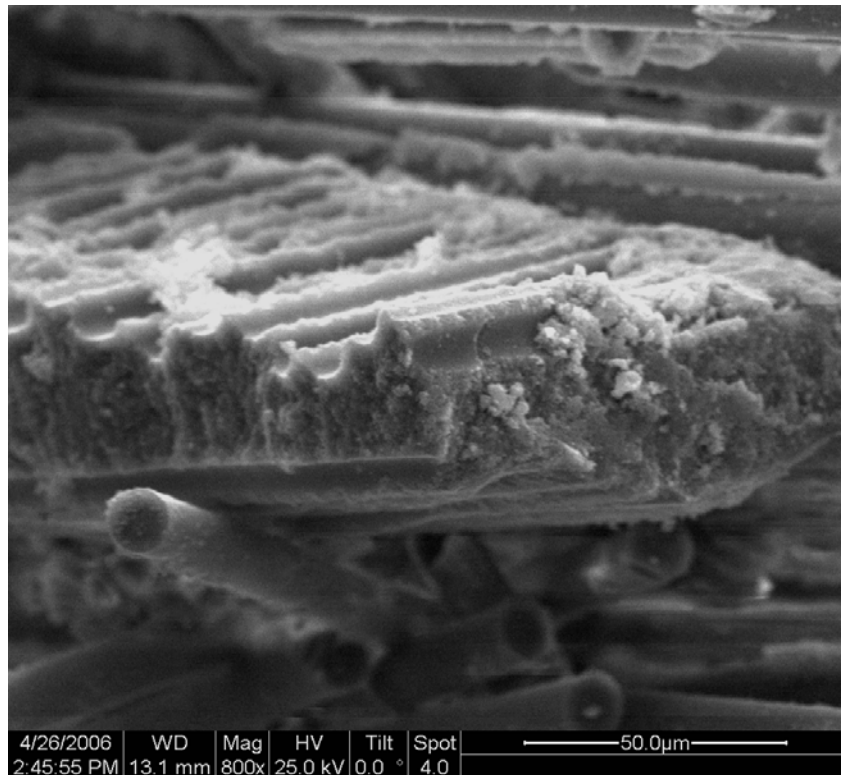
Figure 52. SEM micrograph of alumina matrix.

Figure 53 shows the fibers and the matrix. The matrix was found (1) between the larger fiber bundles, or tows, and (2) between individual fibers. The larger amount of matrix remaining attached to the fiber after a test has been completed indicates that a strong fiber/matrix bond still exists.
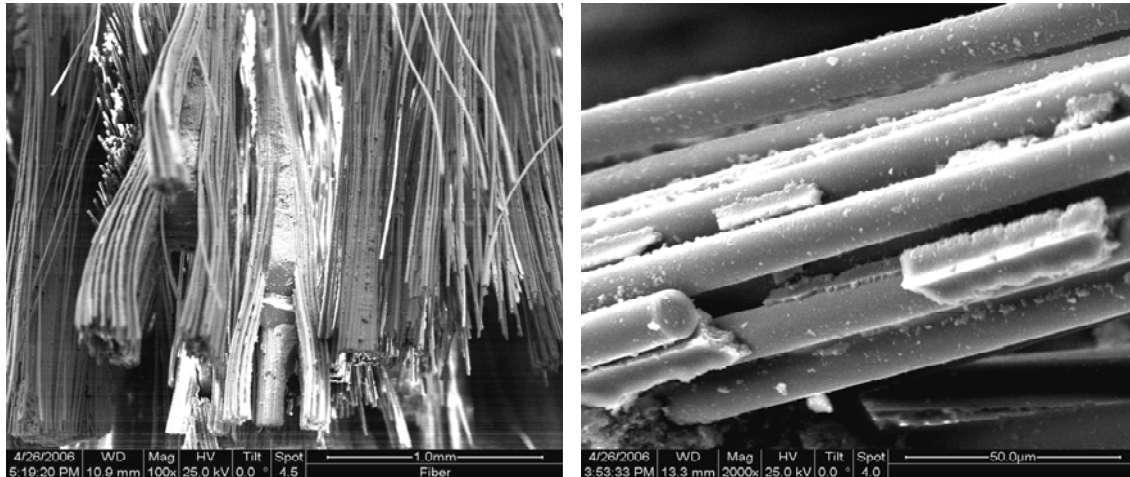
Figure 53. SEM micrographs of N720/A matrix and fiber interface.

Five distinctive microstructural characteristics were identified in the course of the SEM analysis: "waviness" of the fiber bundles, fiber pullout, coordinated planar fracture of fiber bundles, micro cracking of the matrix between the bundles, and micro cracking of the matrix between the individual fibers. Each of these fractures will be discussed below.

The term "waviness" was adopted to describe fiber bundles which did not remain straight but took on a wavy shape (see Figure 54). The "waviness" was found under every load and each environment. However as the load increased so did the degree of "waviness." This microstructural feature was not found in the 0/90° specimens tested by Harlan, but appears only in specimens with the ±45° fiber orientation. At present, it is not understood what causes the "waviness" of the fiber bundles, but there are two possible

explanations that can be offered. One is that the waviness is caused by shear forces acting on the fiber bundles under load. This would also explain why waviness was not found in the 0/90° specimens. In the case of the 0/90° fiber orientation, fibers do not experience shear stress and therefore would not see and "waviness." The second, and simpler, theory suggests that the "waviness" is caused by the weaving of the fiber bundles into fabric plies. When failure occurs and the bundles separate, their "woven" shape remains intact. This is only seen with the ±45° fiber orientation because of the way the fiber bundles separate from each other at an angle. In the 0/90° fiber orientation, the fiber bundles just separate without being pulled away from each other.
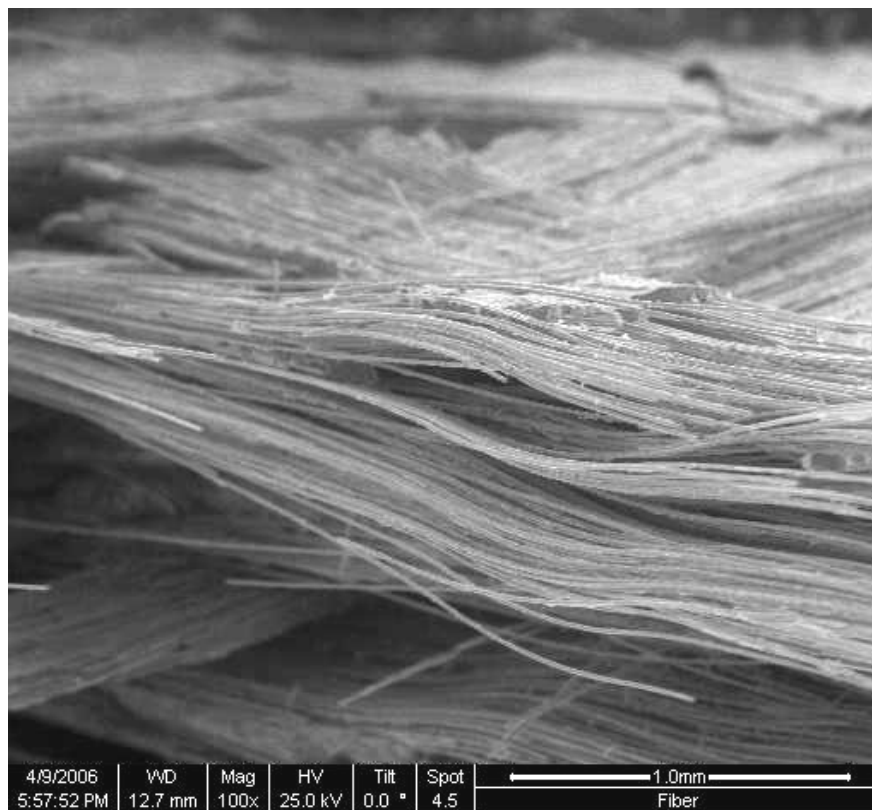
Figure 54. SEM micrograph depicting fiber "waviness."

The second microstructural characteristic observed in each specimen was fiber pullout (see Figure 55). Fiber pullout was very pronounced in each test and test

environment regardless of the applied stress. Individual fiber pullout, which indicates a

breakdown in the bond between the matrix and fiber was more pronounced in tests with

longer times to failure. This type of fracture surface was difficult to observe in the SEM

because of the limited focal distance and the randomness of the fiber failures. The

individual fibers break in different planes where local stress increases can be absorbed by

the surrounding fibers. At first, the fractures are random and equally distributed

throughout the fiber bundle. But, once the number of fiber fractures reaches a critical

level, then the local stress becomes high enough to cause failure of the entire bundle

[22:88-89].
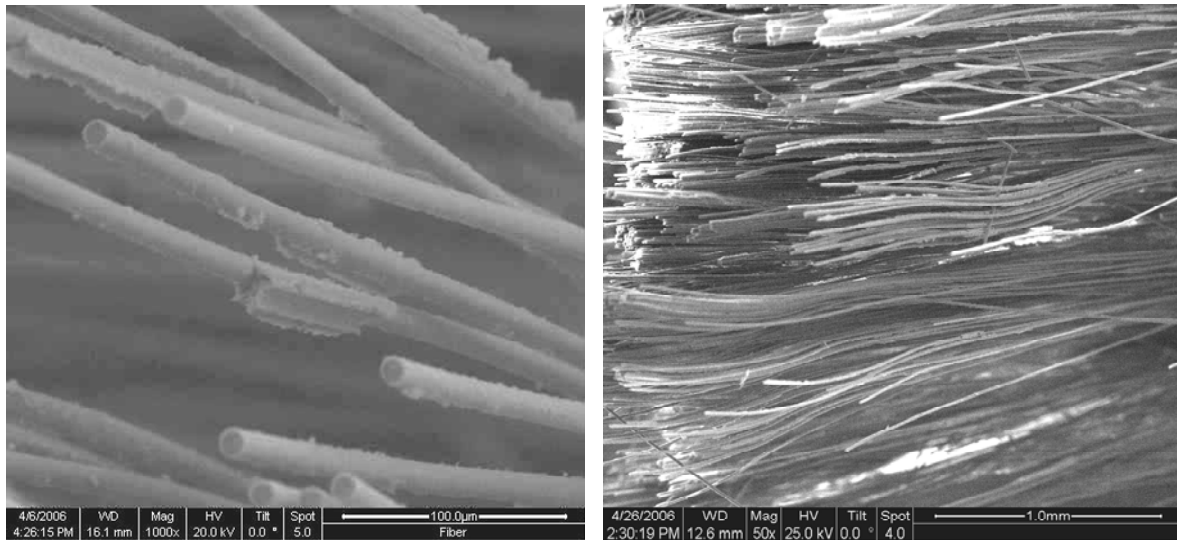
**Figure 55. SEM micrographs depicting fiber pullout in the fracture surfaces of
tested N720/A specimens.**

For most specimens, fracture surfaces were dominated by coordinated planar

fracture (see Figure 56 and Figure 57). Here an entire bundle fails, causing a reduction of

material strength. Overall, most of the fibers remained in large bundles as the failure

occurred. This type of failure indicates strong bonds between the matrix and the

individual fibers.
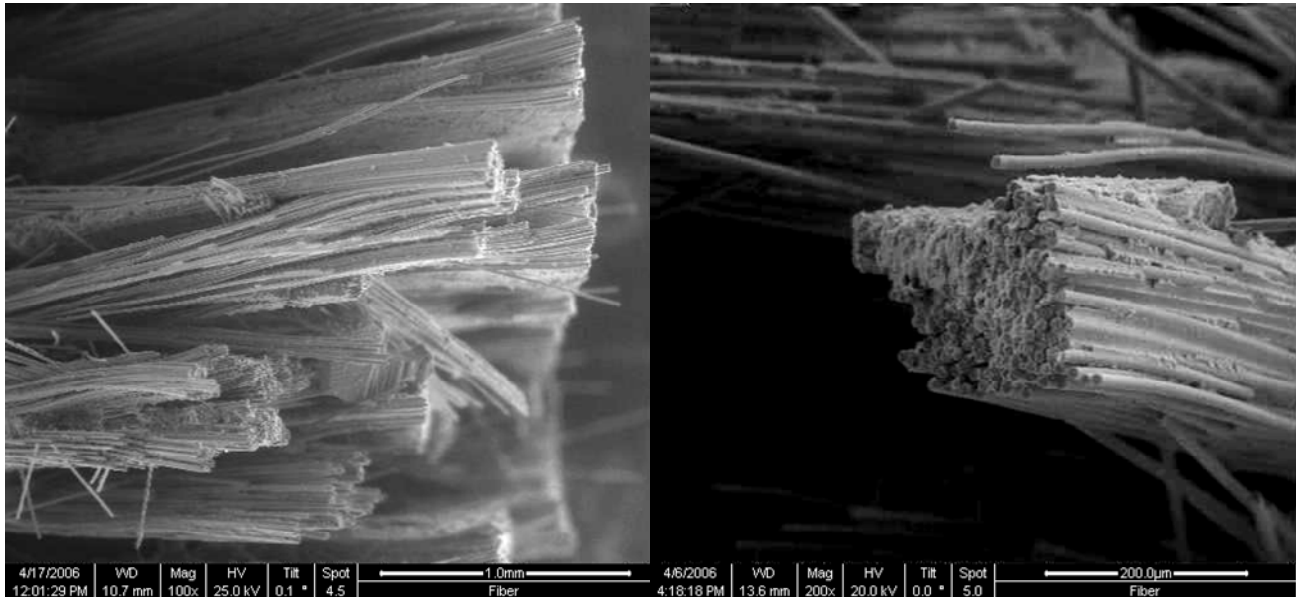
Figure 56. SEM micrographs depicting regions of coordinated planar fracture.
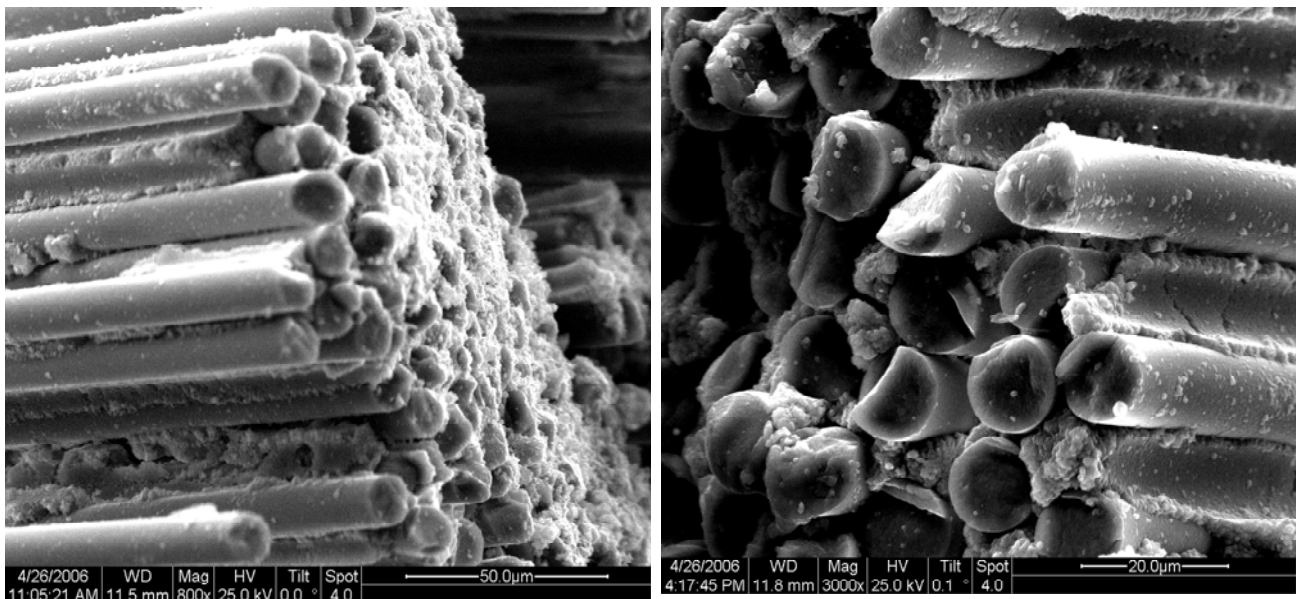
Figure 57. SEM micrographs depicting regions of coordinated planar fracture.

In the case of the matrix dominated ±45° fiber orientation, the specimen is not

fiber dominated, and therefore fiber degradation can not govern the material failure.

Alumina matrix, which is relatively weak and porous, was used in N720/A in order to provide for crack deflection, allowing the cracks to propagate around instead of through the fibers. In the CMC with 0/90° fiber orientation, crack deflection is critical to CMC toughness, because the material response is fiber-dominated. Even if the fibers remain intact, matrix failure will cause the specimen failure. In a porous matrix CMC, matrix cracks originating during processing will become larger and more numerous under load, weakening the overall material. As the loading continues, matrix separates from the individual fibers when the fiber/matrix bonds are weakened and break down. This causes fiber pullout. Matrix cracks and separation of individual fibers from the matrix can be seen Figure 58 and Figure 59.
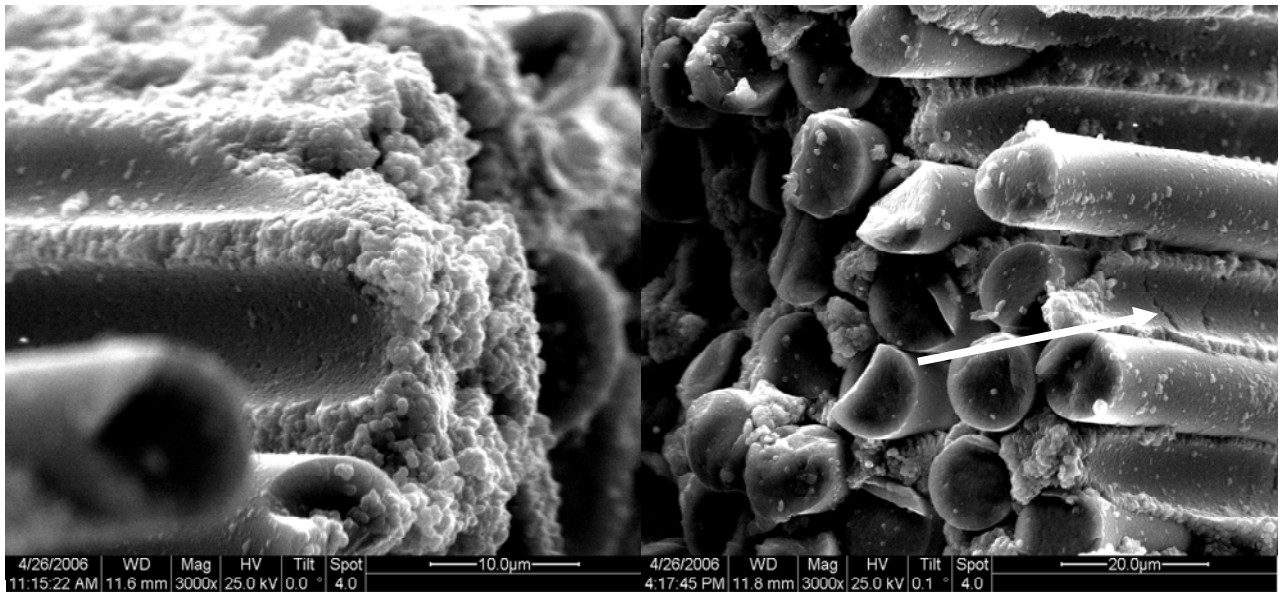
Figure 58. SEM micrographs depicting matrix failure between fibers.
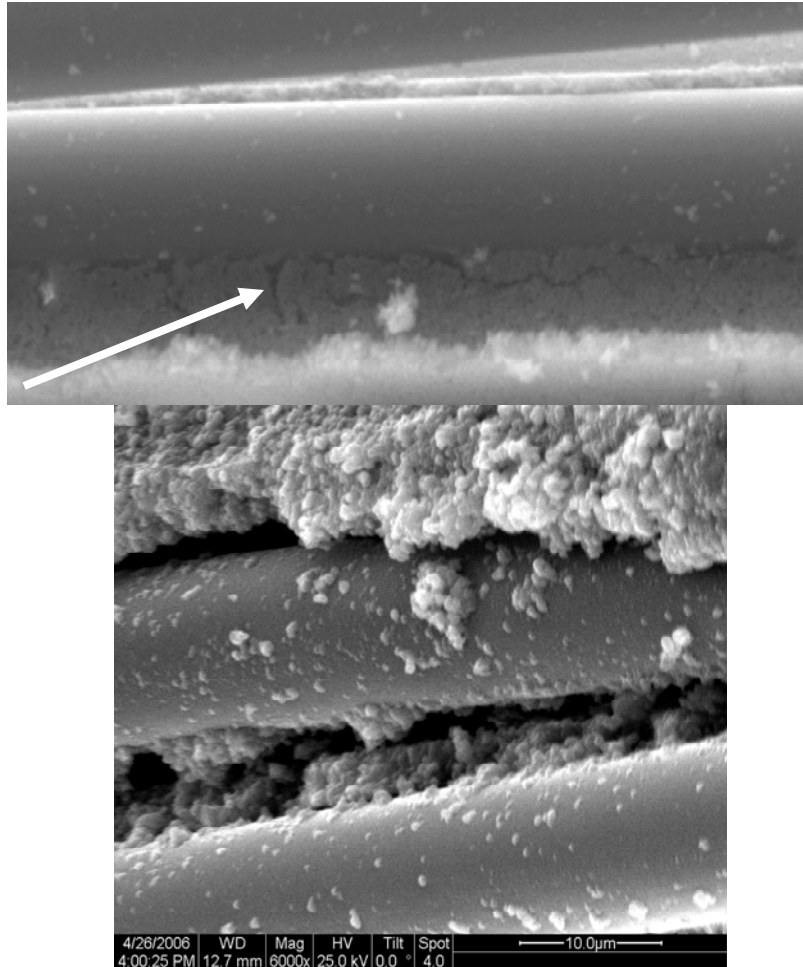
Figure 59. SEM micrographs depicting matrix failure between fibers.

Another characteristic feature of the fracture surfaces was failure of matrix between the larger fiber bundles (see Figure 60 and Figure 61). This type of failure was likely the most damaging to the overall specimen.
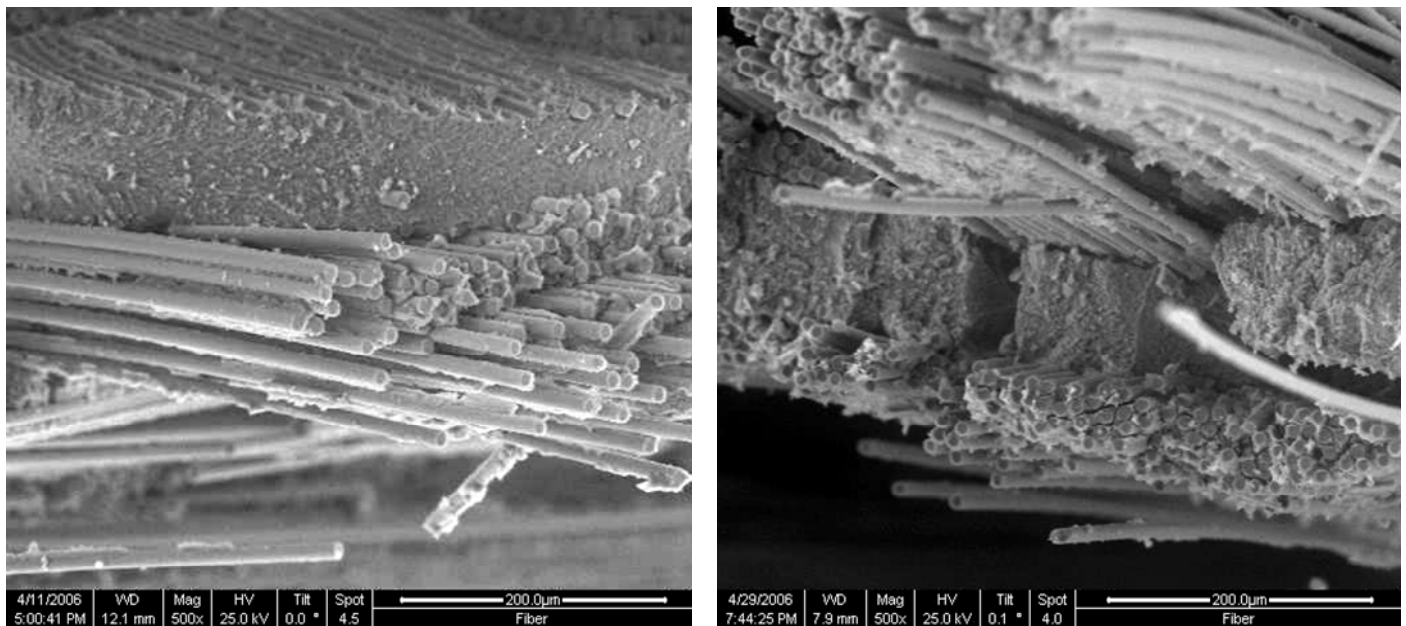
Figure 60. SEM micrographs depicting matrix failure between bundles.
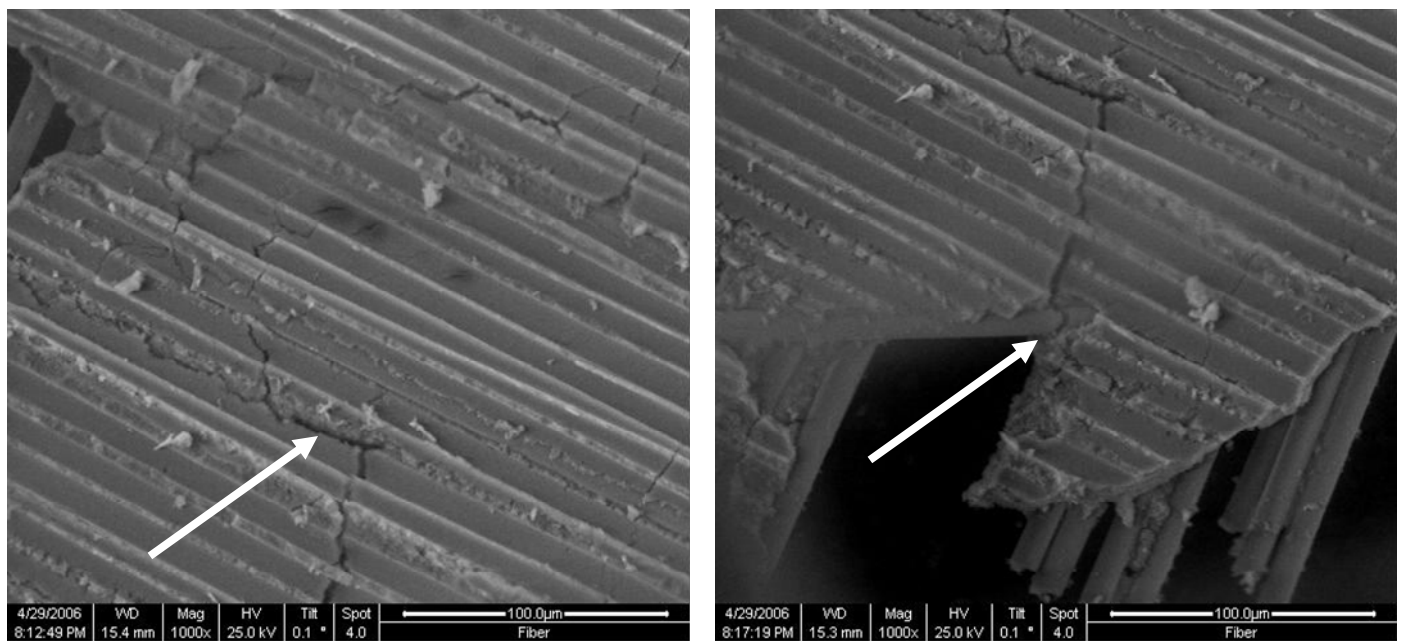
Figure 61. SEM micrographs depicting cracks propagating through matrix.

The fracture surfaces produced at various stress levels had similar appearance. In the case of higher loads, there was less individual fiber pullout and more coordinated bundle failure. The individual fibers which did separate from the matrix at lower loads did not have as much matrix still attached to them as did the fibers pulled out at higher

loads, which still showed large amounts of matrix bounded to them. This can be seen in

Figure 62 and Figure 63, which show the fracture surfaces of specimens tested in the

laboratory air environment.
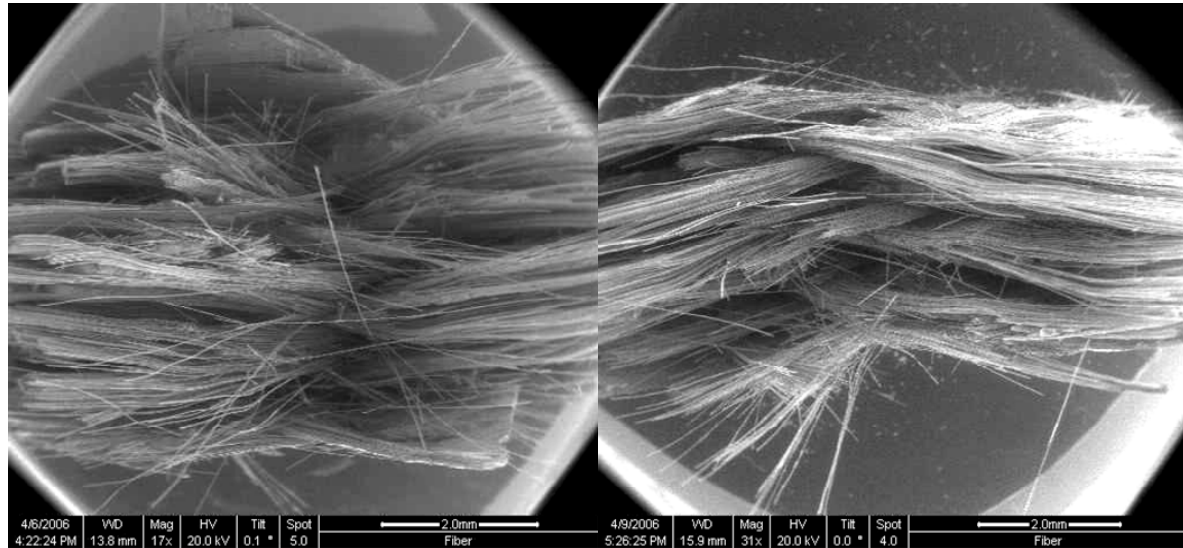
C-1 45 MPa   **C-2 15 MPa**

Figure 62. SEM micrographs depicting fiber pull produced at different stress levels.
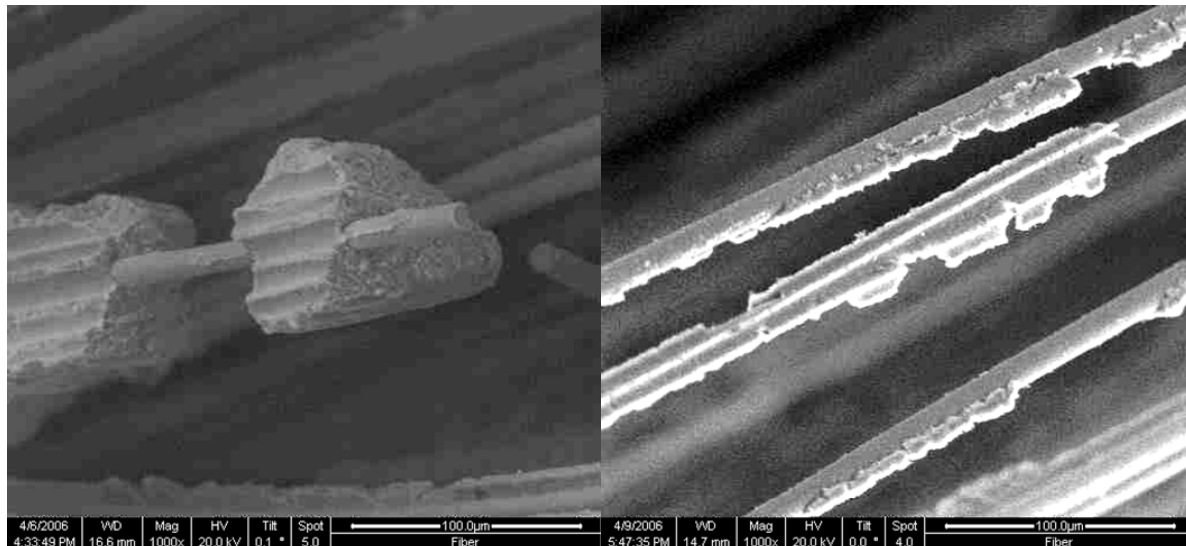
C-1 45 MPa   **C-2 15 MPa**

Figure 63. SEM micrographs depicting fiber pull produced at different stress levels.

Environment did seem to have an impact on the matrix. It is believed that in the air and steam environment the porous matrix may become denser. So, when a fiber is pulled out, the matrix does not collapse into the trough left by the fiber but retains its original shape (see Figure 64). However, in the argon environment, the matrix appeared to be much more porous (see Figure 65). More matrix cracks were found in specimens tested in argon than in those tested in the air or steam environment. The argon environment appeared to have increased porosity and decreased the strength of the matrix. At present the reasons for that are not well understood.
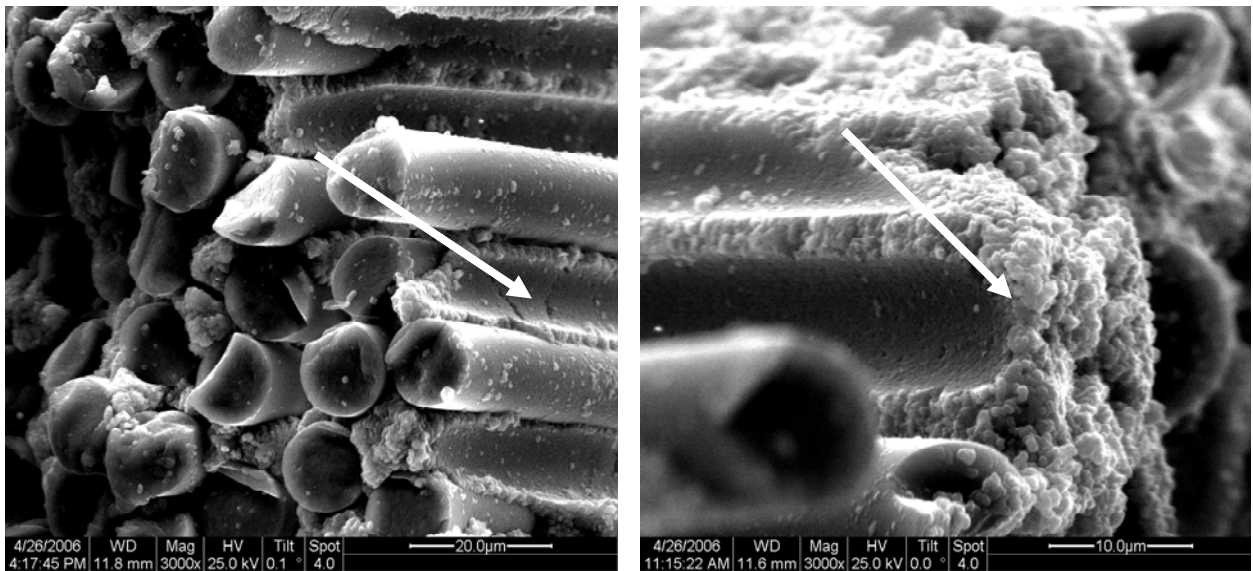
Figure 64. SEM micrograph depicting the matrix of specimens in air and steam.
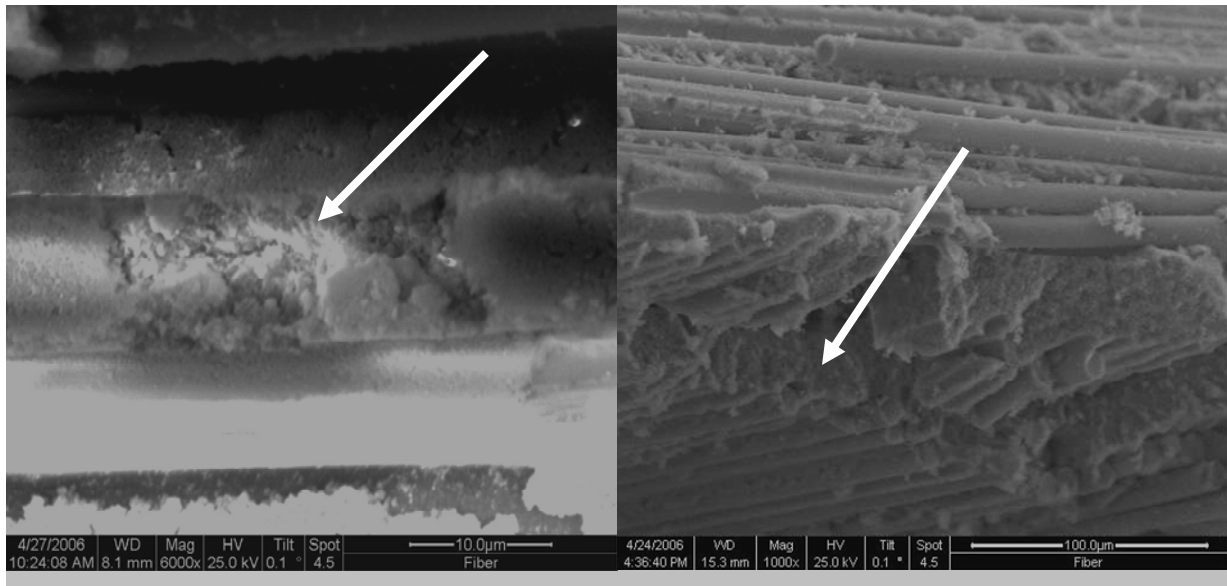
Figure 65. SEM micrograph depicting the matrix of specimens in argon.

Fracture surfaces of the 0/90° specimens tested in creep had a different appearance [13], exhibiting less fiber pull-out then the fracture surfaces of the ±45° specimens (see Figure **66**).
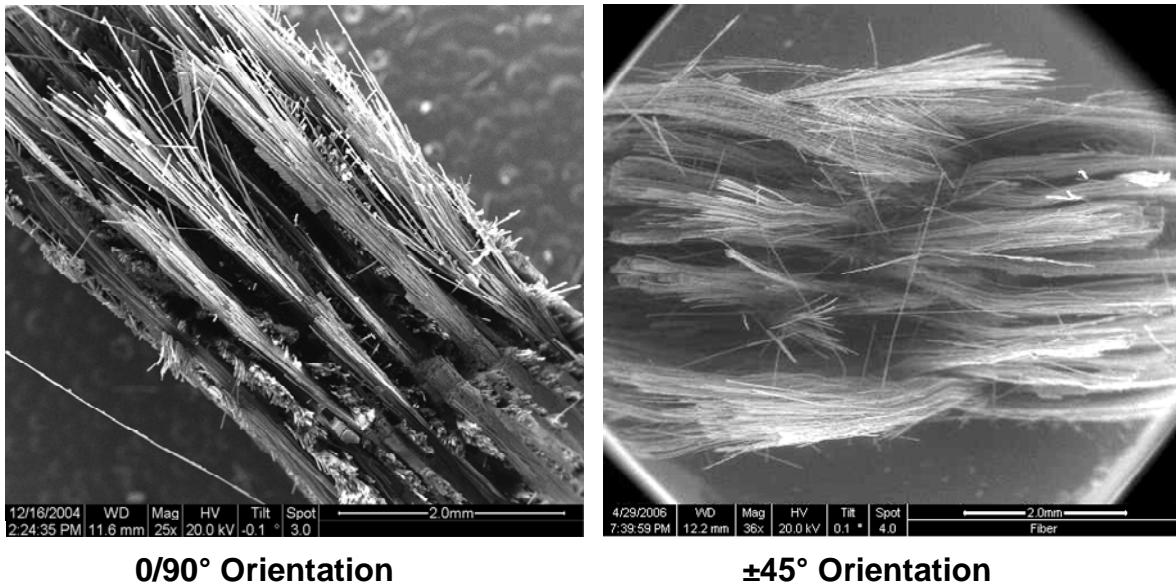
0/90° Orientation   **±45° Orientation**

Figure 66. SEM micrographs depicting fracture surfaces of N720/A specimens with 0/90° and ±45° fiber orientations.

5.4 Energy Dispersive X-ray Spectroscopy (EDS)

The main objective of the spectroscopic investigation was to identify elemental differences, if any, between the specimens tested in different environments. The oxide/oxide CMCs were originally developed for use in oxidizing environments, for example steam, where the ability of the material to remain chemically stable is important. Since N720/A was originally developed for use in aerospace applications, such as an aircraft turbine engine, it must be able to maintain properties and perform when subjected to a water vapor environment.

Wannaparhun et al. [38] examined the N720/A CMC at high temperatures and in a water vapor environment and concluded that silicon could be leached out from the mullite phase of the fiber under these conditions. The mullite released the silicon in the form of $Si(OH)_4(g)$ where it re-condensed within the alumina matrix [38:39]. The mullite phase was added to the N720 fiber in order to improve the low creep resistance of a purely alumina fiber. Wannaparhun et al. suggested that the leaching of silicon, or migration of silicon species, might lead to a reduced creep life of a material in an oxidized environment. Wannaparhun et al. suggested that the presence of either oxygen or hydrogen in the environment could cause the silicon species to migrate, weakening the fiber, and overall reducing the creep resistance of the material.

A qualitative EDS analysis was performed in order to determine whether migration of silicon species occurred in specimens subjected to creep loading at 1200°C in the laboratory air, 100% steam, and 100% argon environments. The EDS analysis may be able to explain why specimens tested in steam and especially argon produced higher creep rates and lower creep lives. A summary of the specimens used in the EDS analysis

79

is given in Table 12, where test environment, creep stress, time to failure, and location of

the EDS analysis are provided for each specimen. Specimens C-1, C-8, and C-12 were

coated with carbon for use in the high vacuum mode of the SEM.

Table 12. Specimens used in EDS analysis.

Specimen #	Environment	Creep Stress (MPa)	Time to Failure (h)	Accumulated Creep Strain (%)	Location of Matrix Analysis
C-1	Air	45	0.033	0.65	Interior
C-4	Air	40	23.716	11.08	Edge
C-8	Steam	45	0.016	0.65	Interior
C-11	Steam	40	0.733	5.05	Edge
C-12	Argon	45	0.006	3.72	Interior
C-16	Argon	35	100	20.90	Edge

The ±45° fiber orientation and V shaped fracture surfaces made achieving clear,

detailed data from the EDS very difficult. Instead of trying to collect data across the

entire fracture surface of a specimen, the electron beam spot mode was utilized to

precisely control the beam location. The manufacture of the analysis system, EDAX,

suggested the working distance to the specimen be set to 10 mm, the counts per second

(CPS), to around 1000-2000, and the dead time, between 20-40%. All of these

recommendations were followed. However, because of the matrix location deep within

the fracture surface relative to the x-ray, often a CPS of 500-700 could only be obtained.

Figure 67 shows a qualitative EDS analysis of the as-received material. Four

main peaks are clearly visible. The far left peak represents carbon which is present due to

coating, then come oxygen and aluminum peaks from the alumina and mullite, and

finally a silicon peak can be seen on the far right. Silicon is found within the mullite. The

as-received matrix showed no silicon peak. The search for migration of silicon species

from fiber into the matrix began in the regions of matrix originally located near the fibers [22:78].
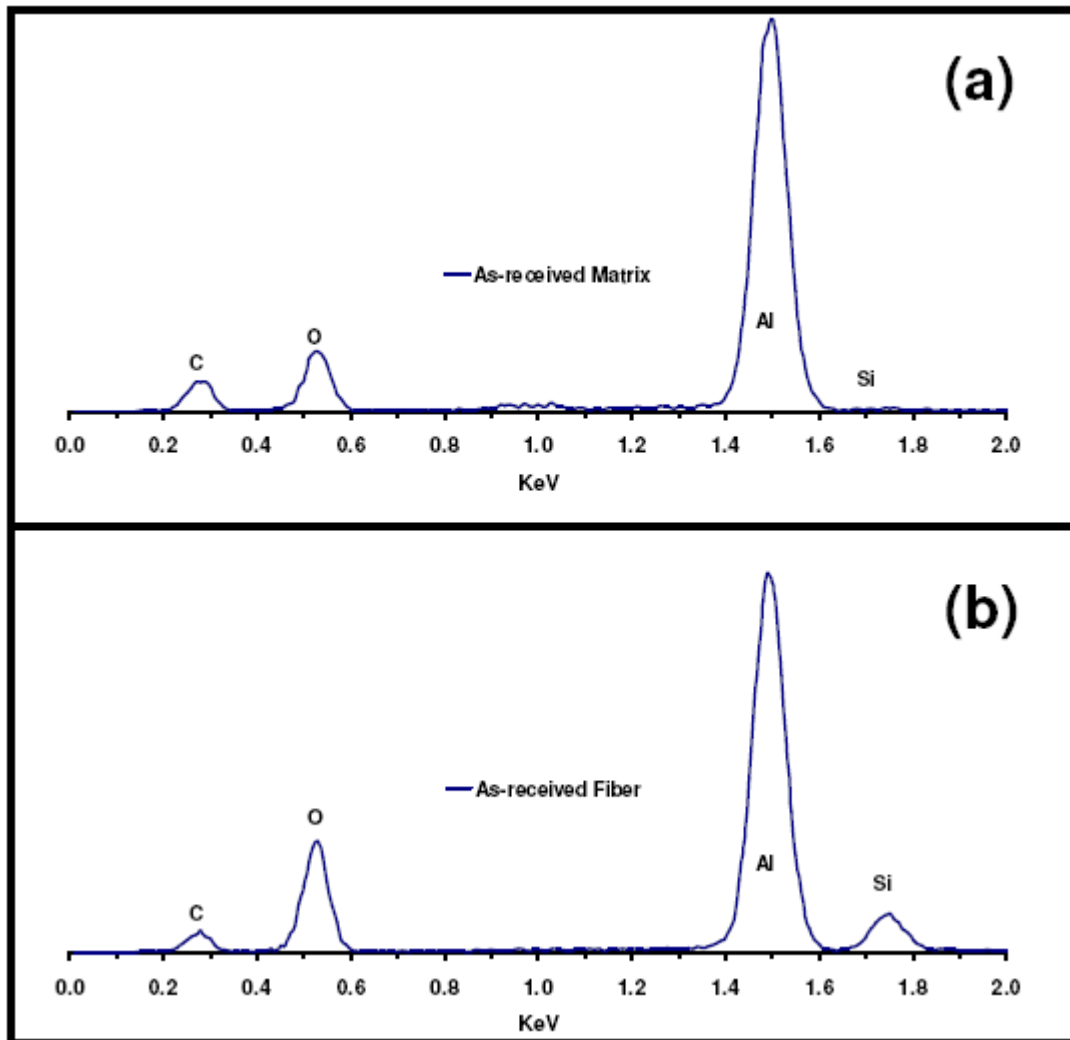
Figure 67. EDS spectra of as-received N720/A composite: (a) matrix and (b) fiber [22:77].

Selection of the matrix region during EDS analysis and placement of the electron beam was important when trying to collect accurate data. If the electron beam was focused on matrix located next to a fiber, the data collected could include the fiber. This would contaminate the results. So, to analyze the spectra of the matrix located as close to

the fiber as possible, and where at the same time no fiber spectra data could be collected, the electron beam was focused on regions of the fracture surface where fiber had pulled away from the matrix. By choosing these locations, an analysis of the matrix region which had direct contact with the fiber could be carried out. The images in Figure 68 show the location of each EDS analysis. The arrows point to the direct spots where the electron beam was focused. For comparison, an EDS analysis was also performed for the matrix regions that did not have direct contact with the fibers (see Figure 69).

C-4 Air

C-11 Steam

C-16 Argon
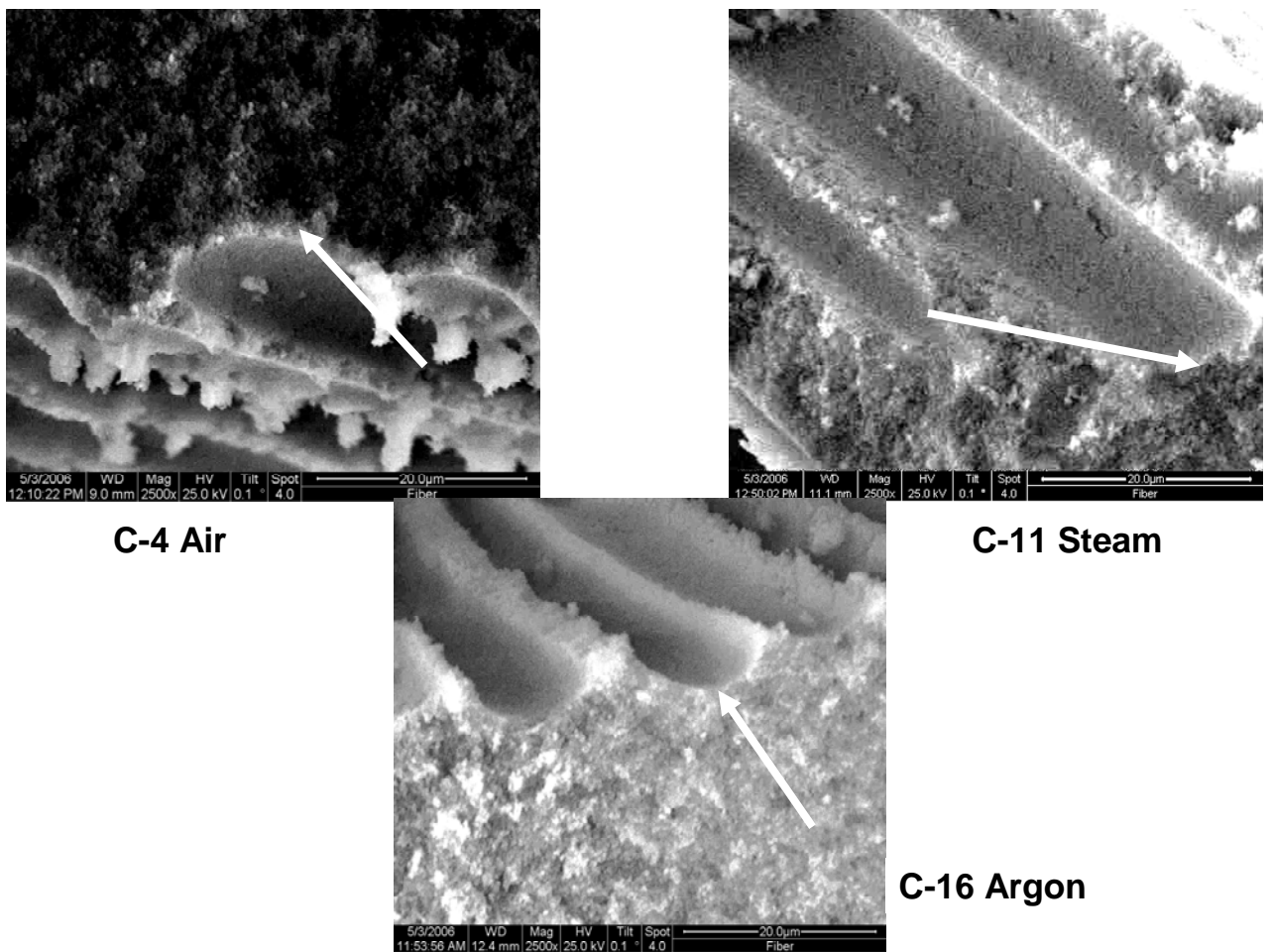
Figure 68. SEM micrographs showing-locations of electron beams at the edge of the matrix for EDS analysis.

C-1 Air

C-8 Steam

C-1 Argon
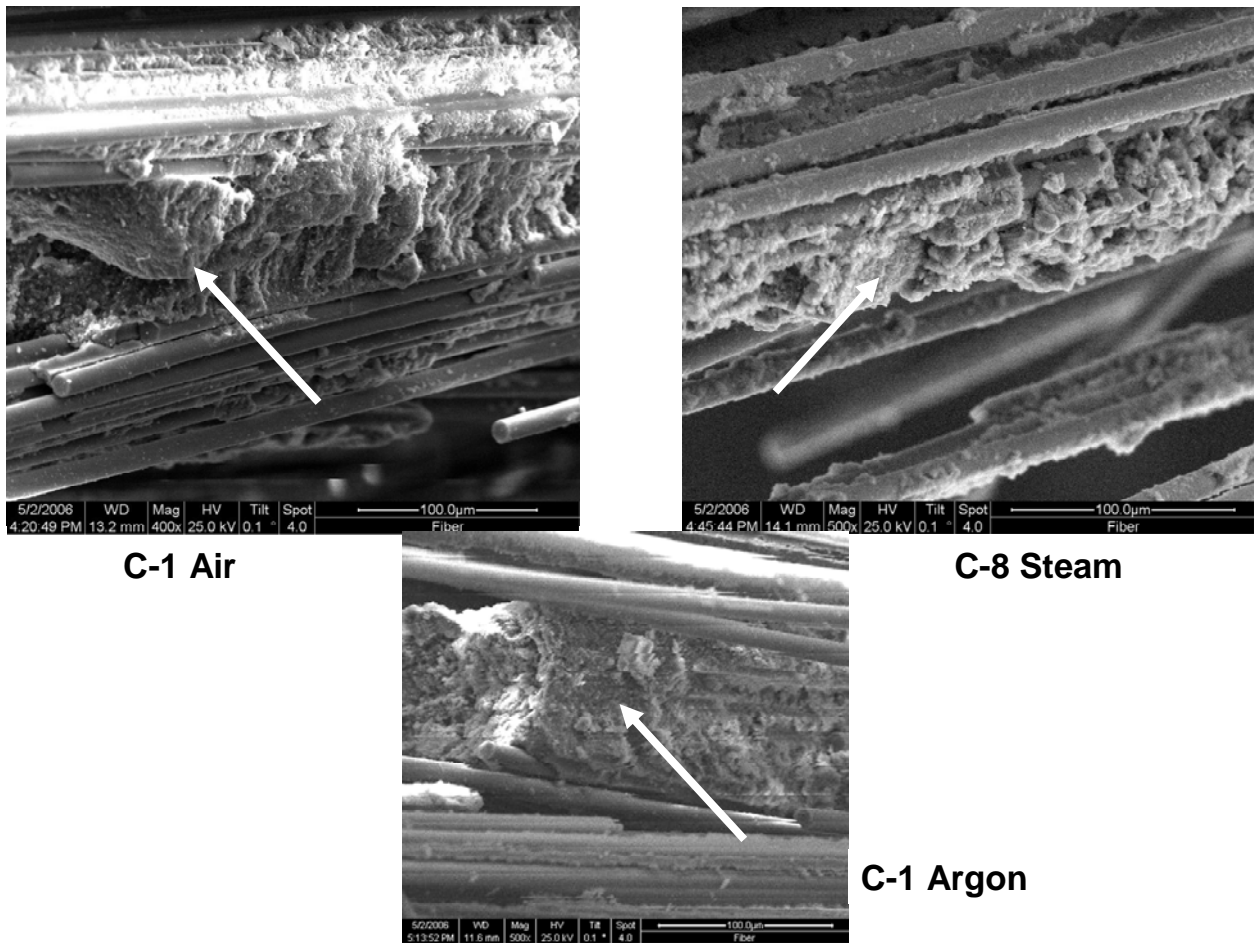
Figure 69. SEM micrographs showing locations of electron beams in the matrix for EDS analysis.

Results of the EDS qualitative analysis were evaluated in two ways. First, results obtained in a given location of the focused electron beam, in specimens tested in different environments were compared. Second, results obtained for specimens tested in a given environment, but with a different focal point within the matrix, next to and away from fibers, were compared. Results are presented in Figure 70 through Figure 74. All data was normalized to a CPS of 700 for aluminum. The normalized data can be accurately compared and contrasted on the same scale. One can observe, that post failure, a silicon peak is present in the matrix. This can be seen for each test environment and at each focal point of the electron beam. The largest amount of silicon species migration is seen in the

argon environment. In the interior of the matrix where matrix was not in contact with the fibers, very little if any silicon is observed. However, when the focal point is centered at the edge of the matrix, where matrix was in direct contact with fibers, a much larger amount of silicon is seen. A sharp increase in silicon species migration is also seen in specimens tested in the steam environment compared to the as received specimen. Note that there is more silicon present in the interior of the matrix of the C-8 specimen, tested in steam, than at the edge of the matrix of the C-11 specimen, also tested in steam but at the lower stress level. The most reasonable explanation may be specimen-to-specimen variability. The data may also be influenced by a hidden fiber and the presence of noise could cause the presence of silicon to look larger than it really is. Both specimens C-8 and C-11 show an increase of silicon in the matrix compared to the as received specimen.
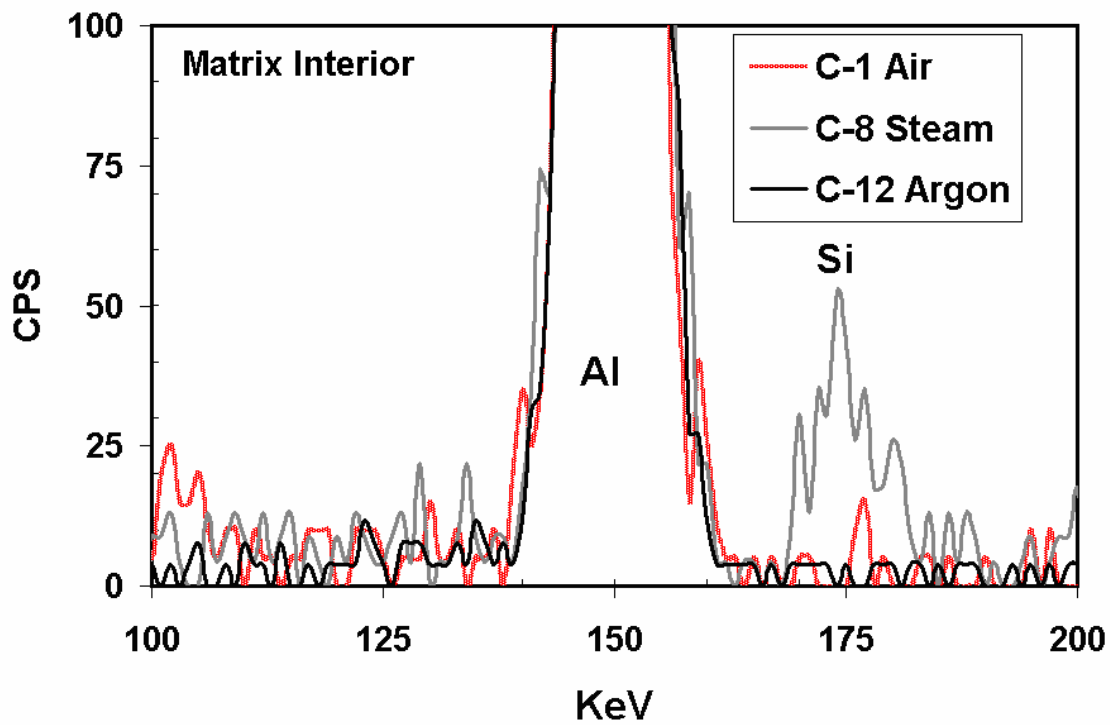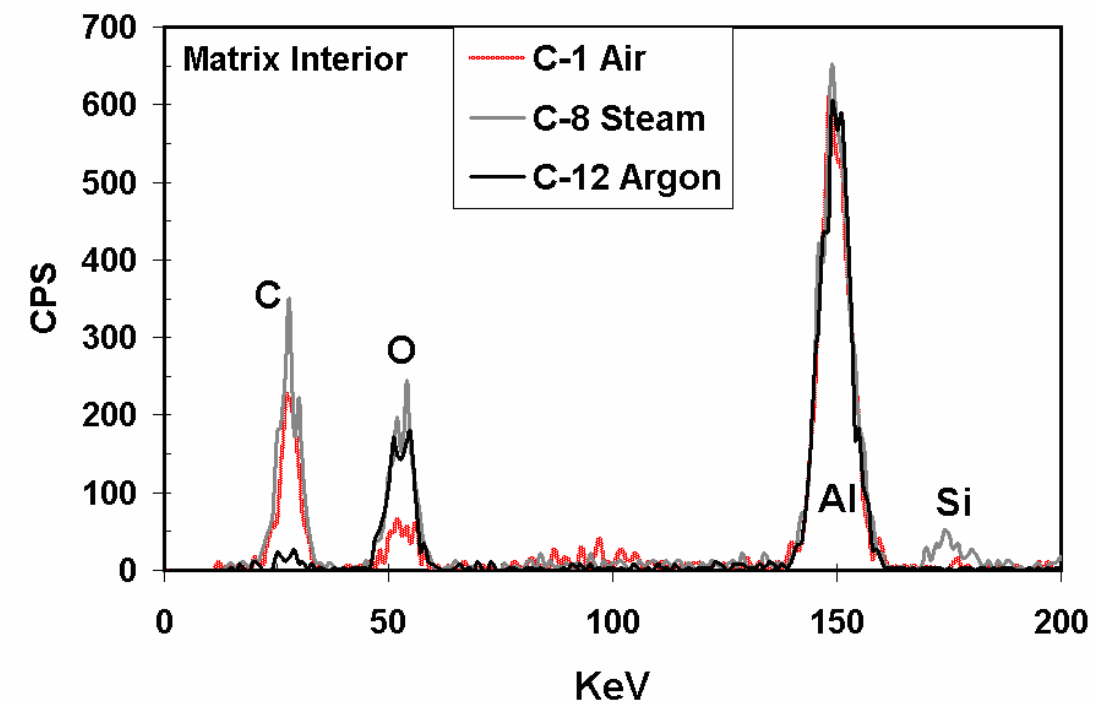
Figure 70. EDS spectra of the interior matrix in all three environments.
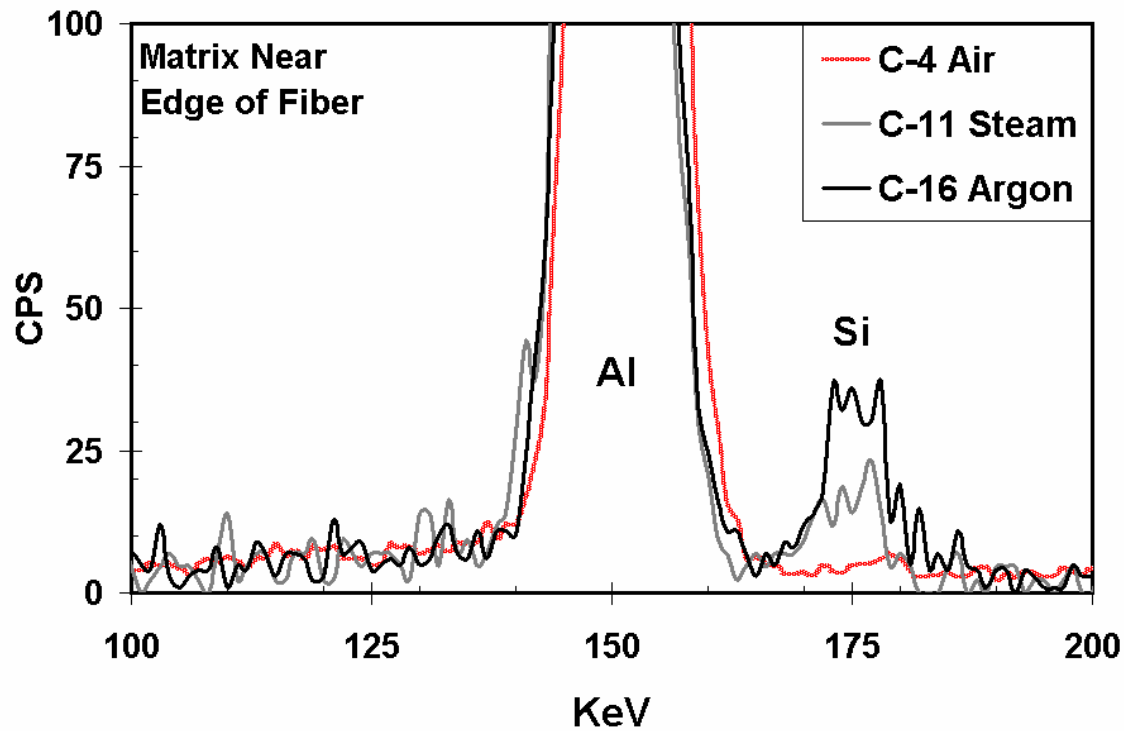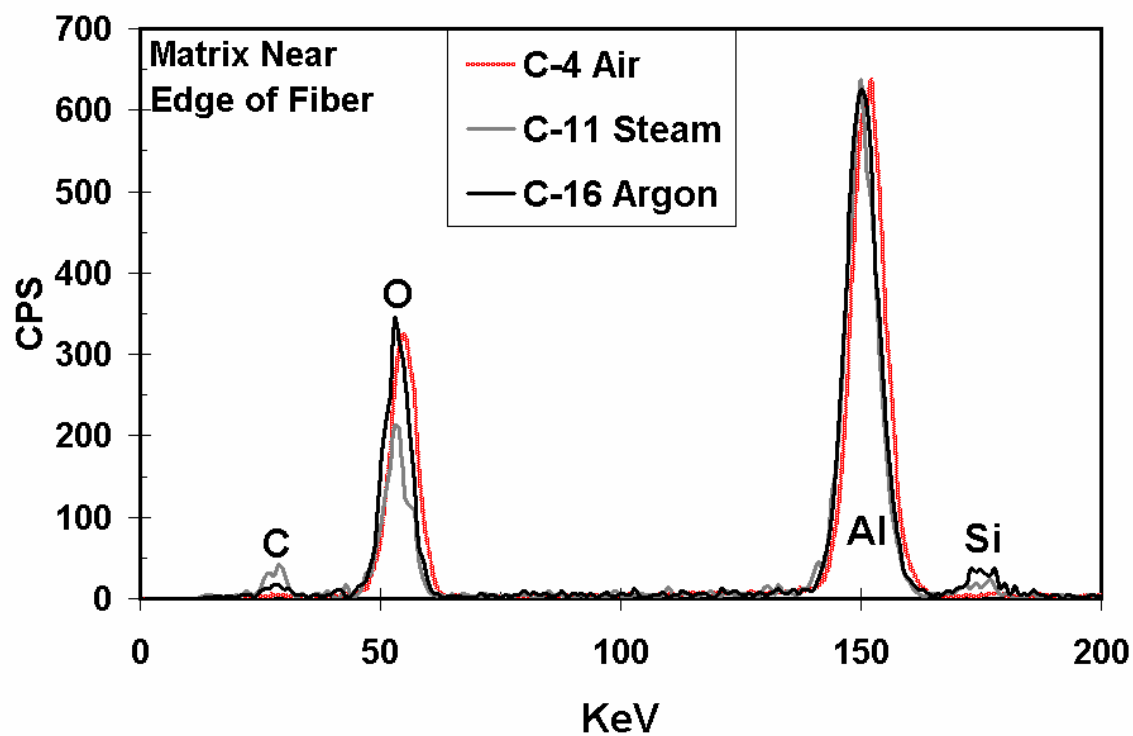
Figure 71. EDS spectra of the matrix near edge of fiber in all three environments.

Following an analysis of specimens tested in different environments, specimens tested in the same environment were examined, using different electron beam focal points. The graphs in Figure 72 to Figure 74 show the amount of silicon present in the interior of the matrix (where matrix had no direct contact with fibers) compared to that present near the edge of the matrix (where matrix was in direct contact with fibers) In air, there is little change in the amount of silicon observed in the two locations. The specimens tested in the 100% steam environment show an increase in silicon in the matrix compared to an untested specimen. Finally, in specimens tested in the argon environment, the presence of silicon goes from almost zero in the matrix interior to a large amount at the matrix edge. This indicates a significant amount of silicon species migration in the 100% argon environment. This is contradictory to how an oxide/oxide CMC should respond in an inert environment where no oxygen is present. It was assumed that migration of silicon species was enabled and/or accelerated by the presence of oxygen. The current results reveal that migration of silicon species occurs in the absence of oxygen. Apparently the presence of oxygen is not required to initiate such migration. Further study is needed to fully understand the mechanism behind this phenomenon. However, the present results are of immediate use to the CMC processing community, indicating that sintering in argon may not be desirable.
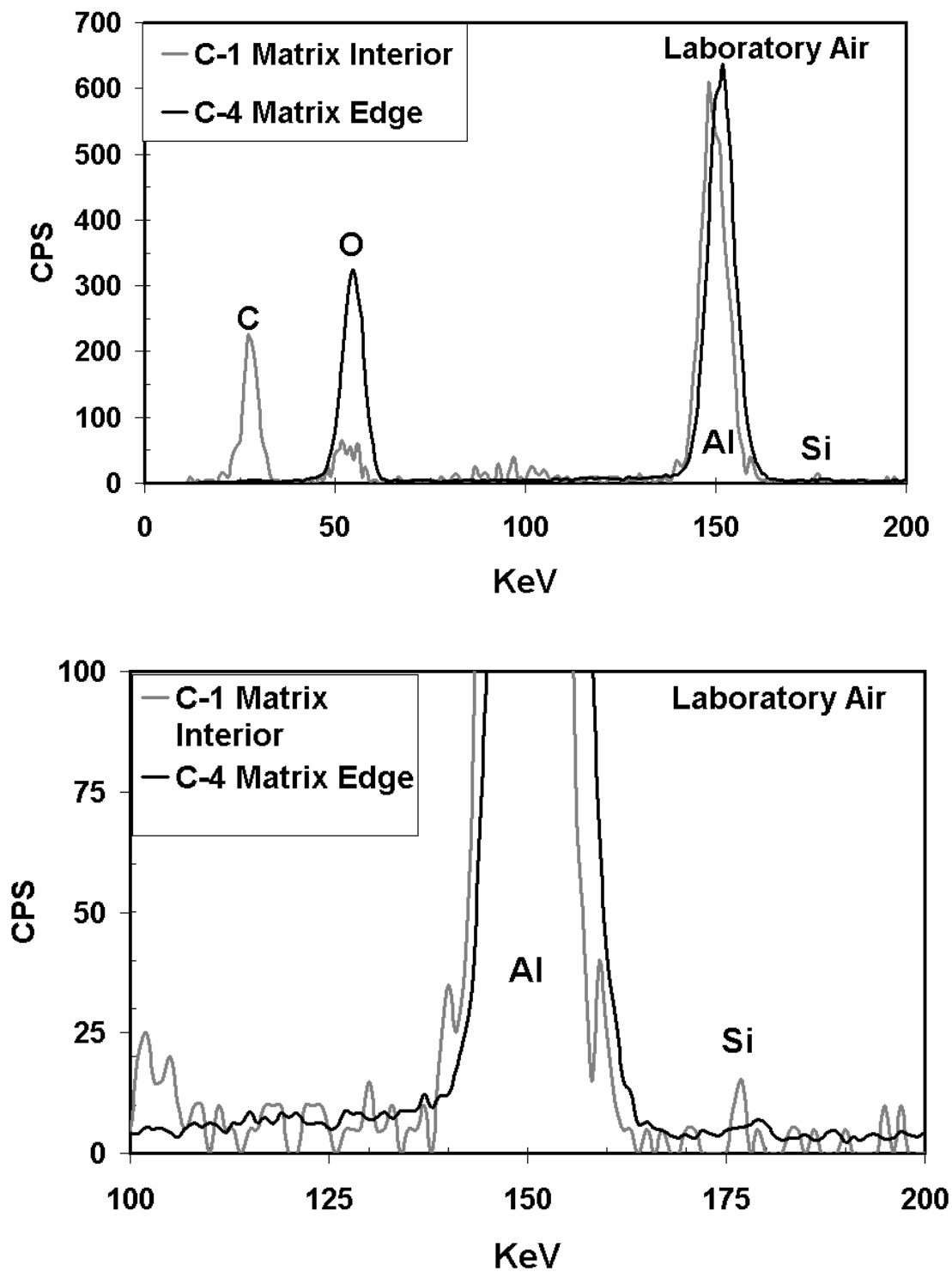
Figure 72. EDS spectra of the matrix interior compared to the spectra of the matrix edge in the specimens tested in laboratory air.
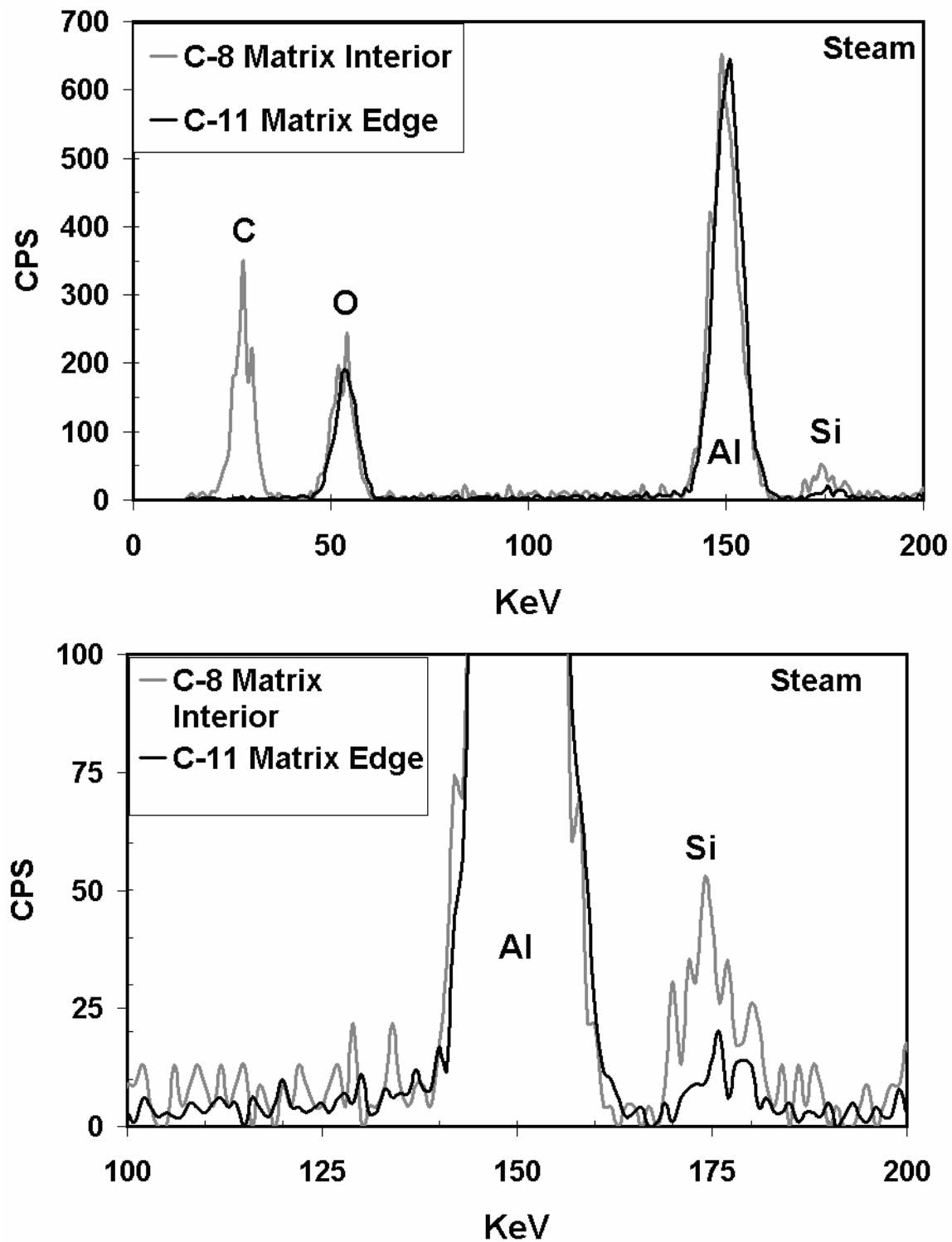
Figure 73. EDS spectra of the matrix interior compared to the spectra of the matrix edge in the specimens tested in 100% Steam.
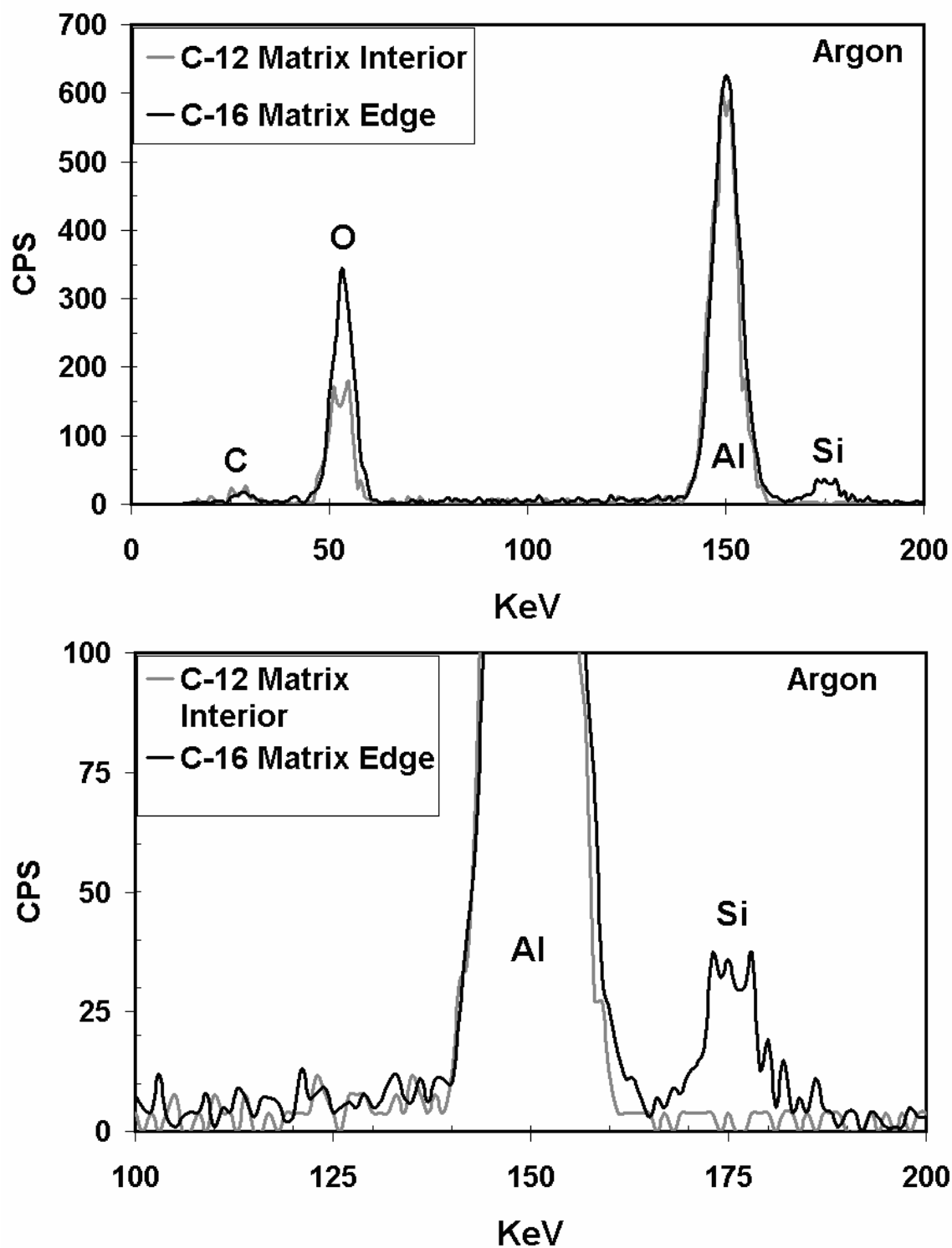
Figure 74. EDS spectra of the matrix interior compared to the spectra of the matrix edge in the specimens tested in 100% argon.

In prior investigation, Mehrman [22] conducted EDS analysis of N720/A specimens tested in fatigue at 1200°C in air and in steam. Mehrman [22] found that the highest amount of silicon species migration occurred at the fiber/matrix interface of the specimens tested in steam [22:82].
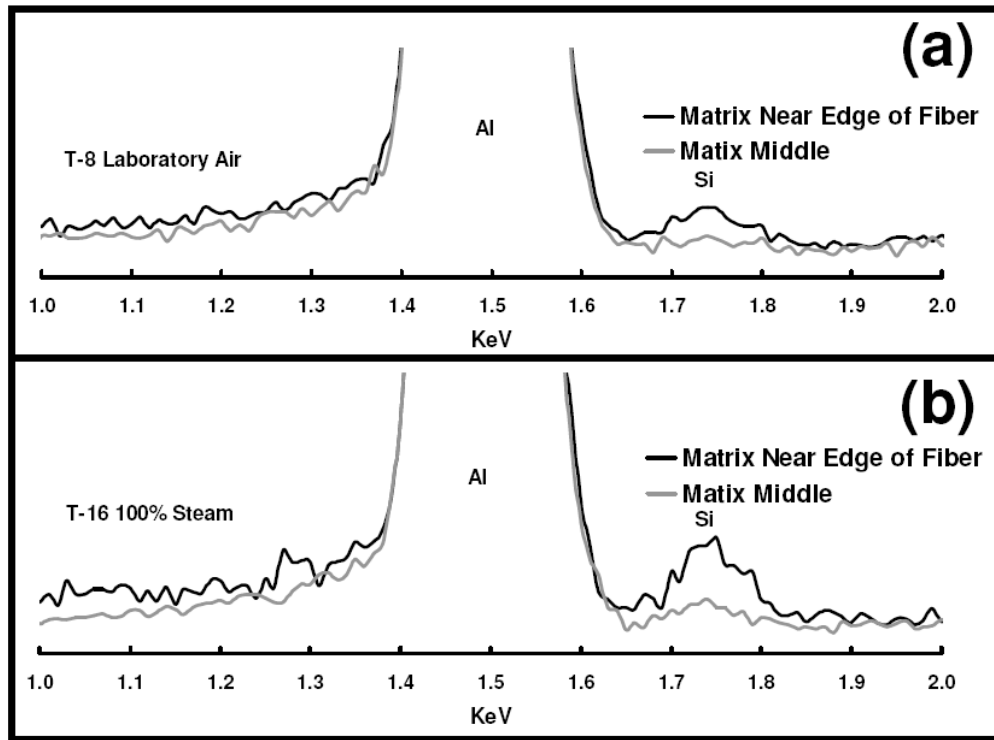
Figure 75. EDS spectra of the matrix near the fiber edge of N720/A CMC compared to the spectra of matrix ~25μm away form the fiber edge tested in: (a) laboratory air and (b) steam environment [22:83].

Wannaparhun et al. [38] as well as Mehrman [22] believed that the presence of oxygen was directly responsible for the migration related to silicon. This research shows that the highest levels of silicon species migration occurred in a 100% argon environment, where no oxygen was present. This research indicates that the lack of oxygen in the environment may be responsible for the migration of silicon species from the fiber to the matrix.

VI.   Conclusions and Recommendations

6.1   Conclusions

This research effort evaluated the creep-rupture behavior of Nextel[TM] 720/A with a ±45˚ fiber orientation in air, steam, and argon environments. Mechanical tests were preformed to determine the creep response of the CMC. Then, the composite microstructure was analyzed using an optical microscope and an SEM. Finally, a qualitative spectroscopy analysis was performed using an EDS. Results of this research show that the ±45° N720/A cross-ply exhibits a much lower creep strength compared to the 0/90° N720/A cross-ply.

6.1.1   Mechanical Behavior

Monotonic tensile tests were performed in order to determine the ultimate tensile strength of the ±45˚ N720/A cross-ply. The UTS was approximately 55 MPa, the elastic modulus was 46 GPa, and the failure strain was 0.265%.

The creep-rupture tests were performed in three different environments: laboratory air, 100% steam, and 100% argon. Creep stress levels were 45, 40, 35, and 15 MPa. Results revealed that the applied stress governs the damage accumulation which leads to a decrease in creep life.

The shortest creep life was produced at the highest stress of 45 MPa. Duration of all 45 MPa creep tests were less than 2 min. Furthermore, tertiary creep developed early in these tests. The 40 MPa test conducted in air survived for 23 h. All creep tests conducted at creep stress levels of 40 MPa failed much sooner. Mechanical tests ≤ 35 MPa achieved run-out conditions of 100 h. These tests all exhibited primary creep and

secondary creep regimes. The tests conducted at 35 MPa accumulated the largest creep strains.

For a given creep stress, specimens tested in the laboratory air environment produced lower creep rates then specimens tested in other environments. Tests conducted in the 100% argon environment produced higher creep rates, but similar creep lives compared to specimens tested at the same creep stress in air and in steam. Environment did not appear to have a significant influence on the creep life of ±45° specimens. The results suggest that the presence of an oxidizing environment, such as steam, causes degradation of the fiber rather than degrading the matrix. The highest creep-rates and the largest creep strains were produced in the 100% argon environment. No oxidation could occur in 100% argon. In conclusion, N720/A composites with a ±45˚ fiber orientation exhibited relatively good creep resistance, regardless of environment, at 1200˚C at stresses ≤ 35 MPa. At stresses above 35 MPa creep resistance was poor, but independent of the test environment.

6.1.2   Composite Microstructure

Fractography was performed using both the optical microscope and the SEM in order to examine and characterize the fracture surfaces produced in creep-rupture tests. The optical microscope showed that each specimen exhibited a V shaped fracture surface. However, this type of fracture surface was not produced in 35 MPa tests conducted in steam and argon where large creep strains were accumulated. These specimens showed a flatter fracture surface. The fractography also revealed that the overall larger damage areas were found in specimens tested in a 100% argon environment.

The SEM examination allowed for a more detailed analysis of the fracture surfaces. The prevailing microstructural features were: "waviness," fiber pullout and fiber fracture, coordinated planar fracture of fiber bundles, micro cracking of the matrix between the fiber bundles, and micro-cracking of the matrix between the individual fibers. Similar features were observed in each specimen regardless of the applied stress or test environment. Matrix degradation appears to be the main cause of specimen failure. In the air and steam environments, the matrix appeared to densify and maintain its original shape through micro-cracking and fiber failure. The matrix observed in the argon environment appeared to be more porous and loosely packed. More matrix cracks were found in specimens tested in the argon environment.

6.1.3   Spectroscopy

The qualitative EDS analysis showed evidence of silicon species migration from the mullite phase of the fiber to the alumina matrix. This was most prominently seen in steam and in argon (where oxygen was not present). Mehrman [22] previously theorized that the presence of an oxidizing environment was directly related to silicon species migration. However, Mehrman only collected data in air and in steam environments. The qualitative analysis performed in this research examined specimens tested in air, steam, and argon environments and revealed that larger amounts of silicon species migration occurred not in an oxidizing environment, but in an oxygen-deprived environment. Larger amounts of silicon species migration observed in steam and in argon suggest that depletion of the mullite phase of the fiber occurs in these environments. This depletion of the mullite phase may be the mechanism behind the degraded creep performance of the material in these environments.

94

6.2   Recommendations

Each new discovery on the effects of environment and fiber orientation of creep behavior of N720/A composite brought new questions to be answered. Although much was learned about the effect of the ±45° fiber orientation on creep resistance of N720/A, there is still much to be explored. First, N720/A performs differently in each environment. Harlan [13] reported that the presence of steam significantly reduced the creep resistance [13:70]. This research did not reveal a dramatic effect of steam on creep behavior. Further research must be conducted to understand why steam affects the strength of the fibers more than the strength of the matrix. In addition, ±45° N720/A cross-ply displayed the shortest creep life and the largest creep strains when tested in the argon environment. As an oxide/oxide CMC, N720/A should perform best in a zero oxygen environment. Why did the presence of argon cause such drastic increase in creep rates and creep strain accumulations? The only way to answer this question is to perform more tests on the N720/A composite in a 100% argon environment using both 0/90° and ±45° specimens.

This research included a thorough EDS analysis which determined that silicon species were migrating from the mullite phase of the fiber to the alumina matrix. Mehrman [22] suggested that migration occurred because of the oxidizing environment [22:85]. The EDS analysis performed here shows that migration occurs not only in steam, but also in argon, where no oxygen is present. A more thorough EDS analysis of polished specimens should be conducted to try and quantify the amount of silicon species migration in laboratory air, steam, and argon environments. This type of EDS analysis should be carried out using a Transmission Electron Microscope (TEM) in order to get

more accurate data. A TEM should also be used to analyze and identify any grain structure differences in specimens tested in different environments and the as-received material. With the use of a TEM, one can try to understand the changes, which occur within the grains as the silicon leaches from the mullite phase of the fiber, as well as any changes in the grain size that may occur under different loading conditions. In addition, further micro-structural analysis should be performed to determine the effects of loading and environment on the density of the alumina matrix. The density of the matrix is directly related to the damage tolerance of the material.

One possible solution to increasing the strength of the N720/A CMC with the ±45° fiber orientation would be to use fiber coating. Saruhun et al. [32] demonstrated a process for coating N720 fiber in fabric form with carbon using a CVD process. They believe that a fugitive carbon/oxide double layer system would improve crack deflection and fiber sliding. However, addition of an interphase coating to the material would increase the overall cost of the CMC. The N720/A composite offers high strength at a lower cost compared to other CMCs.

Appendix A: Detailed Test Summary

Table 13. Detailed test summary.

Specimen #	Test	Enviroment	Creep Stress Mpa	E Gpa	Time to Failure hr	e_{fail} %	$e_{thermal}$ %	Accumulated Creep Strain %	$a_{thermal}$ 1/C	Residual Strength Mpa
T-1	Tensile	air	54.9	46	0.009	0.265	0.76	NA	6.00E-06	NA
C-1	Creep	air	45	45.8	0.033	1.48	0.67	0.65	6.00E-06	NA
C-2	Creep	air	15	46.1	100	0.161(in tension)	0.66	3.38	6.00E-06	61.07
C-3	Creep	air	35	45.9	100	0.161(in tension)	0.60	13.30	5.00E-06	61
C-4	Creep	air	40	48.1	52.000	12.07	0.63	11.08	6.00E-06	NA
C-8	Creep	steam	45	45.2	0.016	0.712	1.34	0.65	1.30E-04	NA
C-9	Creep	steam	15	44.2	100	0.147(in tension)	0.90	4.80	8.00E-04	67
C-10	Creep	steam	35	43.9	100	0.16(in tension)	0.82	16.52	9.00E-04	53.4
C-11	Creep	steam	40	41.3	0.733	5.07	0.80	5.05	9.00E-04	NA
C-12	Creep	argon	45	44.2	0.006	4.07	0.85	3.72	7.00E-04	NA
C-13	Creep	argon	30	47	2392	NA	1.18	4.46	7.00E-04	NA
C-14	Creep	argon	40	43.5	0.009	2.59	0.88	2.36	8.00E-04	NA
C-15	Creep	argon	15	49.4	100	0.10(in tension)	0.76	5.67	6.00E-04	73.04
C-16	Creep	argon	35	47	100	.024(in tension)	0.78	20.9	6.00E-04	49.39
C-17	Creep	argon	45	45	0.000	0.2	0.83	0.72	6.00E-04	NA
C-18	Creep	argon	40	48.8	0.867	3.78	0.9	3.58	7.00E-04	NA

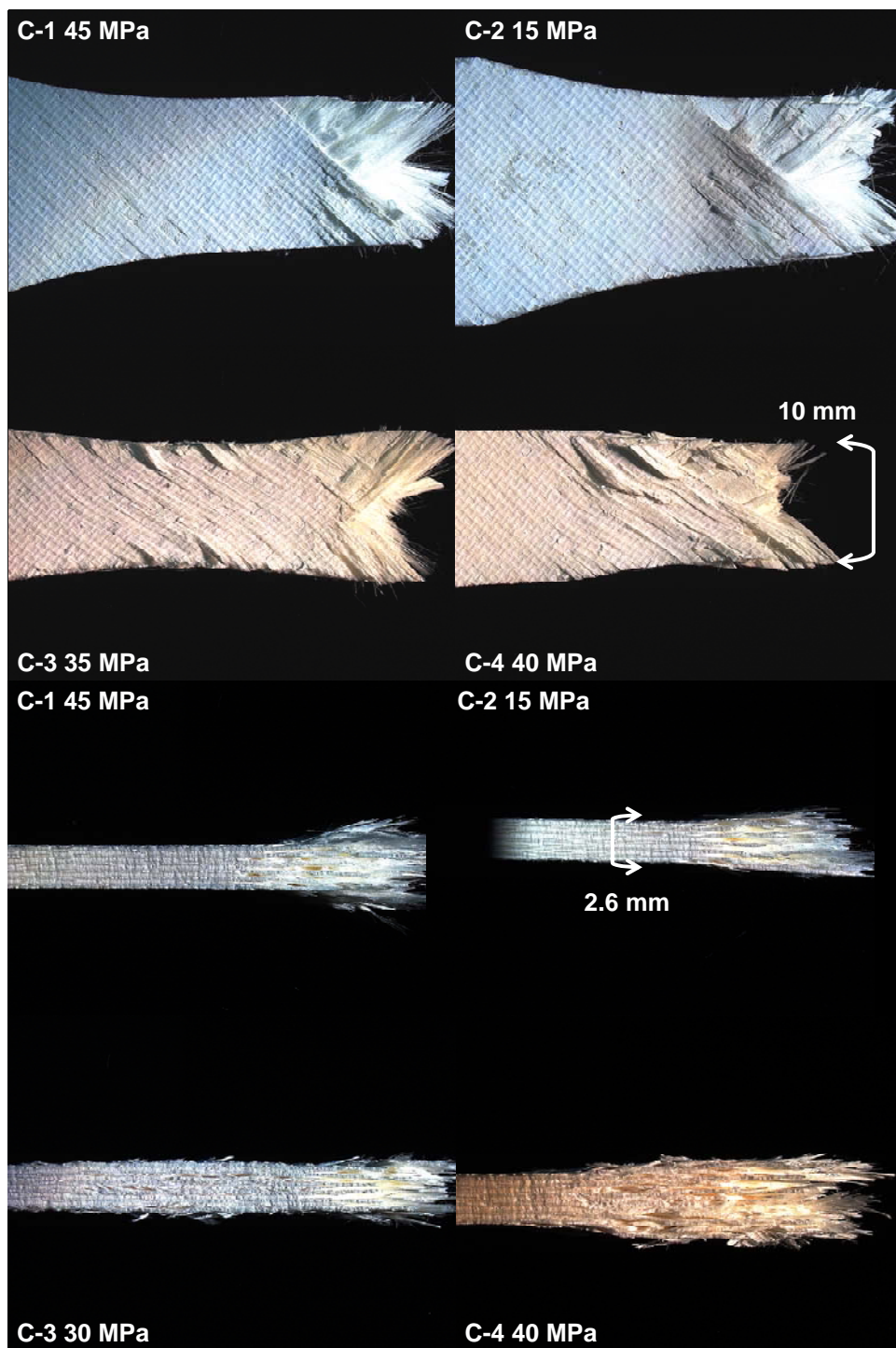**Appendix B: Additional Microstructure Figures**

Figure 76. Fracture surfaces of Nextel[TM]**720/alumina CMC specimens tested in creep at 1200°C in laboratory air environment.**
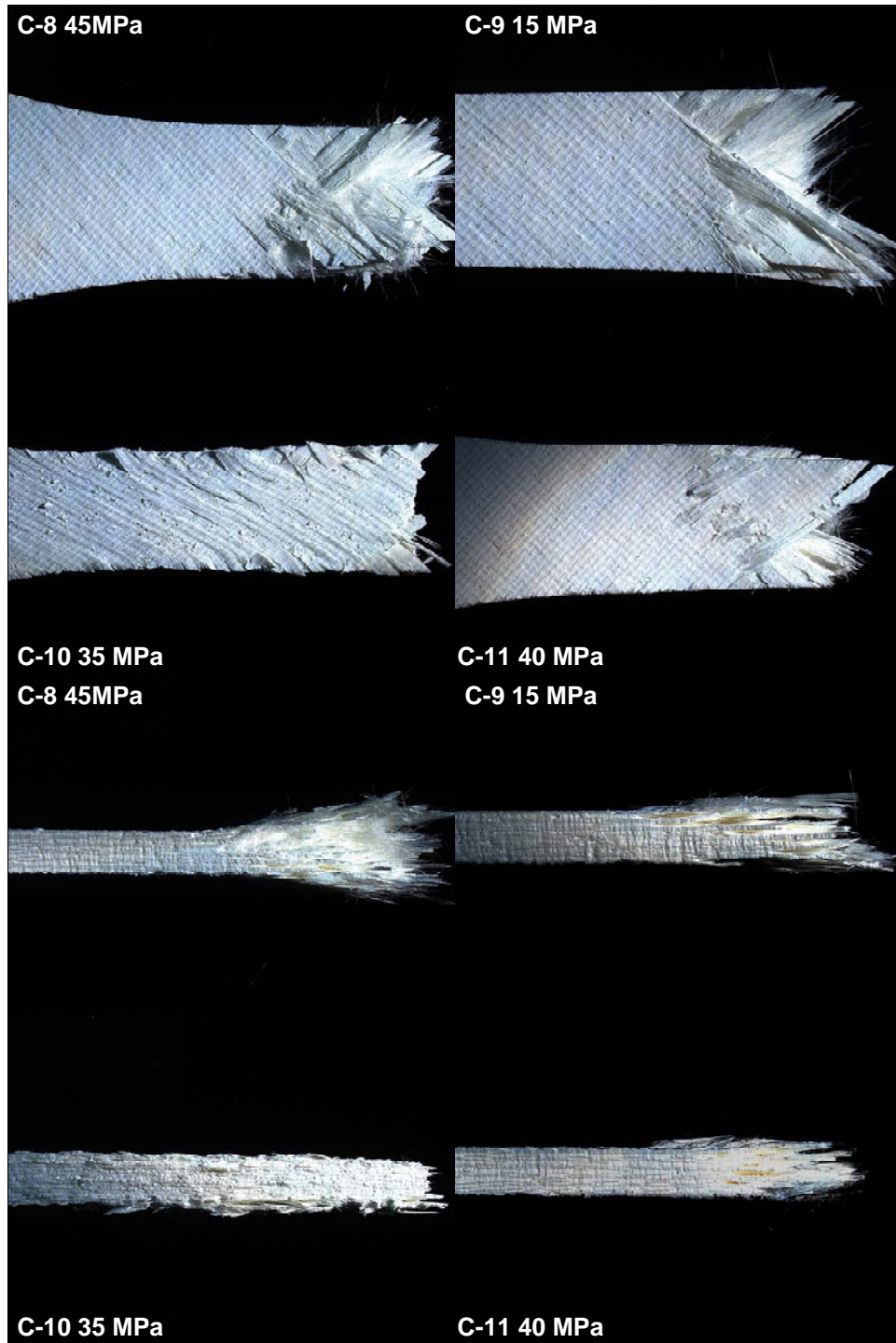
Figure 77. Fracture surfaces of Nextel[TM]720/alumina CMC specimens tested in creep at 1200°C in 100% steam environment.

C-12 45 MPa   **C-14 40 MPa**   **C-15 15 MPa**

C-16 35 MPa   **C-17 45 MPa**   **C-18 40 MPa**

C-12 45 MPa   **C-14 40 MPa**   **C-15 15 MPa**

C-16 35 MPa   **C-17 45 MPa**   **C-18 40 MPa**
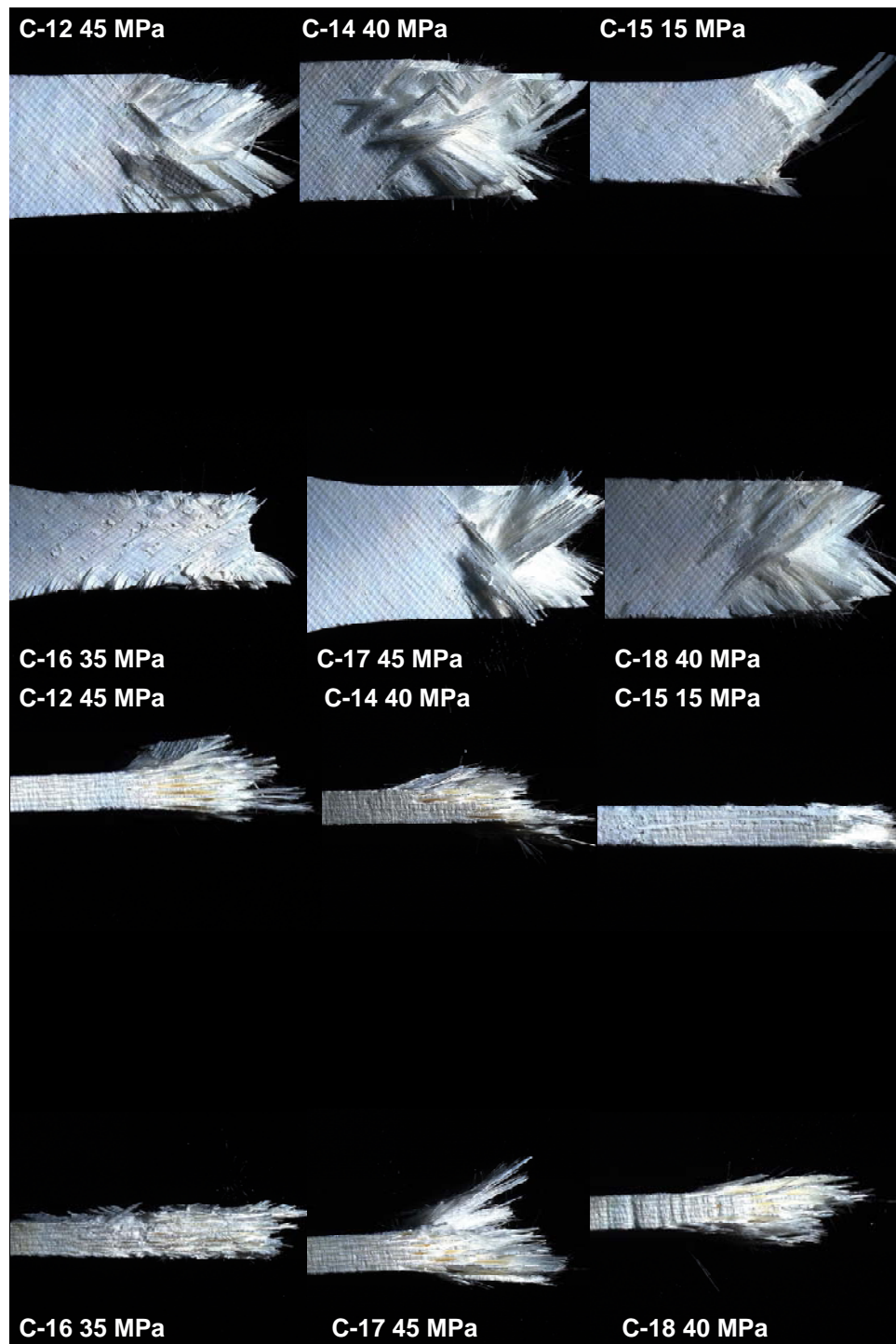
Figure 78.Fracture surfaces of Nextel^{TM}720/alumina CMC specimens tested in creep at 1200°C in 100% argon environment.

Figure 79. Micrograph of Nextel^{TM}720/alumina CMC specimen C-1 tested in creep at 45 MPa at 1200°C in laboratory air environment.

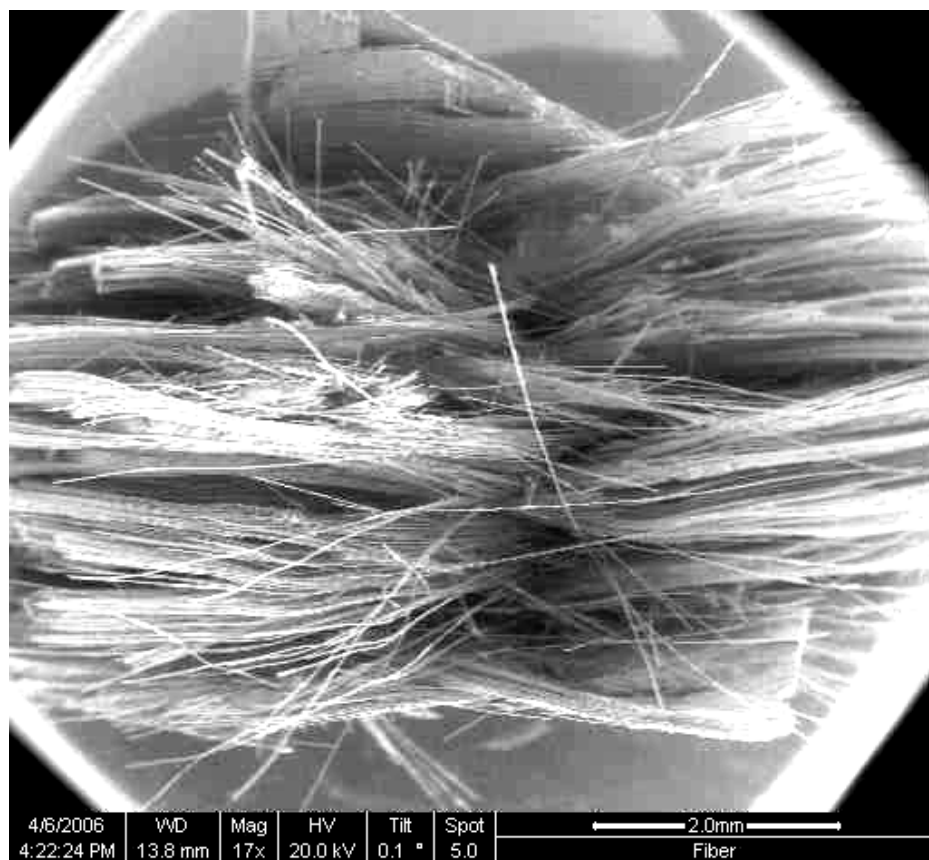**Figure 80. Micrograph of Nextel^{TM}720/alumina CMC specimen C-1 tested in creep at 45 MPa at 1200°C in laboratory air environment: (a) coordinated fiber bundle, (b) individual fiber pullout with large matrix particles found on fiber.**

Figure 81. Micrograph of Nextel^{TM}720/alumina CMC specimen C-2 tested in creep at 15 MPa at 1200°C in laboratory air environment: intact matrix surrounding broken fiber.

Figure 82. Micrograph of Nextel^{TM}720/alumina CMC specimen C-3 tested in creep at 35 MPa at 1200°C in laboratory air environment: intact fiber bundle layers.

(a) 4/11/2006 | 4:37:20 PM | WD 12.6 mm | Mag 1000x | HV 25.0 kV | Tilt 0.1° | Spot 4.5 | 100.0μm | Fiber

(b) 4/11/2006 | 4:35:17 PM | WD 12.5 mm | Mag 500x | HV 25.0 kV | Tilt 0.0° | Spot 4.5 | 200.0μm | Fiber
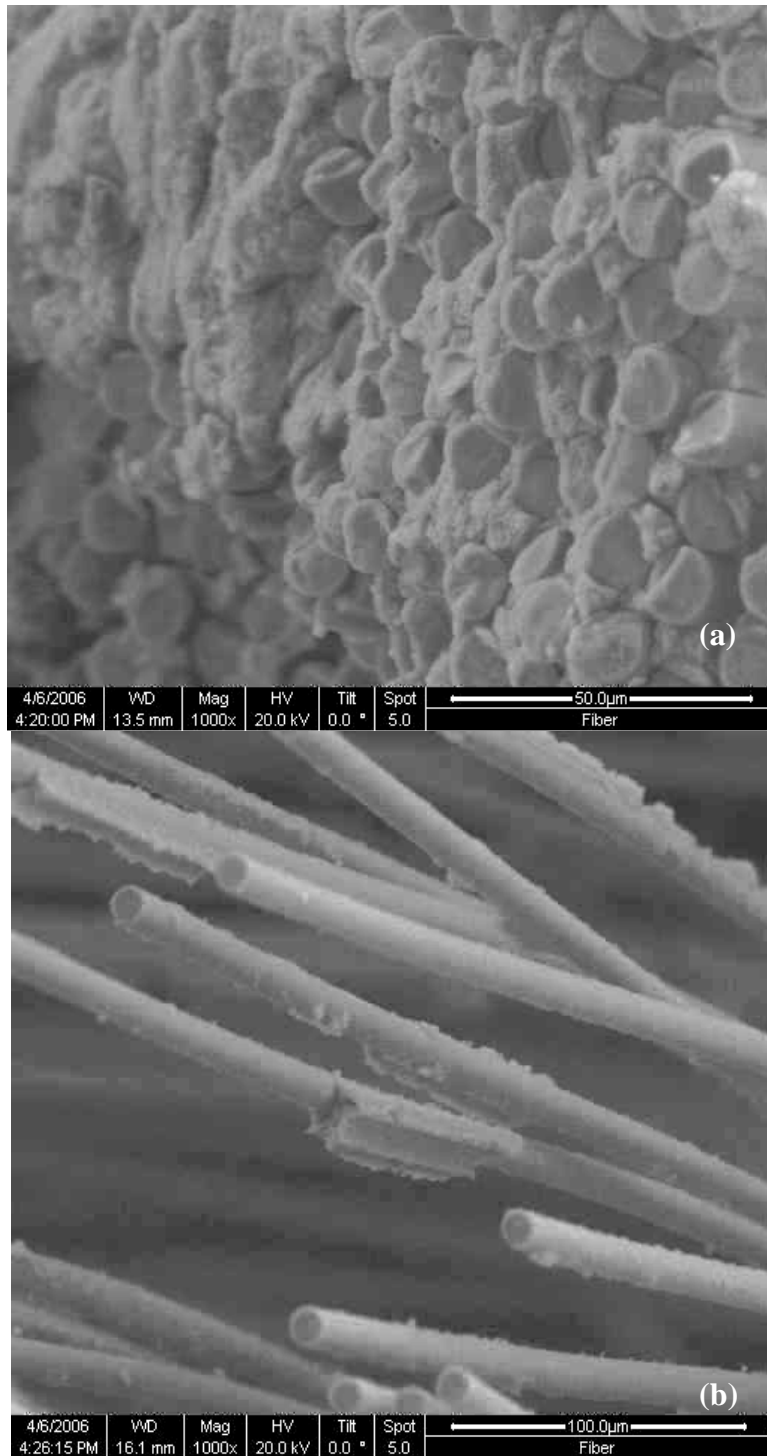
Figure 83. Micrograph of Nextel^{TM}720/alumina CMC specimen C-3 tested in creep at 35 MPa at 1200°C in laboratory air environment: (a) coordinated bundle failure, (b) matrix between fiber bundles with some fiber pullout.
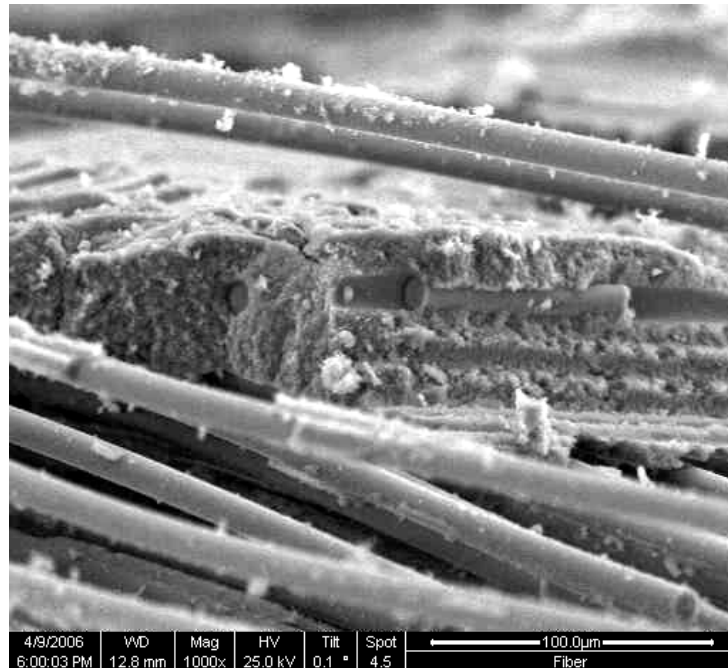
Figure 84. Micrograph of Nextel™720/alumina CMC specimen C-4 tested in creep at 15 MPa at 1200°C in laboratory air environment: (a) shows "waviness" and intact matrix attached to fiber, (b) individual fiber pullout with matrix particles.
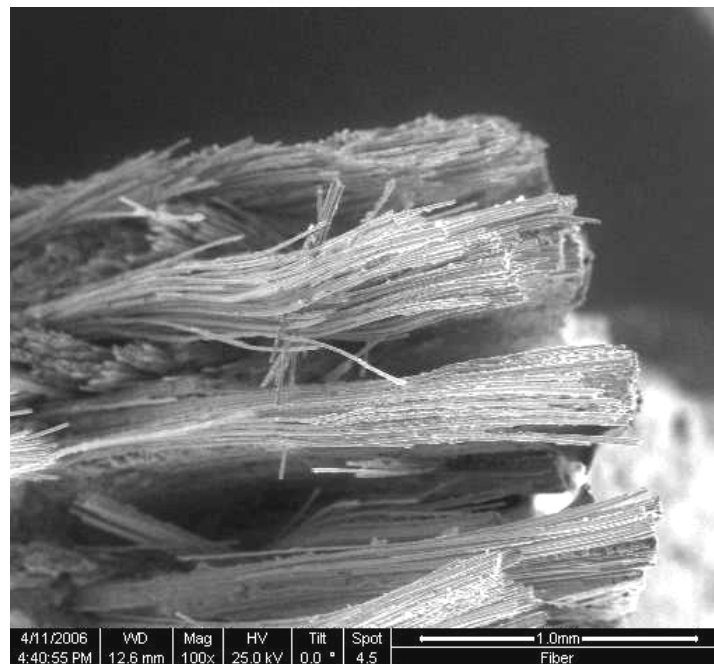
(a)
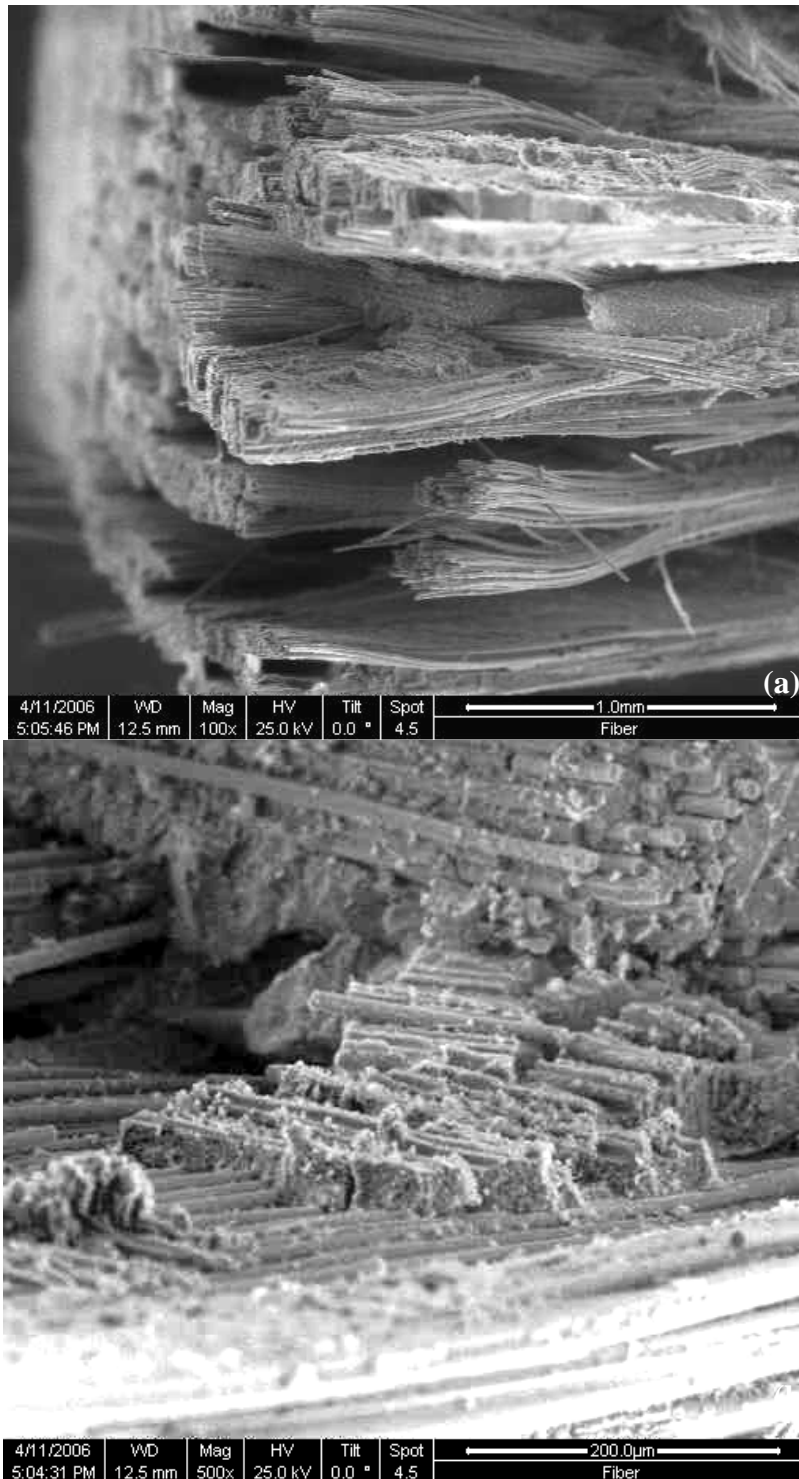
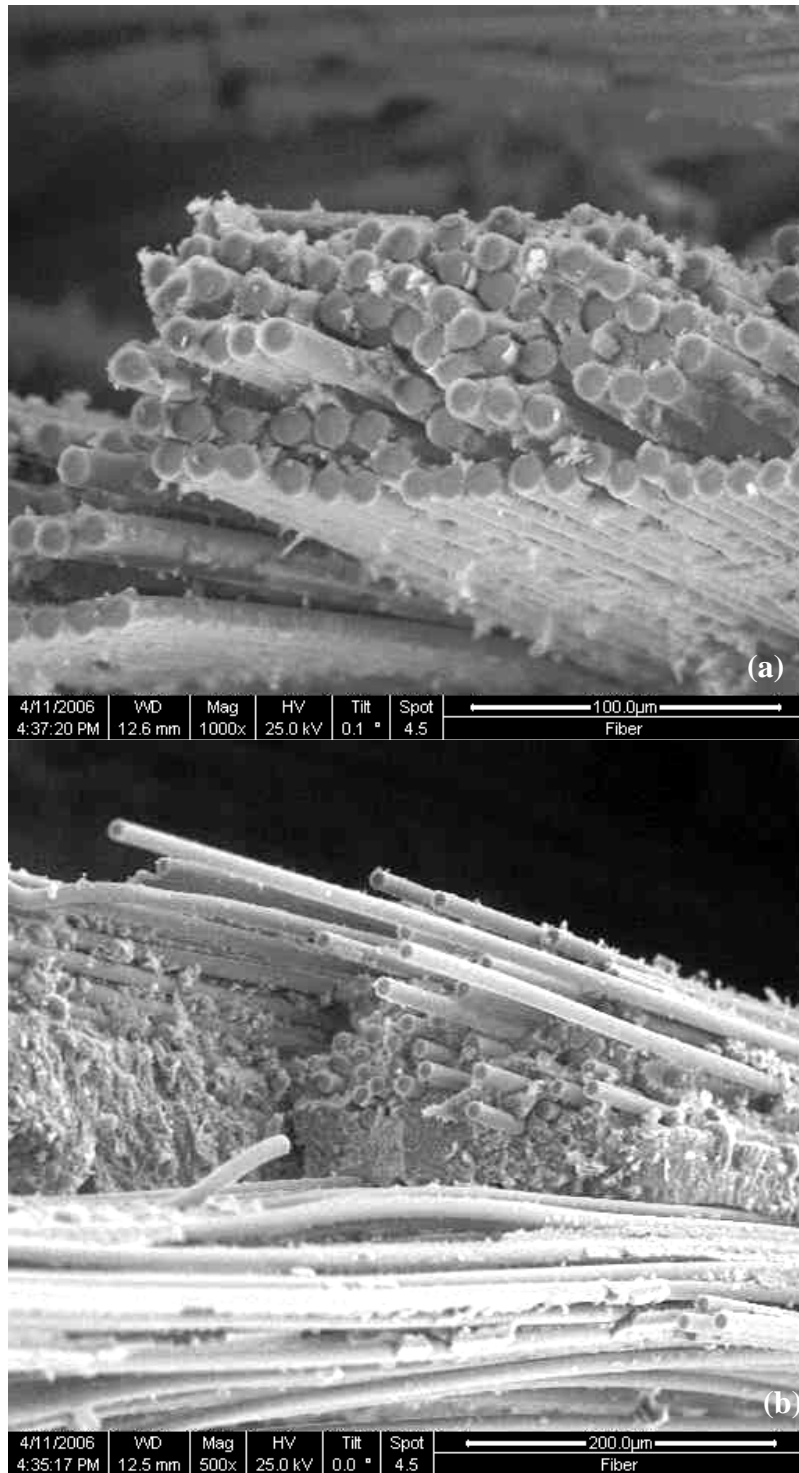**Figure 85. Micrograph of Nextel^{TM}720/alumina CMC specimen C-4 tested in creep at 15 MPa at 1200°C in laboratory air environment: (a) fiber layers separated by matrix, (b) matrix with where fibers have pulled away.**

Figure 86. Micrograph of Nextel^{TM}720/alumina CMC specimen C-8 tested in creep at 45 MPa at 1200°C in 100% steam environment: (a) degradation of matrix separating fibers, (b) large fiber bundles pulled apart.

Figure 87. Micrograph of Nextel^{TM}720/alumina CMC specimen C-9 tested in creep at 15 MPa at 1200°C in 100% steam environment: (a) individual fiber pullout covered in matrix, (b) coordinated bundle failure with some pullout and matrix separating fibers.
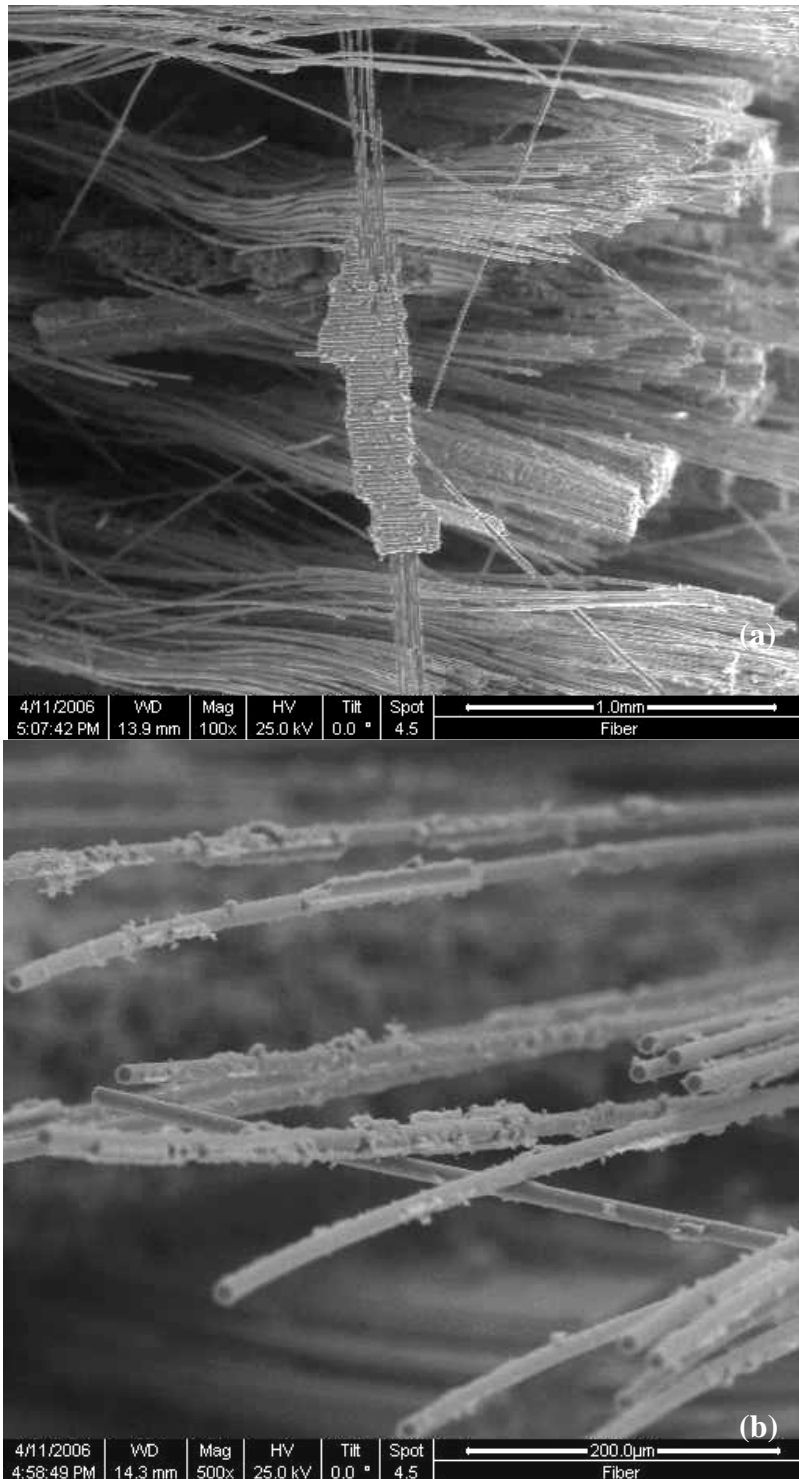
Figure 88. Micrograph of Nextel^{TM}720/alumina CMC specimen C-9 tested in creep at 15 MPa at 1200°C in 100% steam environment: shows intact fiber bundles and layers separated by matrix.

Figure 89. Micrograph of Nextel™720/alumina CMC specimen C-10 tested in creep at 35 MPa at 1200°C in 100% steam environment: (a) "waviness" in fiber bundles, (b) fiber pullout.
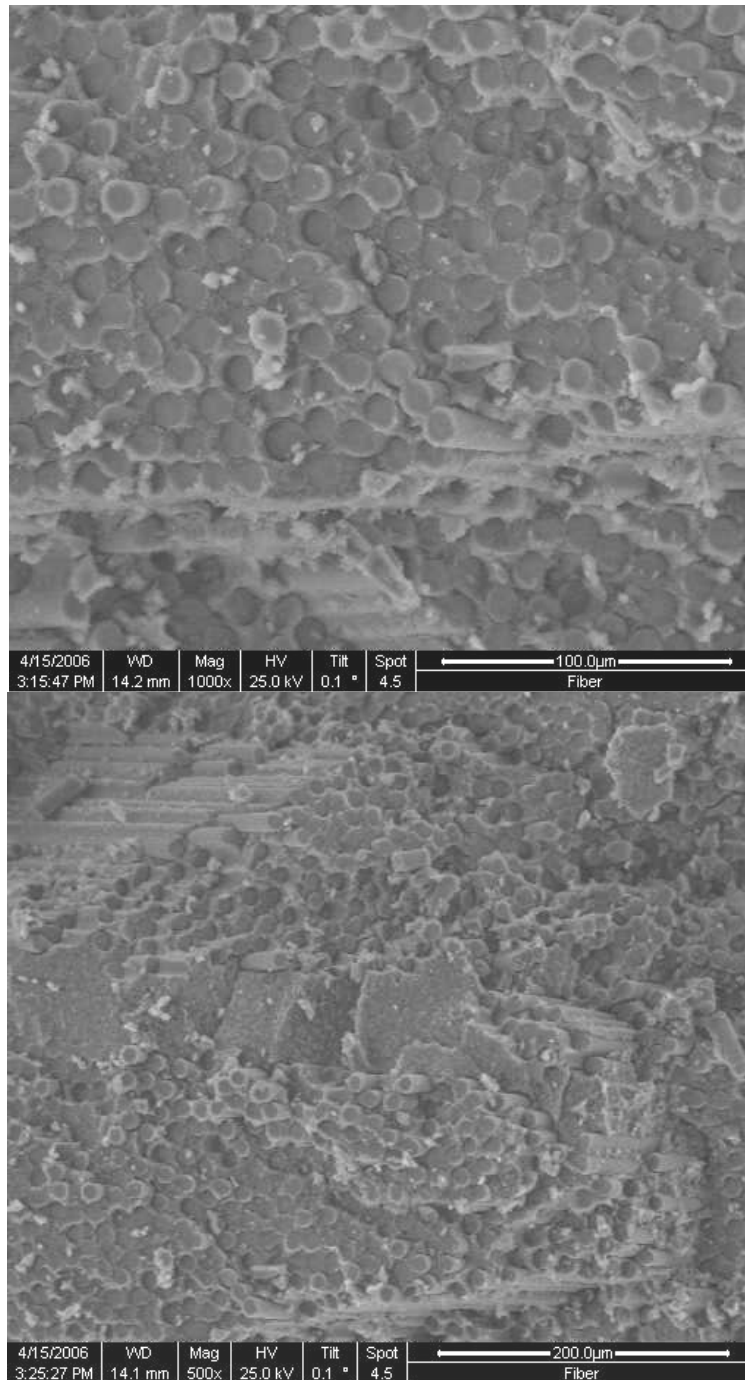
Figure 90. Micrograph of Nextel^{TM}720/alumina CMC specimen C-10 tested in creep at 35 MPa at 1200°C in 100% steam environment: closely packed fibers with littlie separation of pullout.

Figure 91. Micrograph of Nextel^{TM}720/alumina CMC specimen C-11 tested in creep at 40 MPa at 1200°C in 100% steam environment: (a) fiber bundle with individual fiber pullout, (b) breakdown of matrix separating fibers.

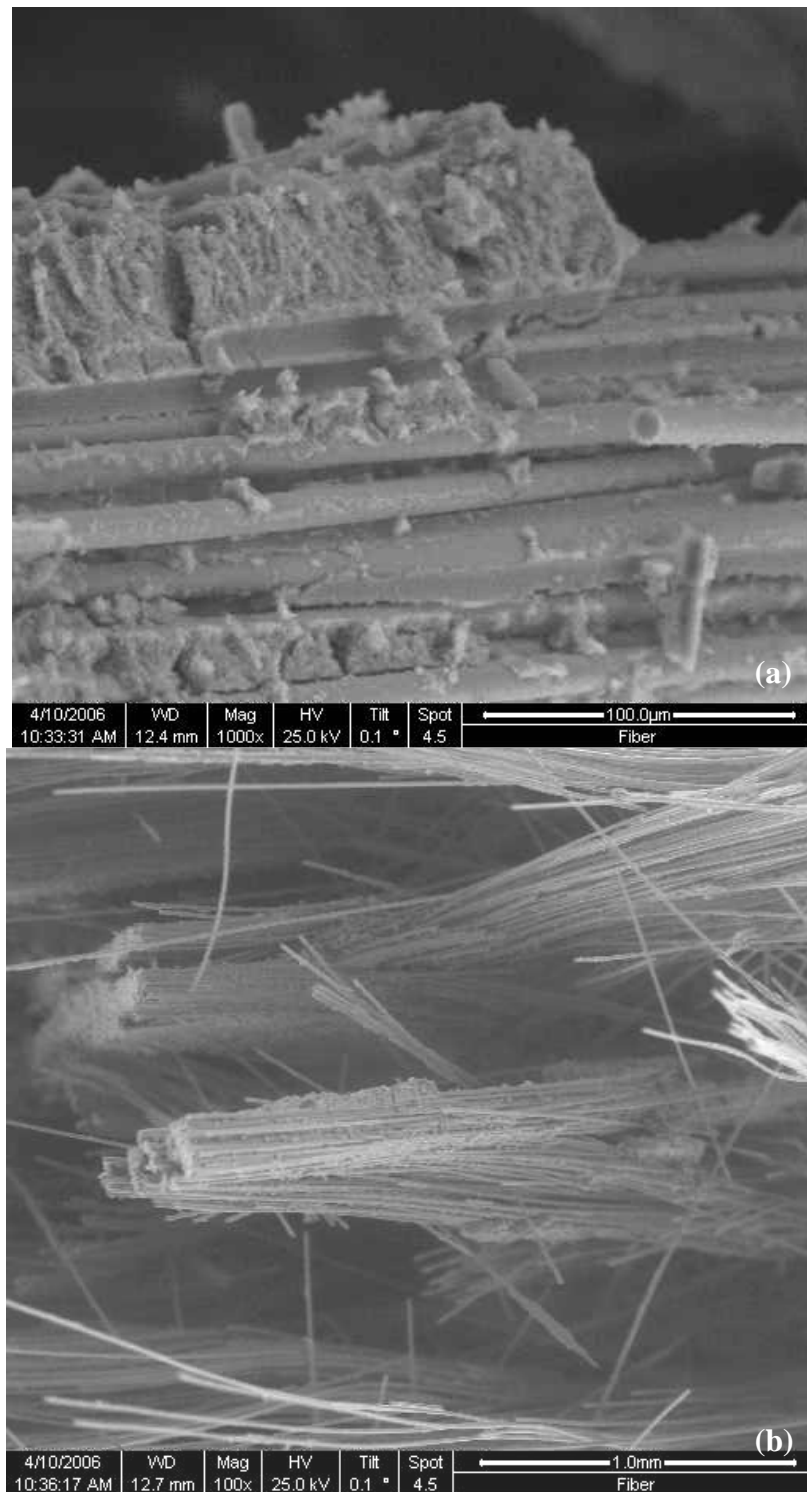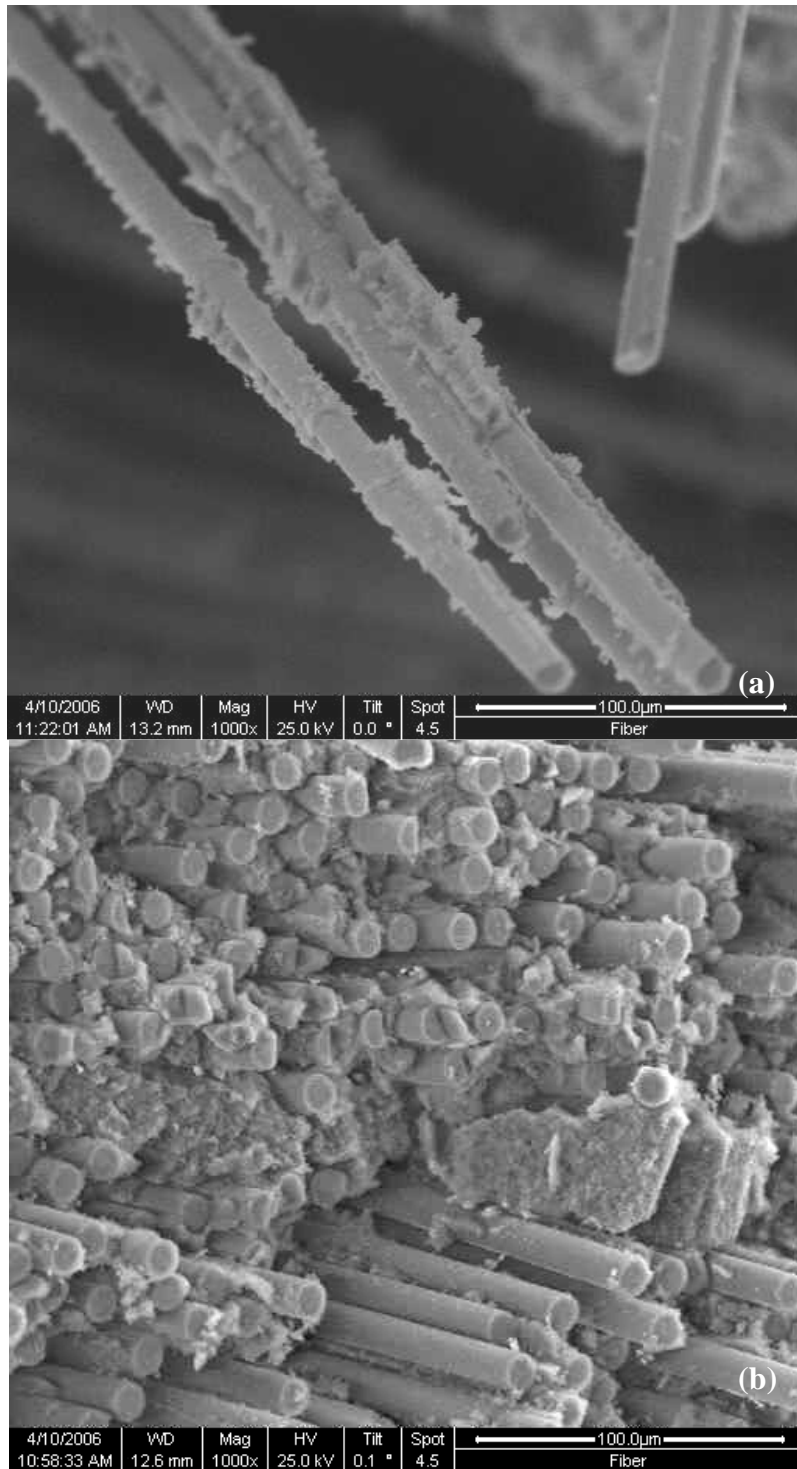**Figure 92. Micrograph of Nextel^{TM}720/alumina CMC specimen C-11 tested in creep at 40 MPa at 1200°C in 100% steam environment: (a) matrix with a large crack propagating through it and no fibers, (b) matrix concentration on fiber bundle.**

(a)

| 4/17/2006 | WD | Mag | HV | Tilt | Spot | 100.0µm |
| 11:50:20 AM | 12.8 mm | 1000x | 25.0 kV | 0.1 ° | 4.5 | Fiber |

(b)

| 4/17/2006 | WD | Mag | HV | Tilt | Spot | 1.0mm |
| 11:47:00 AM | 13.4 mm | 100x | 25.0 kV | 0.1 ° | 4.5 | Fiber |

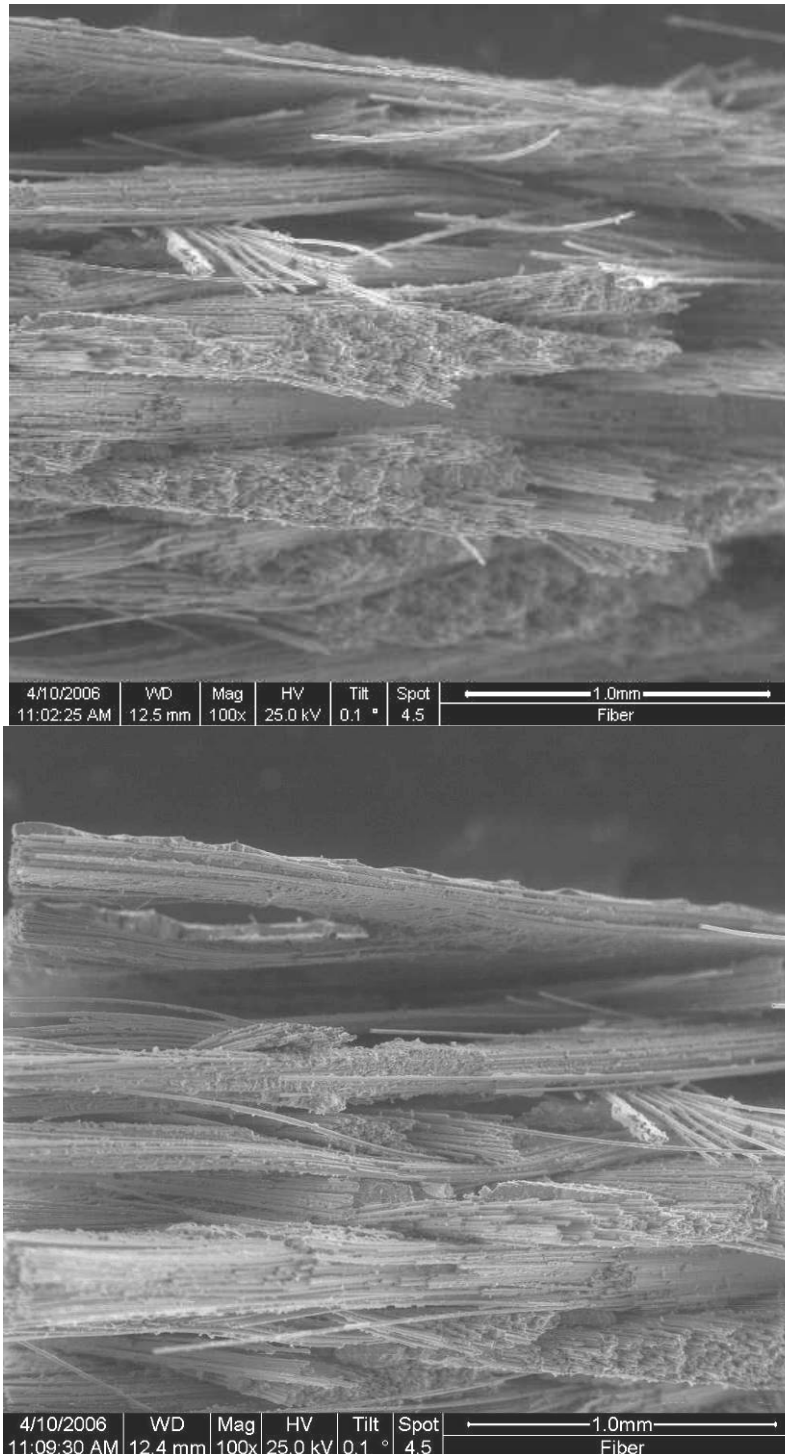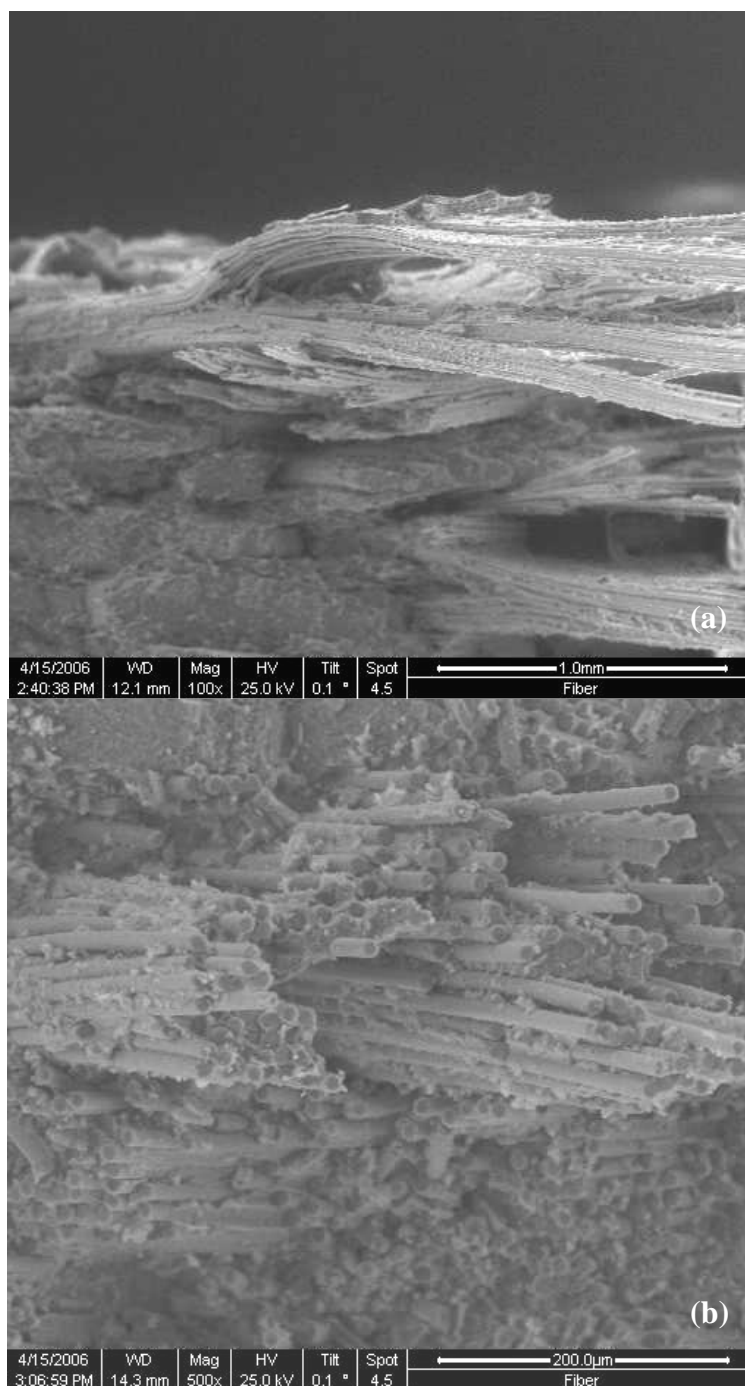**Figure 93. Micrograph of Nextel^{TM}720/alumina CMC specimen C-12 tested in creep at 45 MPa at 1200°C in 100% argon environment: (a) fiber pullout with shearing at the tips, (b) fiber bundle separated by "waviness."**

114

Figure 94. Micrograph of Nextel^{TM}720/alumina CMC specimen C-12 tested in creep at 45 MPa at 1200°C in 100% argon environment: intact matrix separating fiber bundles.

Figure 95. Micrograph of Nextel^{TM}720/alumina CMC specimen C-14 tested in creep at 40 MPa at 1200°C in 100% argon environment: individual fiber pullout with small matrix particles.

Figure 96. Micrograph of Nextel^{TM}720/alumina CMC specimen C-14 tested in creep at 40 MPa at 1200°C in 100% argon environment: (a) matrix separating two fiber bundles facing different directions, (b) organized matrix missing fibers which were pulled away.
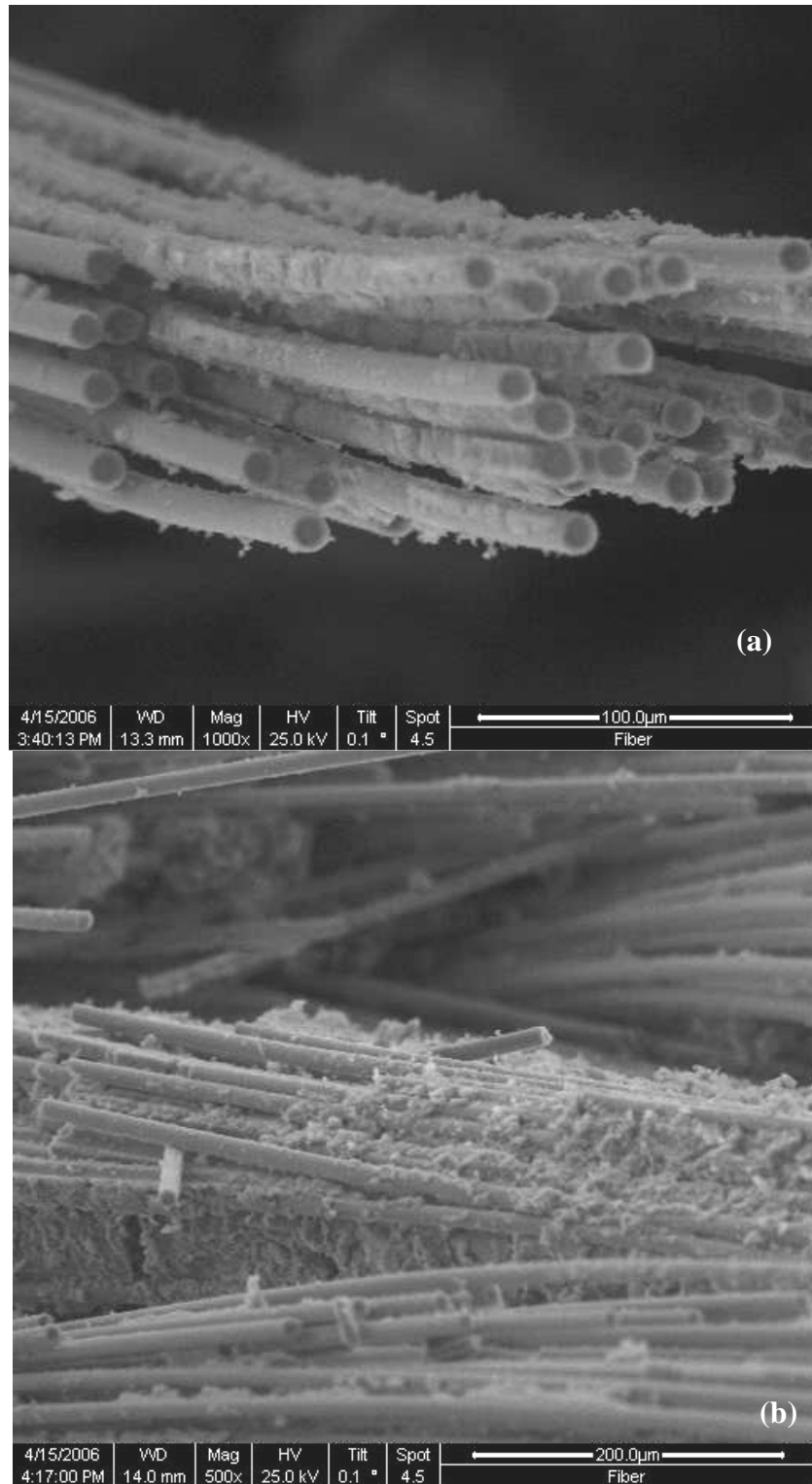
Figure 97. Micrograph of Nextel™720/alumina CMC specimen C-15 tested in creep at 15 MPa at 1200°C in 100% argon environment: (a) coordinated bundle failure, (b) disorganized matrix separating fiber bundles.
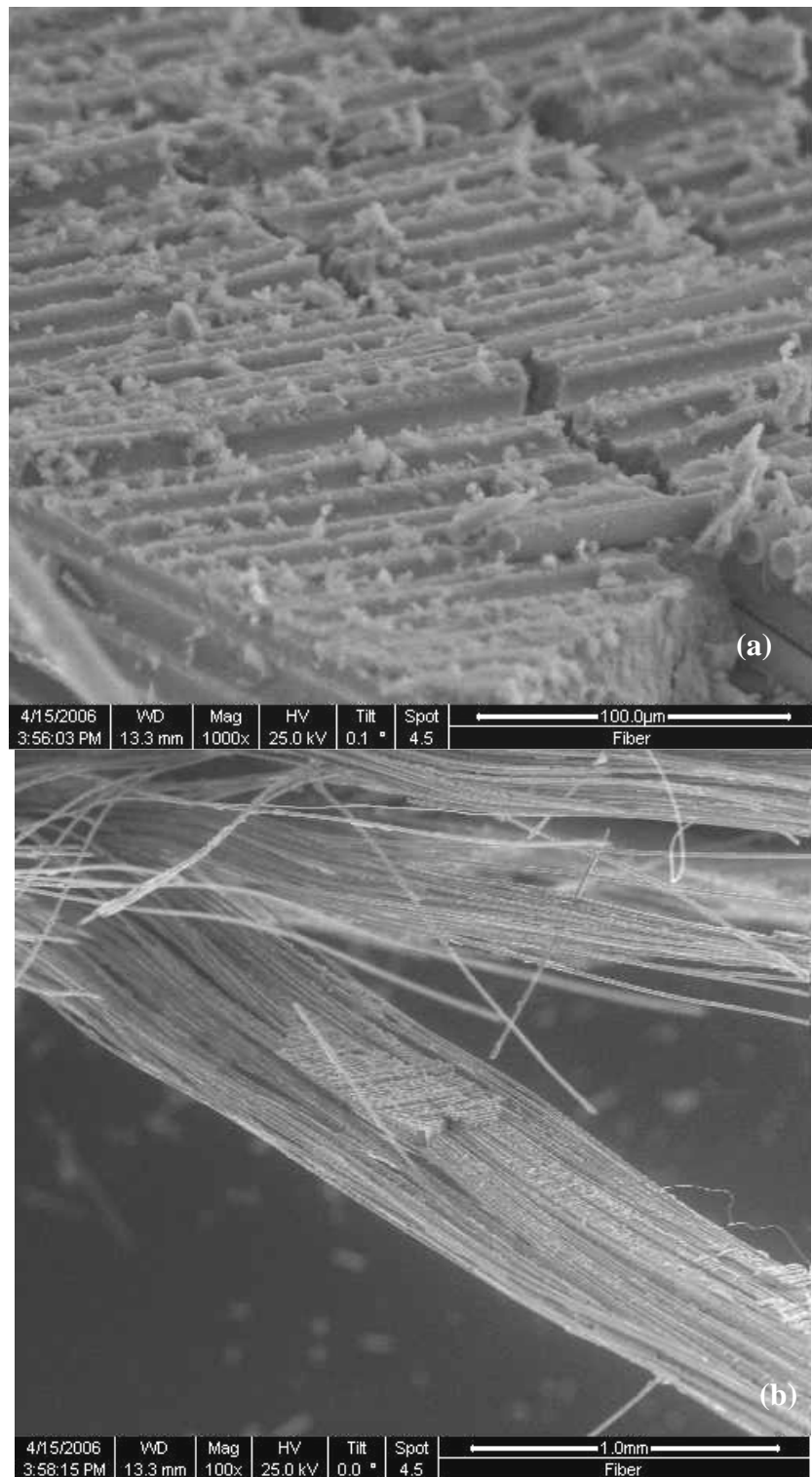
Figure 98. Micrograph of Nextel^TM720/alumina CMC specimen C-15 tested in creep at 15 MPa at 1200°C in 100% argon environment: (a) matrix separating fiber bundles with individual fiber pullout, (b) disorganized matrix missing fibers.
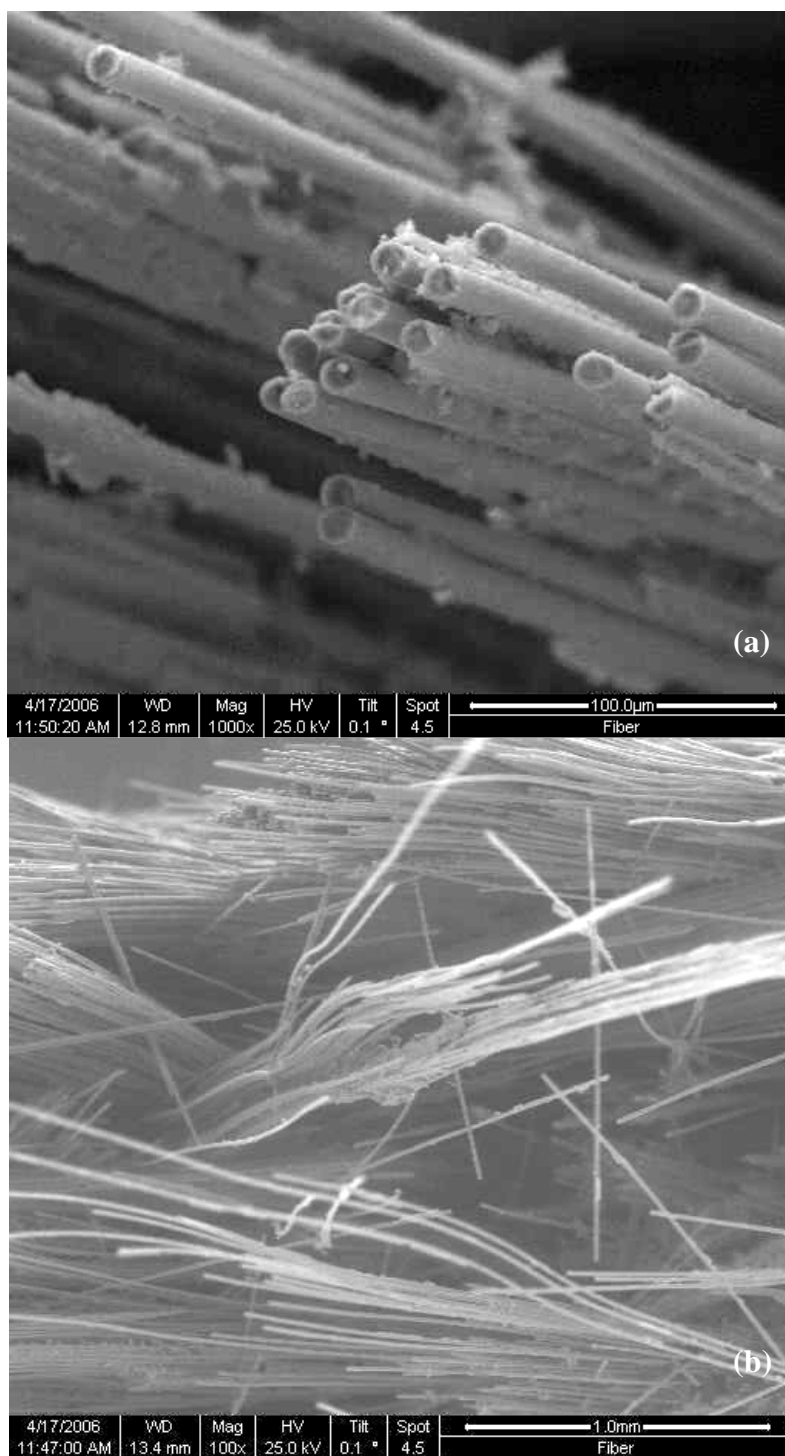
Figure 99. Micrograph of Nextel^{TM}720/alumina CMC specimen C-16 tested in creep at 35 MPa at 1200°C in 100% argon environment: (a) fiber pullout still covered in matrix, (b) matrix separating bundles, notice the curvature of the matrix trough where fibers once where.
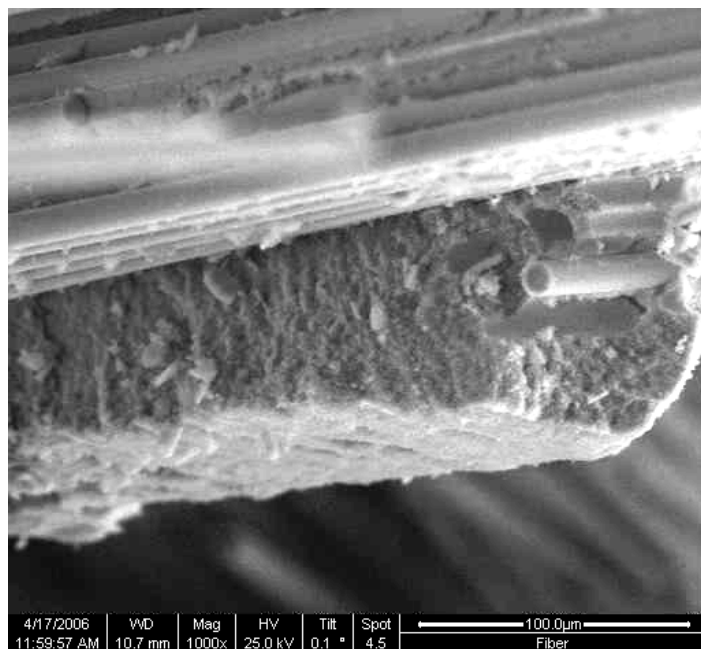
Figure 100. Micrograph of Nextel™720/alumina CMC specimen C-16 tested in creep at 35 MPa at 1200°C in 100% argon environment: (a) individual fiber showing the smoothness of the break and its size, (b) degradation of matrix between fibers.
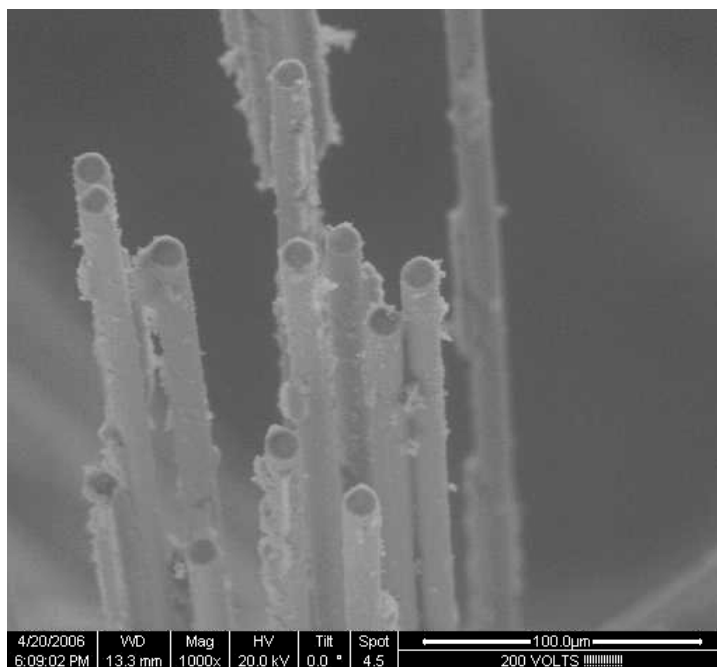
Figure 101. Micrograph of Nextel^{TM}720/alumina CMC specimen C-17 tested in creep at 45 MPa at 1200°C in 100% argon environment: (a) individual fiber with irregular fracture pattern, (b) crack propagating between matrix separating fibers.
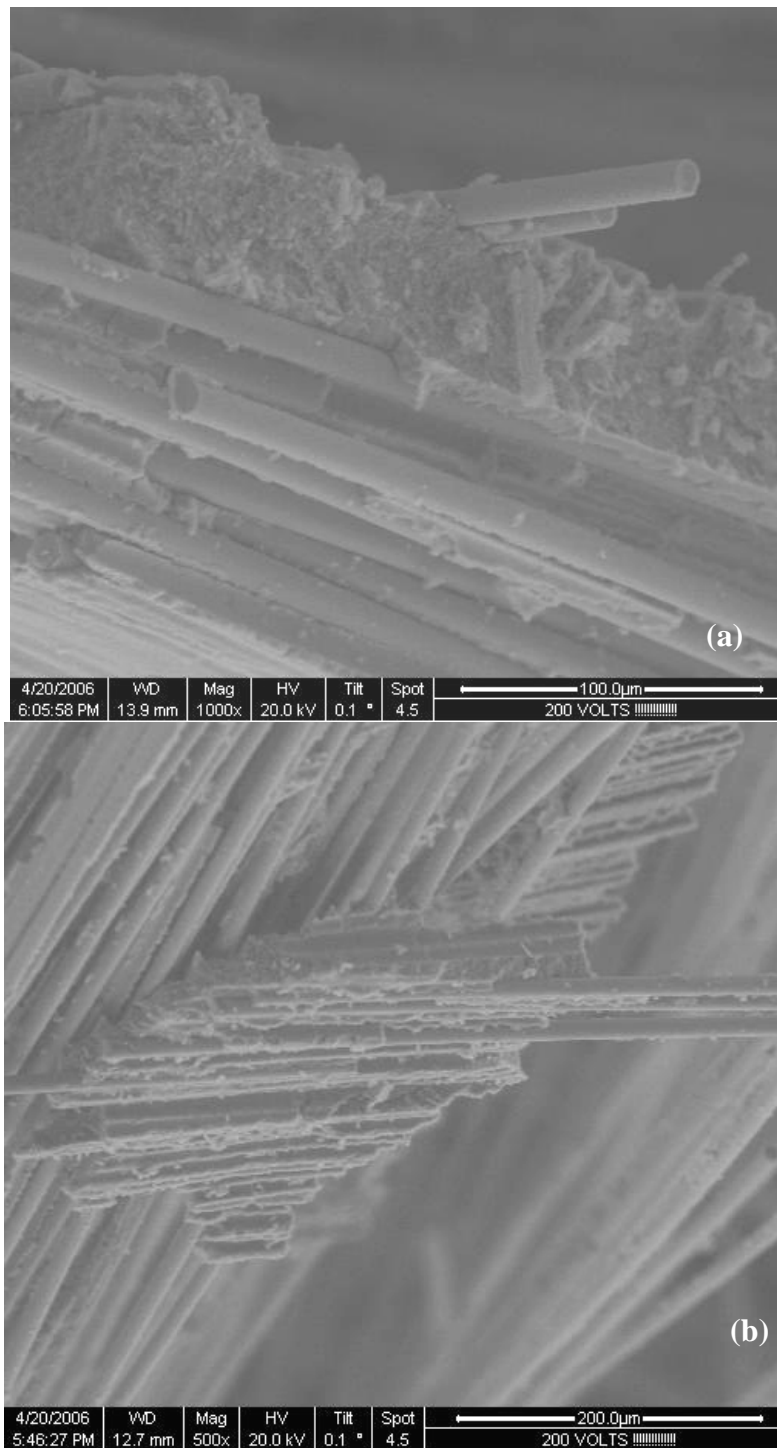
Figure 102. Micrograph of Nextel^{TM}720/alumina CMC specimen C-18 tested in creep at 40 MPa at 1200°C in 100% argon environment: (a) individual fiber pullout from matrix, (b) fracture surfaces from coordinated fiber bundle failure.
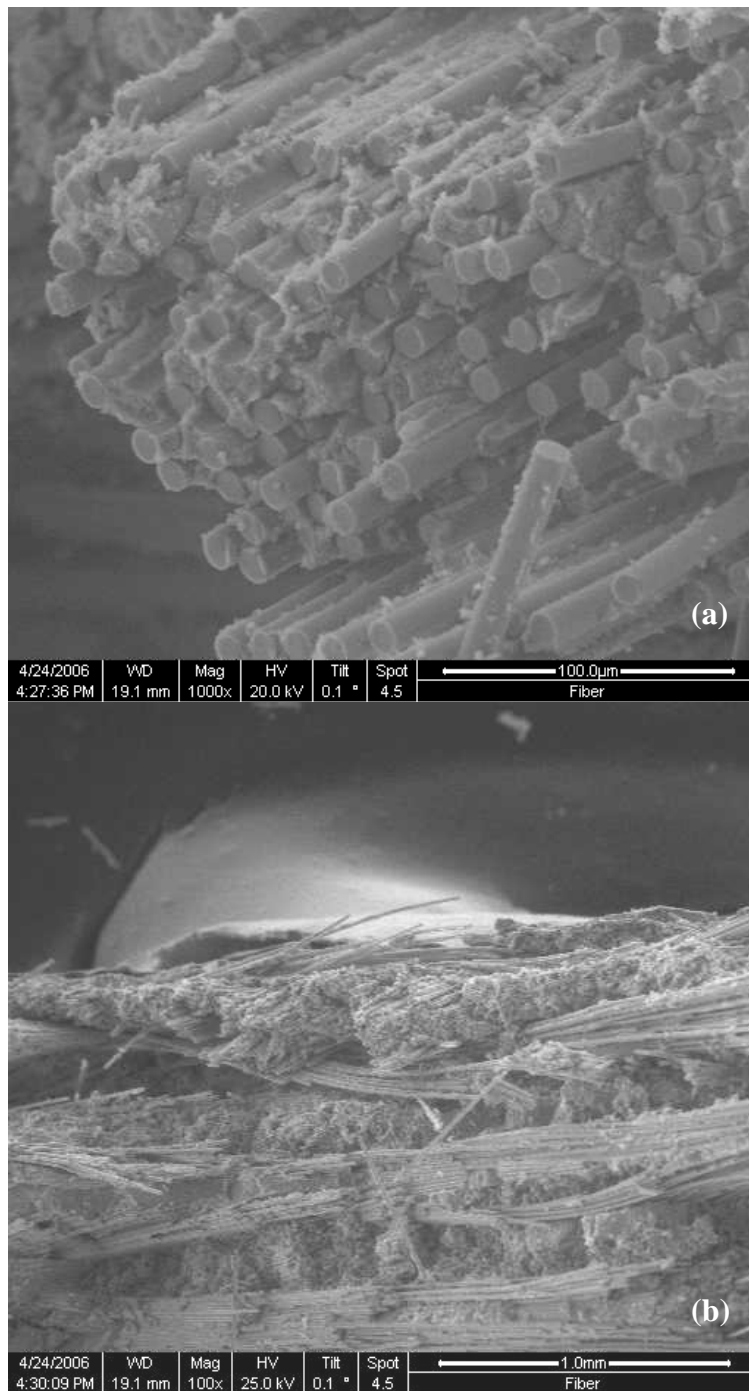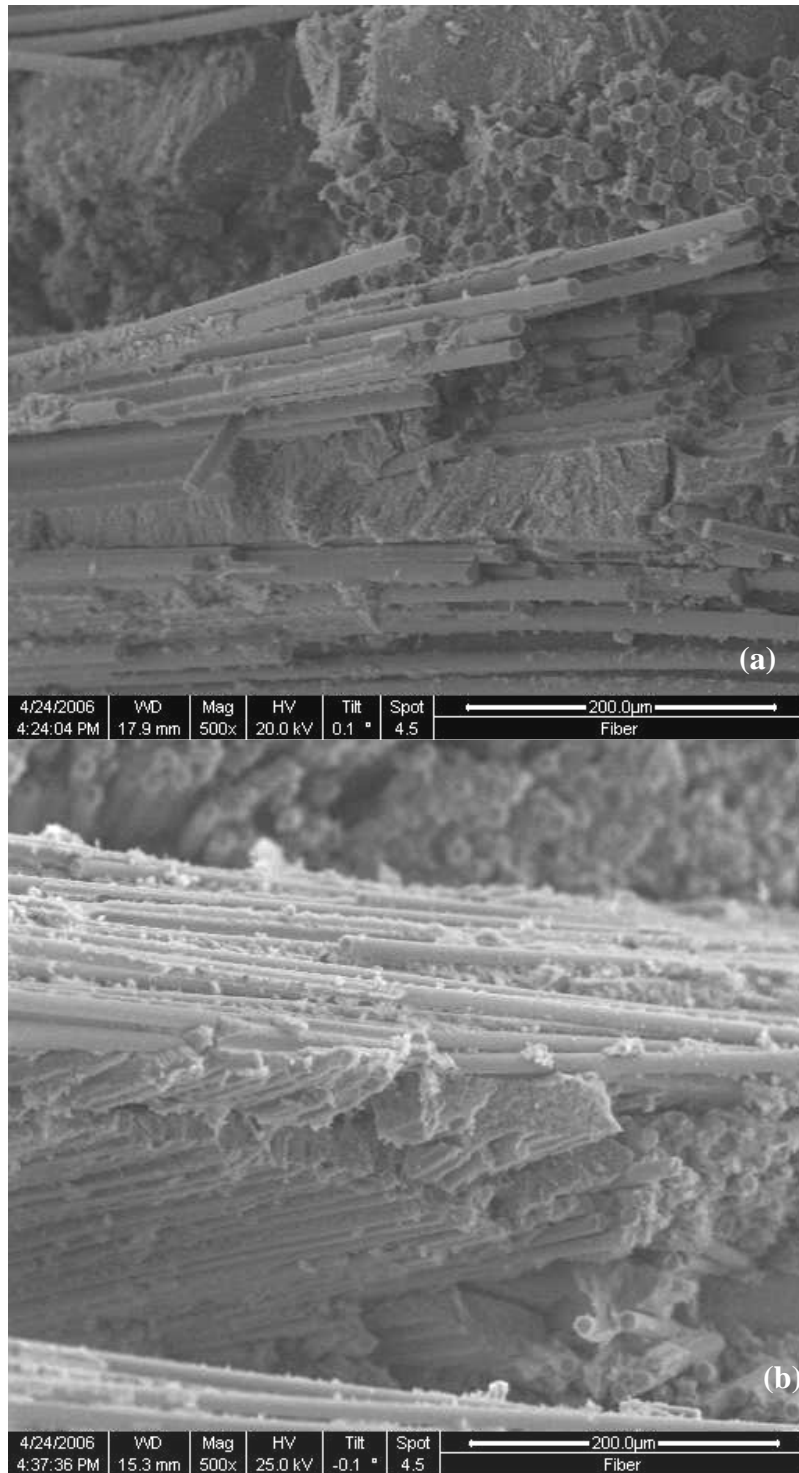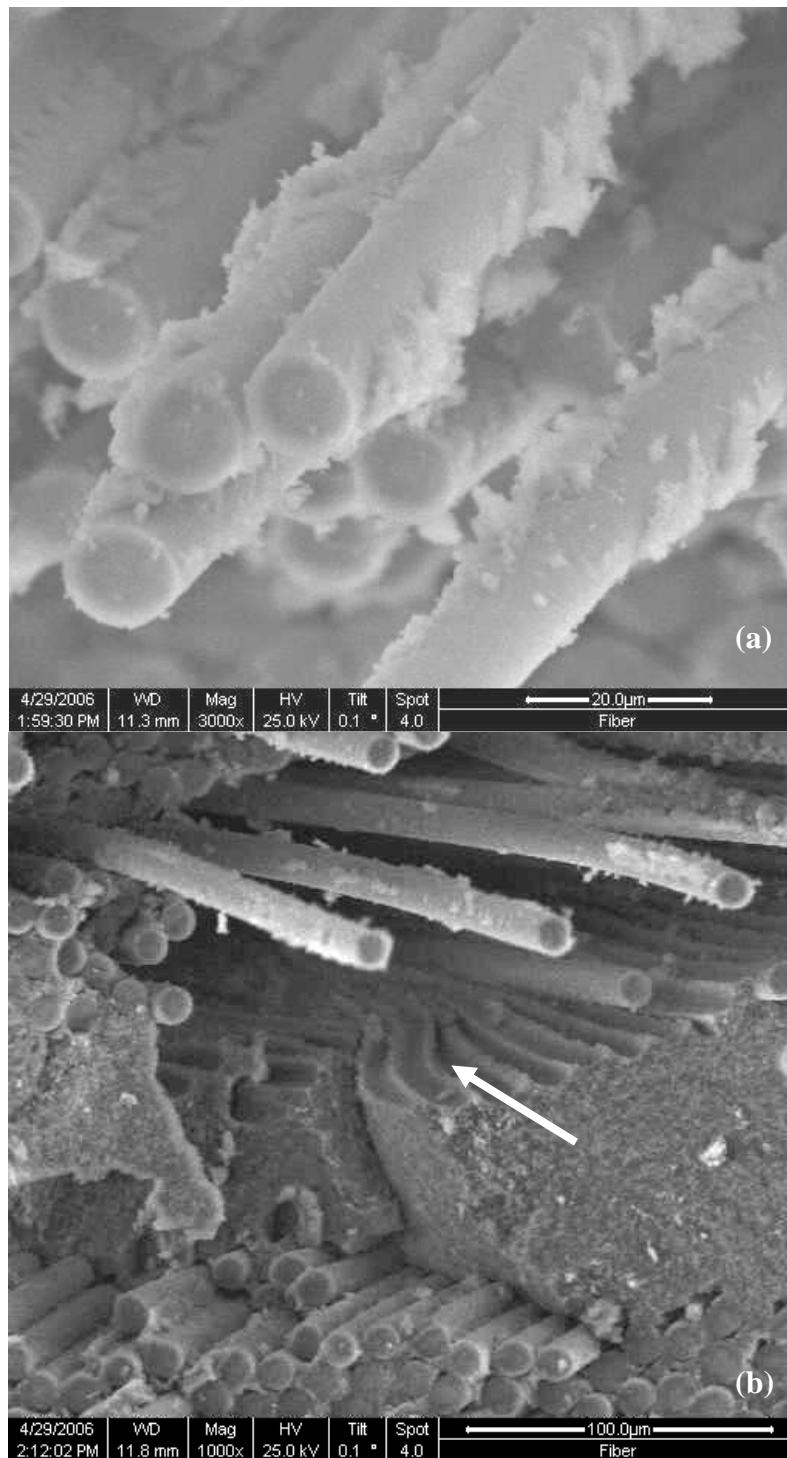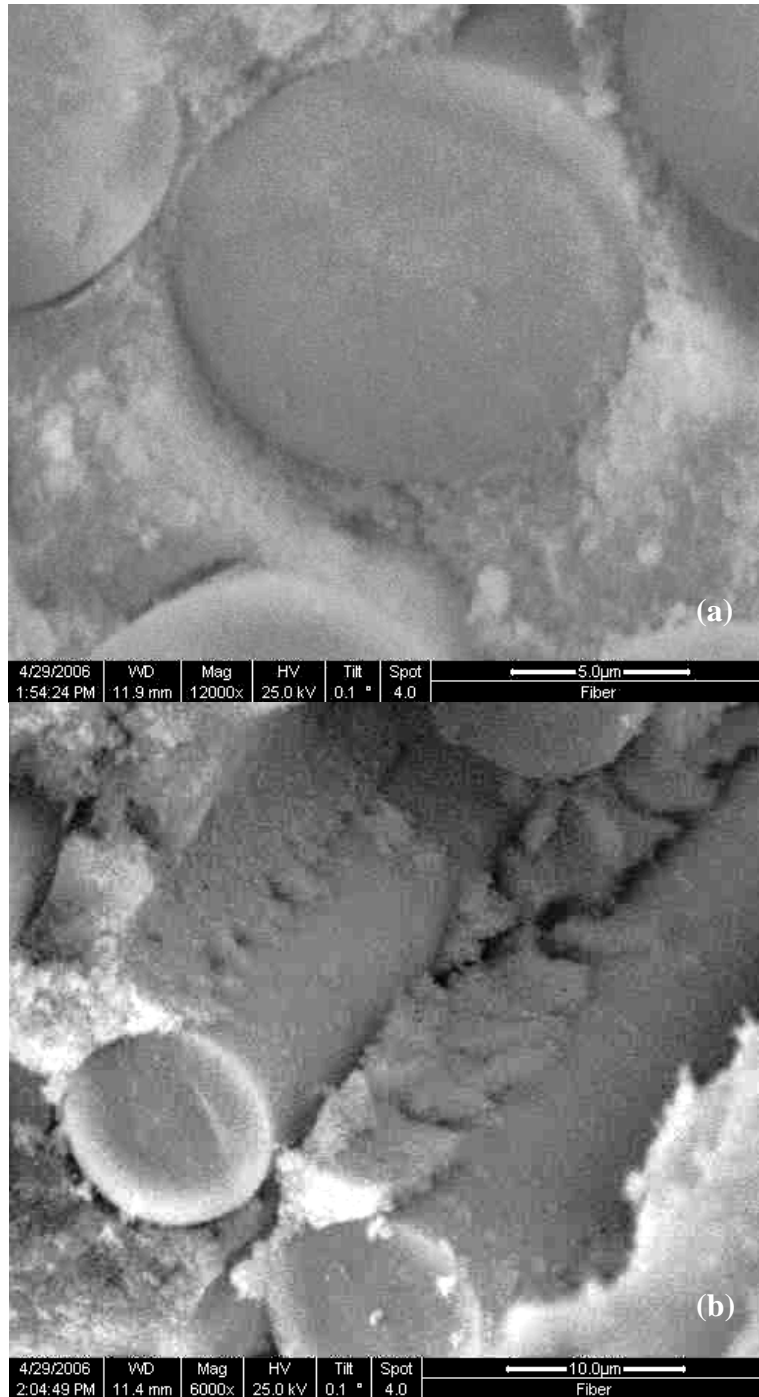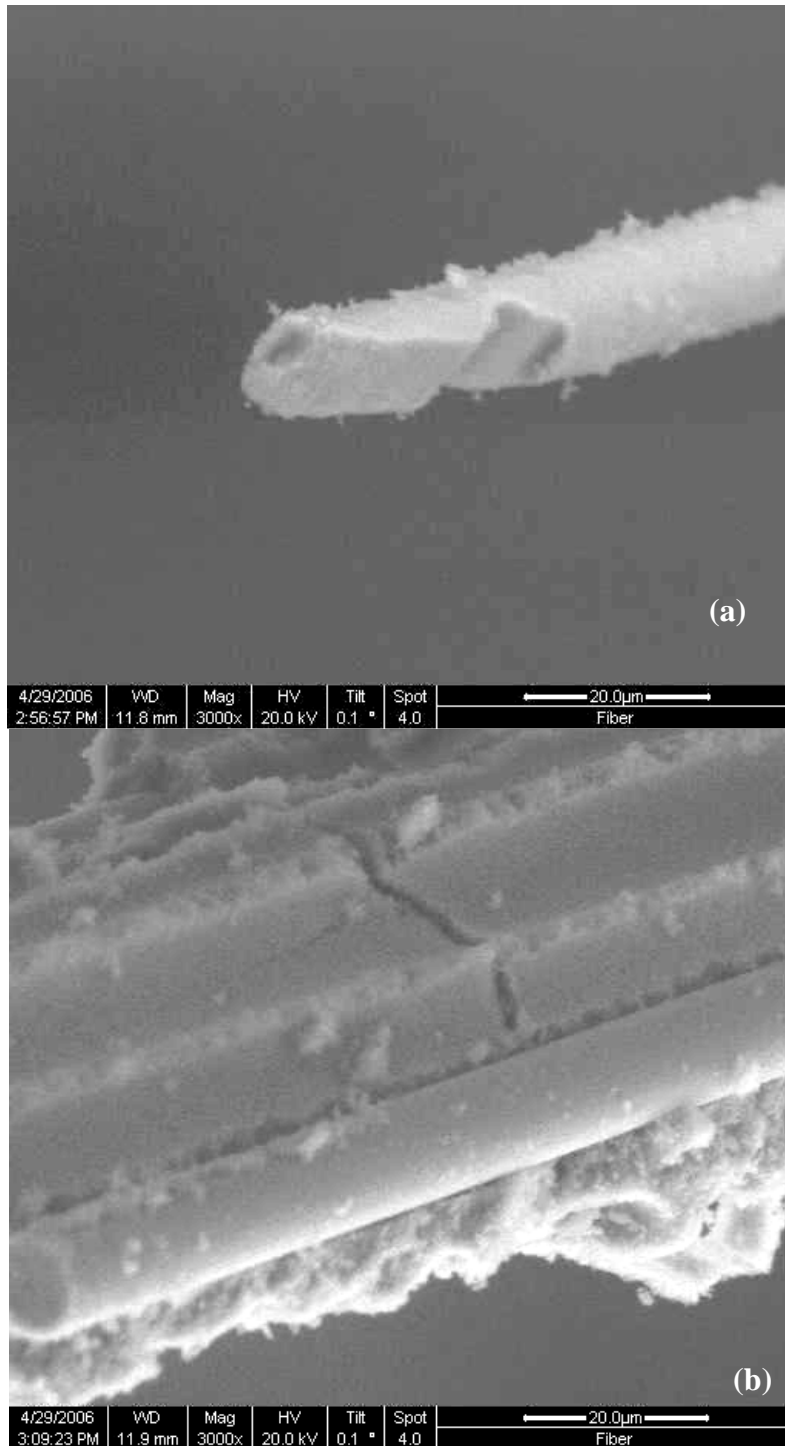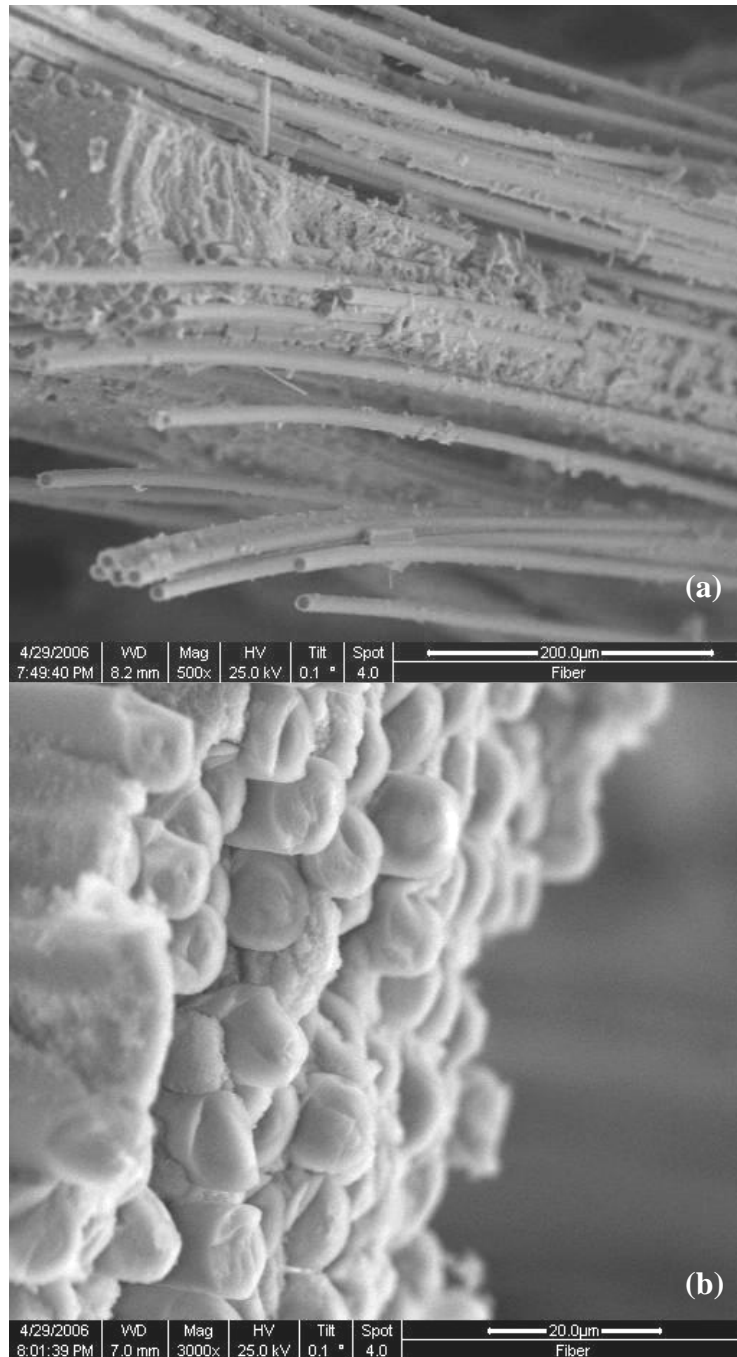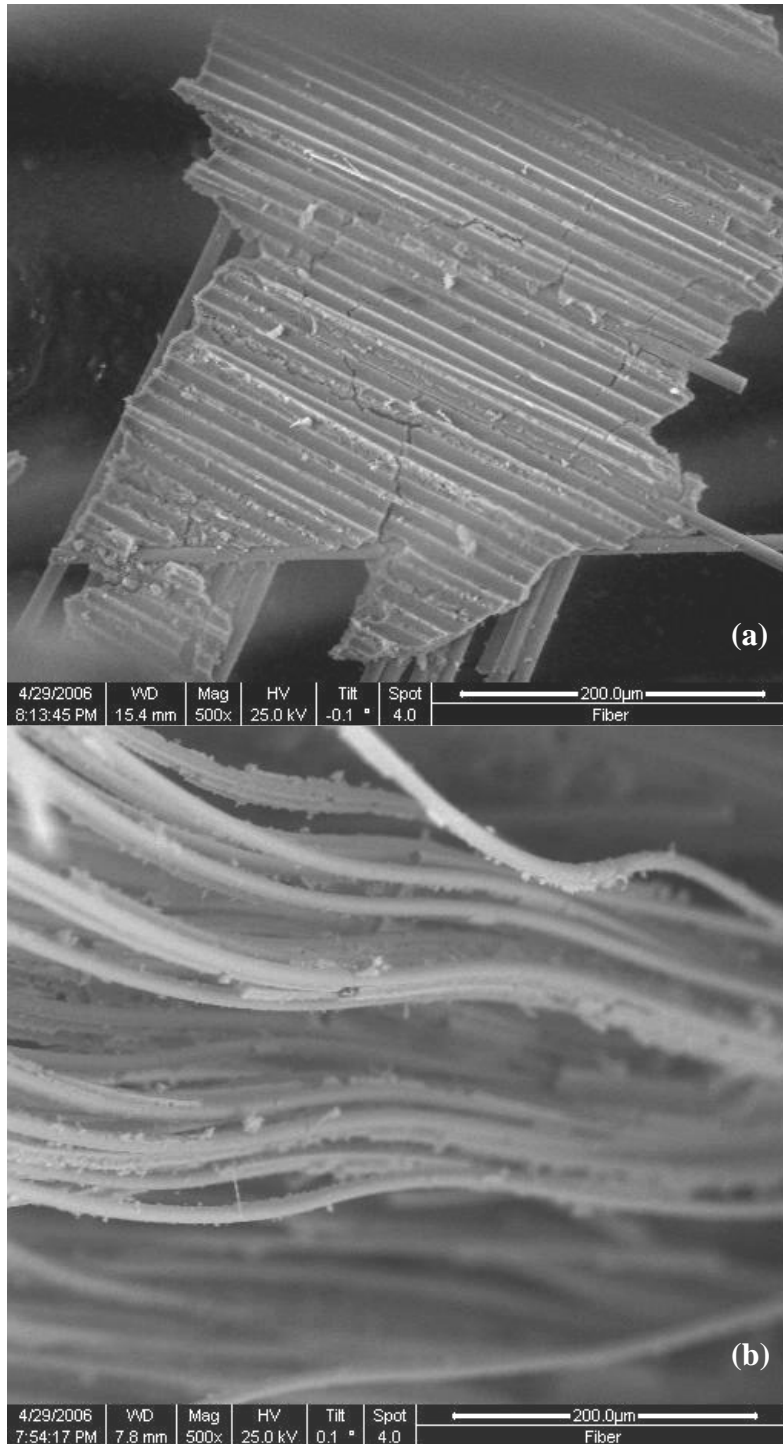
Figure 103. Micrograph of Nextel™720/alumina CMC specimen C-18 tested in creep at 40 MPa at 1200°C in 100% argon environment: (a) crack propagating through matrix with missing fibers, (b) organized "Waviness" of individual fibers.

Bibliography

1. "787 Dreamliner." Boeing. 1 Apr. 2006
   <http://www.boeing.com/commercial/787family/background.html>.

2. "F-22 Raptor Materials and Processes." Globalsecurity.Org. 19 Dec. 2005. 12 Mar.
   2006 <http://www.globalsecurity.org/military/systems/aircraft/f-22-mp.htm>.

3. "X-37." <u>Future X-Pages</u>. 22 Oct. 2004. NASA. 10 Feb. 2006 <www.hq.nasa.gov/.../
   History/x-33/x37-pix1.jpg>. "Effect of interphase characteristics on long-term
   durability of oxide-based fiber-reinforced composites," *Composites: Part A*, 32:1095-
   1103 (2001).

4. *All You Wanted to Know About Electron Microscopy…but Didn't Dare to Ask.*
   Hillsboro, OR: FEI Company, no date. http//www.feicompany.com. 10 Feb 2006

5. Antti, M. -L., Lara Curzio, E., and Warren, R. "Thermal degradation of an oxide
   fiber (Nextel 720)/aluminosilicate composite," Journal of the European Ceramic
   Society, 24: 565-578 (2004).

6. Antti, M-L, and Edgar Lara-Curzio. "Effect of Notches, Specimen Size, and Fiber
   Orientation on the Monotonic Tensile Behavior of Composites at Ambient and
   Elevated Temperatures," in 25th Annual Conference on Composites Advanced
   Ceramics Materials, and Structures: A. Ed. Mrityunjay Singh and Todd Jensen.
   Westerville, OH: The American Ceramic Society, 2001.

7. ASTM C 1337, "Standard Test Method for Creep and Creep Rupture of Continuous
   Fiber-Reinforced Ceramic Composites under Tensile Loading at Elevated
   Temperatures," *Annual Book of ASTM Standards*, Vol. 15.01, American Society for
   Testing and Materials, West Conshohocken PA (2000).

8. Buchanan, Dennis J., Reji John, and Larry P. Zawada. "Creep Rupture Behavior of
   ±45° Oxide/Oxide Nextel[TM]720/AS Composite," in *25th Annual Conference on
   Composites Advanced Ceramics Materials, and Structures: A*. Ed. Waltruad M.
   Kriven and Hau-Tay Lin. Westerville, OH: The American Ceramic Society, 2003.

9. Butner, Steve. Composite Optics Inc. Ceramics, San Diego CA. Email
   Correspondence. April 2006.

10. Casas, L., and Martínez-Esnaola J.M. "Microstructural characterization of an
    alumina/mullite composite tested in creep," *Materials Science and Engineering*,
    A368: 139-144 (2004).

11. Chawla, K.K. *Ceramic Matrix Composites* (2nd Edition). Boston: Kluwer Academic Publishers, 2003.

12. Harada, Yoshihisa, Suzuki, Takayuki, and Hirano, Kazumi. "Influence of Moisture on Ultra-High-Temperature Tensile Creep Behavior of in Situ Single-Crystal Oxide Ceramic Alumina/Yttrium Aluminum Garnet Eutectic Composite," *Journal of the American Ceramic Society*, 86: 951-958 (2003).

13. Harlan, Lee B. *Creep-Rupture Behavior of an Oxide/Oxide Ceramic Matrix Composite at Elevated Temperatures in Air and Steam Environments.* MS thesis, AFIT/GA/ENY/05-M05. School of Engineering and Management, Air Force Institute of Technology (AU), Wright-Patterson AFB OH, March 2005.

14. Haslam, J.J., Berroth, K.E., and Lange, F.F. "Processing and properties of an all-oxide composite with a porous matrix," *Journal of the European Ceramic Society*, 20: 607-618 (2000).

15. Jackson, Patrick R. *Characterization of Compressive Creep Behavior of Oxide/Oxide Composite with Monazite Coating at Elevated Temperature.* MS thesis, AFIT/GA/ENY/06-M17. School of Engineering and Management, Air Force Institute of Technology (AU), Wright-Patterson AFB OH, March 2006.

16. Johnson, David W. and others. Ceramic Fibers and Coatings: Advanced Materials for the Twenty-First Century. The National Academy of Sciences: Washington D.C., 1998.

17. Kaya, C., Butler, E.G., Selcuk, A., Boccaccini, A.R., and Lewis, M.H. "Mullite (Nextel™ 720) fiber-reinforced mullite matrix composites exhibiting favorable thermomechanical properties," *Journal of the European Ceramic Society*, 22: 2333-2342 (2002).

18. Kerans, Ronald J. and Triplicane A. Parthasarathy. "Crack Deflection in Ceramic Composites and Fiber Coating Design Criteria," Composites: Part A: Applied Science and Manufacturing, 30: 521-24 (1999).

19. Levi, Carlos G., Yang, James Y., Dalgleish, Brian J., Zok, Frank W., and Evans, Anthony G. "Processing and Performance of an All-Oxide Ceramic Composite," *Journal of the American Ceramic Society*, 81: 2077-2086 (1998).

20. Mattoni, M.A., Yang, J.Y., Levi, C.G., Zok, F.W., Zawada, L.P. "Effects of Combustor Rig Exposure on a Porous-Matrix Oxide Composite, "International Journal of Applied Ceramic Technology, 2(2):133-140 (2005).

21. Mecham, Michael. "Composite Power." <u>Aviation Week</u> 17 Apr. 2006: 47-52.

22. Mehrman, John M. Effects of Hold Times on Fatigue Behavior of Nextel[TM] 720/Alumina Ceramic Matrix Composite at 1200°C in Air and in Steam Environment. MS thesis, AFIT/GA/ENY/06-M23. School of Engineering and Management, Air Force Institute of Technology (AU), Wright-Patterson AFB OH, March 2006.

23. *Minnesota Mining and Manufacturing Company (3M™)*. "Nextel™ Ceramic Textiles Technical Notebook," Company produced technical notebook. no date

24. Musil, Sean S. Characterization of Creep Behavior of Oxide/Oxide Composite with Monazite Coating at Elevated Temperature. MS thesis, AFIT/GAE/ENY/05-M14. School of Engineering and Management, Air Force Institute of Technology (AU), Wright-Patterson AFB OH, March 2005.

25. Ohnabe, Hisaichi, Masaki, Shoju, Onozuka, Masakazu, Miyahara, Kaoru and Sasa, Tadashi. "Potential application of ceramic matrix composites to aero-engine components," *Composites: Part A: applied science and manufacturing*, 30: 489-496 (1999).

26. Parlier, Michel and Ritti, M.H. "State of the art and perspectives for oxide/oxide composites," *Aerospace Science and Technology*, 7: 211-221 (2003).

27. Parthasarthy, T.A., Zawada, L.P., John, R., Cinibulk, M.K., Zelina, J. "Evaluation of Oxide/oxide Composites in a Novel Combustor Wall Application," International Journal of Applied Ceramic Technology, 2(2):122-132 (2005).

28. Pierce, Jennifer, and Hartman, Greg. "Matrix and Composite Characterization of N720/A." Prepared for COI Ceramics, Inc., 9617 Distribution Avenue, San Diego CA 92121. September 2001.

29. Ruggles-Wrenn, M.B., private communications (2005-2006).

30. Ruggles-Wrenn, M.B., S. Mall, C.A. Eber, and L.B. Harlan. "Effect of Steam Environment on High-Temperature Mechanical Behavior of Nextel[TM]720/Alumina (N720/A) Continuous Fiber Ceramic Composite," Composites: Part A: Applied Science and Manufacturing, in press (2006)

31. Ruggles-Wrenn, M.B., S.S. Musil, S. Mall, and K.A. Keller. "Creep Behavior of Nextel[TM]610/Monazite/Alumina Composite at Elevated Temperatures," *Composites Science and Technology*, in press (2006).

32. Saruhan, B., Schmucker, M., Bartsch, M., Schneider, H., Nubian, K., Wahl, G., "Effect of Interphase Characteristics on Long-Term Durability of Oxide-based Fiber-Reinforced Composites," *Composites: Part A,* 32:1095-1103 (2001).

33. Schmidt, S., Beyer, S., Knabe, H., Immich, H., Meistring, R., and Gessler, A. "Advanced ceramic matrix composite materials for current and future propulsion technology applications," *Acta Astronautica*, 55: 409-420 (2004).

34. Simon, R.A. "Progress in Processing and Performance of Porous-Matrix Oxide/Oxide Composites," *International Journal of Applied Ceramic Technology,* 2(2):141-149 (2005).

35. Steel, Steven G. *Monotonic and Fatigue Loading Behavior of an Oxide/Oxide Ceramic Matrix Composite*. MS thesis, AFIT/GMS/ENY/00M-02. Graduate School of Engineering and Management, Air Force Institute of Technology (AU), Wright-Patterson AFB OH, March 2000.

36. Van Rijswijk, K, W.d. Brouwer, and A Beukers. "Composites." Application of Natural Fiber. 2003. Food and Agriculture Organization of the United Nations. 11 Mar. 2006 <10. www.fao.org/docrep/ 007/ad416e/ad416e07.jpg\>.

37. Wallace, James. "Boeing Unveils B787." Seattle Post (2005). 1 Apr. 2006 <http://www.airmech.co.uk/forums/showthread.php?t=710>.

38. Wannaparhum, S., Seal, S., Desai, V.H., Varghese, P., Campbell, C.X."Combined Spectroscopic and Thermodynamic Investigation of Nextel 720/Alumina Ceramic Matrix Composite in Air and Water Vapor at 1100°C", Journal of the American Ceramic Society, 86(9):1628-30 (2003).

39. Wilson, D.M. and Visser, L.R. "High performance oxide fibers for metal and ceramic composites," *Composites: Part A: applied science and manufacturing*, 32: 1143-1153 (2001).

40. Zawada, Larry P., Hay, Randall S., Lee, Shin S., and Staehler, James. "Characterization and High-Temperature Mechanical Behavior of an Oxide/Oxide Composite," *Journal of the American Ceramic Society*, 86: 981-990 (2003).

41. Zawada, Larry P., Staehler, James, and Steel, Steven. "Consequence of Intermittent Exposure to Moisture and Salt Fog on the High-Temperature Fatigue Durability of Several Ceramic-Matrix Composites," *Journal of the American Ceramic Society*, 86: 1282-1291 (2003).

42. Zawada, Larry P. and Lee, Shin S. "The Effect of Hold Times on the Fatigue Behavior of an Oxide/Oxide Ceramic Matrix Composite," *Thermal and Mechanical Test Methods and Behavior of Continuous-Fiber Ceramic Composites*, ASTM STP 1309, Michael G. Jenkins, Stephen T. Gonczy, Edgar Lara-Curzio, Noel E. Ashbaugh, and Larry P. Zawada, Eds., American Society for Testing and Materials, 1997.

Vita

    Ensign Gregory T Siegert, United States Navy, graduated from the Marist School in Atlanta, Georgia. He entered undergraduate studies at Villanova University in Villanova, Pennsylvania where he graduated with a Bachelor of Science degree in Mechanical Engineering with a minor in Naval Science in May 2005. He was commissioned through the Villanova University Naval Reserve Officer Training Corps. Upon graduation he was designated a Student Naval Aviator and given orders to the Graduate School of Engineering and Management, Air Force Institute of Technology. Upon achievement of a masters of science in Aeronautical Engineering, ENS Siegert will continue on to initial pilot training with Training Wing 5 at Naval Air Station Pensacola, Fl.

REPORT DOCUMENTATION PAGE

1. REPORT DATE *(DD-MM-YYYY)* 13-06-2006	2. REPORT TYPE **Master's Thesis**	3. DATES COVERED *(From – To)* June 2005 – June 2006

TITLE AND SUBTITLE Effect of Environment on Creep Behavior of an oxide/oxide CFCC with ±45° fiber orientation	5a. CONTRACT NUMBER
	5b. GRANT NUMBER
	5c. PROGRAM ELEMENT NUMBER
AUTHOR(S) Siegert Gregory, T., ENS, USN	5d. PROJECT NUMBER
	5e. TASK NUMBER
	5f. WORK UNIT NUMBER

7. PERFORMING ORGANIZATION NAMES(S) AND ADDRESS(S) Air Force Institute of Technology Graduate School of Engineering and Management (AFIT/EN) 2950 Hobson Way WPAFB OH 45433-7765	8. PERFORMING ORGANIZATION REPORT NUMBER AFIT/GAE/ENY/06-J15

9. SPONSORING/MONITORING AGENCY NAME(S) AND ADDRESS(ES) AFRL/PRTC AFRL/MLLN Attn: Dr. Joseph Zelina Attn: Dr. Ronald Kerans 1950 Fifth Street 2977 P Street WPAFB OH 45433-7251 WPAFB OH 45433-7734	10. SPONSOR/MONITOR'S ACRONYM(S)
	11. SPONSOR/MONITOR'S REPORT NUMBER(S)

12. DISTRIBUTION/AVAILABILITY STATEMENT
APPROVED FOR PUBLIC RELEASE; DISTRIBUTION UNLIMITED.

13. SUPPLEMENTARY NOTES

14. ABSTRACT
Aerospace applications require materials capable of maintaining superior mechanical properties while operating at high temperatures and oxidizing environments. Nextel™ 720/A (N720/A), an oxide/oxide ceramic matrix composite (CMC) with a porous alumina matrix was developed specifically to provide improved long-term properties and performance at 1200°C. This research evaluated the creep behavior of N720/A with a ±45° fiber orientation at 1200°C in: laboratory air, 100% steam, and 100% argon environments. Creep-rupture tests at the creep stress levels of: 45, 40, 35, and 15 MPa were conducted in each environment.

The ultimate tensile strength of N720/A with ±45˚ fiber orientation was 55 MPa, the elastic modulus (E) was 45 GPa, and failure strain was 0.265%. The creep-rupture results showed a decrease in creep life with increasing creep stress. The material was found to perform best in air, followed by steam, and then argon. Prior to this effort, N720/A was believed to perform best in non oxidizing environments such as argon. Tests at stress levels $\leq$ 35 MPa revealed good creep resistance achieving a run out of 100 h in all test environments at 1200°C. Fracture surface observations with a Scanning Electron Microscope showed a correlation between coordinated fiber bundle failure and increased creep life. A qualitative spectral analysis provided evidence of silicon species migration from the mullite phase of the fiber to the matrix in each environment, but increasingly so in steam and argon.

15. SUBJECT TERMS
Ceramic Matrix Composites, Composite Materials, Ceramic Fibers, Ceramic Materials, Fiber Reinforced Composites, Alumina, Mullite, Creep, Oxides

16. SECURITY CLASSIFICATION OF:			17. LIMITATION OF ABSTRACT	18. NUMBER OF PAGES	19a. NAME OF RESPONSIBLE PERSON Dr. Marina B. Ruggles-Wrenn, AFIT/ENY
REPORT **U**	ABSTRACT **U**	c. THIS PAGE **U**	**UU**	145	19b. TELEPHONE NUMBER *(Include area code)* (937) 255-3636, ext 4641; e-mail: marina.ruggles-wrenn@afit.edu

Standard Form 298 (Rev: 8-98)
Prescribed by ANSI Std. Z39-18